ALMA MATER STUDIORUM - UNIVERSITÀ DI BOLOGNA

SCUOLA DI INGEGNERIA E ARCHITETTURA

DIPARTIMENTO DI INGENERIA CIVILE, CHIMICA, AMBIENTALE E DEI MATERIALI - DICAM

CORSO DI LAUREA MAGISTRALE IN CIVIL ENGINEERING

TESI DI LAUREA

in
Groundwater and Contamination Processes

ASSESSING AQUIFER VULNERABILITY TO SEAWATER INTRUSION: APPLICATION OF THE GALDIT-INDEX TO THE EMILIA-ROMAGNA COASTLINE

CANDIDATO
Adrien Corman

RELATORE:
Prof. Vittorio Di Federico

CORRELATORE/CORRELATORI
Dott.ssa Ing. Giada Felisa

Anno Accademico 2016/2017

Sessione I

This thesis is dedicated to my beloved Grandmother

Acknowledgements

With these few words, I would like to thank all the persons who got involved, directly or indirectly, in the conclusion of this master thesis.

In particular,

Professor Vittorio Di Federico, for having accepted to supervise me, for having provided me a topic as interesting and concerning as the problematic of saltwater intrusion, for his guidance and his availability during the past five months;

Dott.ssa Ing. Giada Felisa for her availability, her reading, her advises and for her explanations about the software QGIS©. In addition, I would also like to thank her for providing me all the data required to bring this work to an end in such a short period of time;

Special thanks to PhD student Julia Shustikova who has dedicated a bit of her precious time to introduce me into the world of GIS softwares. Her teaching skills and her knowledge about GIS softwares in general are really impressive and if I now feel captured for this topic it is also her achievement;

My flatmates Ramon and Arsel for their good company, their help and support during all this year in Italy;

My friends from Belgium who had time to visit me here in Italy but also my new international friends from Bologna with whom I have spent lighter moments and who have made this year such an enjoyable experience;

My family, my sister and my grandfather. Among them, special thanks to my parents for their love and inspiration, for their continuous support and advises during these five years of university studies and for having given me the chance to take part in such a rewarding experience;

Last but not least, I would like to thank my twin brother, Gilles, for having shared the last five years of university with me and all the ups and downs that go with them. I thank him sincerely for his daily support and understanding, no matter the distance. All of this wouldn't have been possible without him;

Bologna, 16th July 2017

Abstract

Saltwater intrusion (SWI) in coastal aquifers due to excessive groundwater withdrawals (for civil, agricultural and industrial purposes) has become a major concern affecting a large number of coastal aquifers worldwide. This trend is expected to grow in the very near future due to the expected sea-level rise (SLR) associated with the human-induced climate change. In this context, the following research proposes an assessment of the vulnerability of the Emilia-Romagna coastline (Italy) to SWI under present conditions. This assessment is conducted through the use of the GALDIT-Index, an indicator-based model which is made of 6 parameters that are presumed to control the phenomenon of SWI (***G***roundwater occurrence, ***A***quifer hydraulic conductivity, ***L***evel of groundwater above the mean sea-level, ***D***istance from the shore, ***I***mpact of existing status of SWI, ***T***hickness of the aquifer). The thematic maps of the 6 factors were prepared in a GIS environment. They were given appropriate ratings and weightages and were overlaid in order to produce two vulnerability maps, one for the surface phreatic aquifer and one for the underlying confined one. The results are relatively similar between those two maps and show that the coastline is highly vulnerable over a width of a few kilometres. The coastal plain, on the other hand, is characterized by a moderate vulnerability that tends to be reduced when moving landwards toward higher topography. Those vulnerability maps can generally be used as a tool for management of the coastal groundwater resources.

Key words: Seawater intrusion, Coastal aquifer, Vulnerability mapping, GALDIT index, GIS, Emilia-Romagna coastline

Table of content

List of figures

List of tables

List of acronyms

AC	=	Alternating Current
a.m.s.l.	=	above mean sea-level
ARPAE	=	Agenzia Regionale per la Prevenzione, l'Ambiente e l'Energia dell'Emilia-Romagna (i.e. Agency for Prevention, Environment and Energy of Emilia-Romagna)
b.m.s.l.	=	below mean sea-level
CER	=	Canale Emiliano-Romagnolo (i.e. Channel Emiliano-Romagnolo)
CRS	=	Coordinate Reference System
CVI	=	Coastal Vulnerability Index
DC	=	Direct Current
DEM	=	Digital Elevation Model
DRASTIC	=	overlay index used to assess groundwater vulnerability to pollution (*D*epth to groundwater, net *R*echarge, *A*quifer media, *S*oil media, *T*opography, *I*mpact of the vadose zone media, hydraulic *C*onductivity of the aquifer)
EC	=	Electrical Conductivity
EM	=	Electromagnetic
EPIK	=	overlay index used to assess groundwater vulnerability to pollution (*E*pikarst, *P*rotective cover, *I*nfiltration conditions, *K*arst network development)
ERT	=	Electrical Resistivity Tomography
EU	=	European Union
FDEM method	=	Frequency-Domain Electromagnetic method
FRST	=	Falling Regressive Systems Tract
GIS	=	Geographic Information System
GOD	=	overlay index used to assess groundwater vulnerability to pollution (*G*roundwater hydraulic confinement, *O*verlying strata, *D*epth to groundwater table)
GQI_{SWI}	=	Groundwater Quality Index for Seawater Intrusion
HST	=	Highstand Systems Tract
IDW	=	Inverse Distance Weighting

IPCC	=	Intergovernmental Panel on Climate Change
kya	=	thousand years ago
LST	=	Lowland Systems Tract
mya	=	million years ago
UNISDR	=	United Nations International Strategy for Disaster Reduction
SEPA	=	Scottish Environment Protection Agency
SGSS	=	Servizio Geologico, Sismico e dei Suoli (i.e. Geological, Seismic and Soil Survey of Emilia-Romagna)
SINTACS	=	overlay index used to assess groundwater vulnerability to pollution (water table depth, effective ***I***nfiltration, unsaturated conditions, soil media, ***A***quifer hydrogeologic characteristics, hydraulic ***C***onductivity, topographic ***S***lope)
SL	=	Sea-Level
SLR	=	Sea-Level Rise
SWI	=	Seawater Intrusion
TDEM method	=	Time-Domain Electromagnetic method
TDS	=	Total Dissolved Solids
TEM method	=	Transient Electromagnetic method
TIN	=	Triangulated Irregular Network
TST	=	Transgressive Systems Tract
USGS	=	United State Geological Survey
VES	=	Vertical Electrical Sounding

Chapter 1
Introduction

The study of coastal zones is of primary interest since they are extremely-densely populated areas. Today it is estimated that over half of the world's population live within 200km of the ocean shoreline, an area only taking up 10% of the earth's surface [1]. The uncontrolled use of coastal aquifers as a major source for freshwater supply (i.e. for civil use as well as agricultural and industrial purposes) has put the fragile coastal equilibrium under dramatic pressure. In particular, the subsequent contamination of freshwater by saltwater, commonly referred to as seawater intrusion (SWI), has become a major and concerning threat, affecting both freshwater quality and quantity.

A three-step approach is usually used to assist the development of groundwater protection strategies at local scale. This method includes a monitoring phase, the modelling of the aquifer and numerical simulations. It however presents two major drawbacks: (1) on the one hand it is very unlikely to be extended at a larger scale due to its important cost in terms of time and resources and due to its high dependency on local hydrogeological conditions; (2) on the other hand, it is generally used as a post-intrusion tool. Given the significant cost of post-intrusion remediation techniques, there is a real need for prediction techniques that would allow a rapid and cost-effective assessment of SWI over large areas.

In this context techniques to assess the vulnerability and the risk of groundwater to SWI were developed with the purposes to provide useful thematic maps that may help the people involved with coastal zone management (i.e. policy makers, local governments…) to detect the current and emerging risk areas, to prioritize areas requiring more detailed investigations and to decide where corrective measures have to be taken or where money has to be invested. Even though no generally recognized and accepted approach has been developed yet, those techniques turn out to be promising complementary tools to the current costly classical approach for the future.

In the present study, the aim is to apply one of these emerging techniques, namely the GALDIT-Index, to the Emilia-Romagna coastline in Italy. Saltwater intrusion is expected to become a crucial issue in Italy since this country constitutes a peninsula with a coastline of more or less 7600km long. The GALDIT-Index consists of an indicator-based model which is made of 6 parameters that are presumed to control the phenomenon of SWI:

- The ***G***roundwater occurrence;
- The ***A***quifer hydraulic conductivity;
- The ***L***evel of groundwater above the mean sea-level;
- The ***D***istance from the shore;
- The ***I***mpact of existing status of SWI;
- The ***T***hickness of the aquifer;

The methodology relies on the extensive use of Geographical Information System (GIS). The maps of the 6 parameters were prepared within a GIS environment based on the data that were collected from various sources. They were then rated and overlaid with suitable weights to produce the final vulnerability map of the study area. Those maps can generally be used as a tool for management of the coastal groundwater resources.

The following research is outlined in six chapters in addition to this introductive chapter. Chapters 2, 3 and 4 consist of the bibliographic part of the work while chapters 5, 6 and 7 deal with the actual purpose of the thesis, namely the application of the GALDIT-Index to the Emilia-Romagna coastline.

In particular, Chapter 2 consists of a general introduction of the problematic of SWI. It firstly provides a physical description of a coastal aquifer as well as of the main saltwater-freshwater dynamics characterizing this latter in unperturbed conditions. The main anthropic pressures are secondly introduced to eventually lead to the definition of the concept of SWI.

Chapter 3 proposes a (non-exhaustive) review of the classical approach that is usually used to deal with SWI at local scale. The three tiers of this approach are considered separately, namely the monitoring phase, the modelling of the aquifer and the numeric (or analytic) simulations.

Chapter 4 gives a general (non-exhaustive) overview of the methods that allow for a rapid and cost-effective assessment of the risk or vulnerability of a region to SWI. Those two categories, risk/vulnerability assessment methods, are introduced separately in this chapter through the review of real case studies.

Chapter 5 presents the study area, namely the coastline of the Emilia-Romagna Region (Italy). It includes the description of the main features of this region in terms of topography, climate, land use and hydrology. The various issues affecting this area are also discussed (subsidence, water scarcity, salinization). Finally the study of the geological evolution of the Po River coastal plain is reviewed in order to fix the final scope of this work relating to the depth of the aquifer that has to be considered.

The first part of Chapter 6 consists of the description of the general approach that has been adopted in this work to derive the results. The second part is dedicated to the presentation and to discussion of the results for both the phreatic and the confined aquifer.

Chapter 7 finally presents the conclusions of the thesis and some possible perspectives.

Chapter 2
Coastal aquifers

2.1 Physical description

Coastal aquifers are made of three different features, as shown in Figure 2-1:

- The freshwater zone;
- The saltwater zone;
- The transition zone;

Due to their density contrast, a relative motion occurs between saltwater and freshwater within a coastal aquifer, leading to the natural density-driven intrusion of seawater. Saltwater is generally assumed to be 1.025 times denser than freshwater and therefore tends to move beneath the freshwater in the form of a saltwater wedge. On the other hand, the less-dense freshwater sits above the saltwater wedge taking the shape of a lens. [1]

The transition zone is characterized by a mixing between freshwater and saltwater due to dispersion and molecular diffusion [2]. Density varies across this zone between the highest values of seawater to lower values of freshwater [3]. The width of the transition zone can range from some hundred meters up to several kilometres [2].

For simplification purposes, the freshwater-saltwater transition zone can be assumed as a sharp boundary (i.e. the freshwater-saltwater interface). The depth of this interface may be approximated by the so-called Ghyben-Herzberg model, which results from the work conducted independently by Ghyben (1888) and Herzberg (1901) [2].

This relation is a direct application to coastal groundwater systems of the famous Archimede's Principle which states that the buoyant or lifting force on an object is equal to the weight of the fluid displaced by that object. Freshwater is less dense than saltwater. So if a static lens of fresh groundwater was floating on saltwater in porous material beneath the surface of a coastal area, the weight of the freshwater lens would equal the weight of the saltwater it displaces. This concept is applied below to derive the Ghyben-Herzberg relation. [4]

$$\begin{aligned} &\rho_f(z+h)=\rho_s z \\ \leftrightarrow\ &z(\rho_s-\rho_f)=\rho_s h \\ \leftrightarrow\ &z=\underbrace{\boxed{\frac{\rho_f}{\rho_s-\rho_f}}}_{=\alpha} h \\ \leftrightarrow\ &z=\alpha h \approx 40h \end{aligned} \tag{1}$$

Where:

- z = thickness of the freshwater zone below mean sea − level (b. m. s. l.)[L];
- h = thickness of the freshwater zone above mean sea − level (a. m. s. l.) [L];
- ρ_s = density of saltwater [M/L^3];
- ρ_f = density of freshwater [M/L^3];

This equation (1) relates the elevation of a water table to the depth of the interface between the freshwater and saltwater zones of the aquifer. Roughly speaking, each meter of fresh groundwater elevation a.m.s.l. would correspond to a freshwater column of 40m b.m.s.l. [2], as shown in the Figure 2-1. In other words, if the water table in an unconfined coastal aquifer is lowered by 1 meter, the interface will potentially rise by 40 meters [3].

However, it is important to keep in mind that the Ghyben-Herzberg relation remains a very approximate model and has been derived assuming simple hydrostatic conditions in a homogeneous, unconfined aquifer and considering that the flow in the aquifer is essentially horizontal (a statement that is equivalent to the Dupuit assumption) and perpendicular to the coast [3].

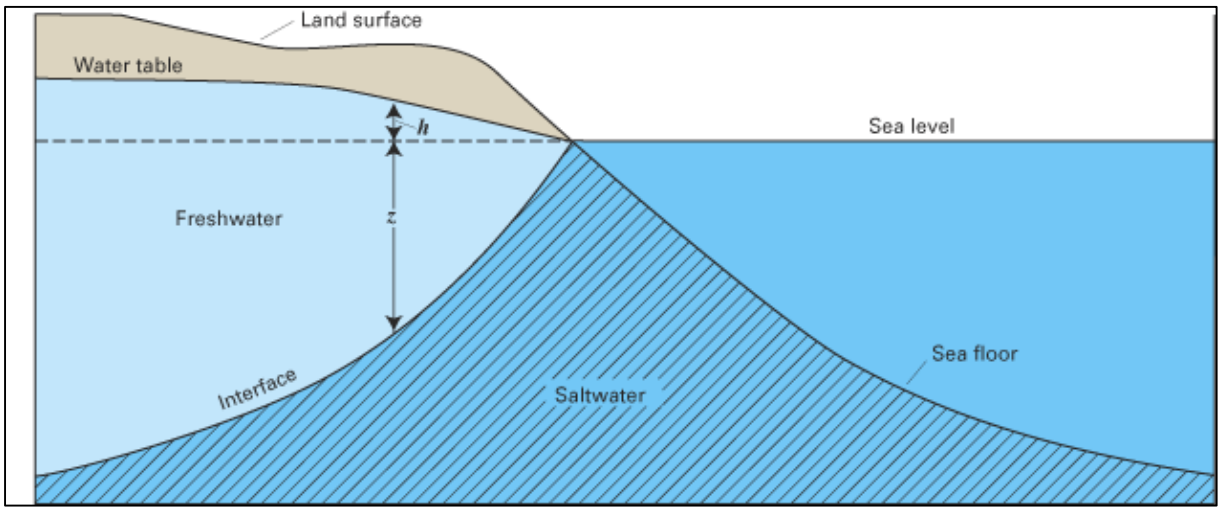

Figure 2-1: Simplified freshwater-saltwater interface in a coastal water-table aquifer [5]

Based on the assumption of sharp interface, another rough formula was developed by Custodio and Bruggeman (1987) to predict the inland penetration distance of the saltwater wedge (i.e. the toe location) under equilibrium conditions [1], [6]:

For confined aquifer:

$$L = \frac{KB^2}{2q_0\alpha} \approx 0.025\frac{KB^2}{2q_0} \tag{2}$$

For unconfined aquifer:

$$q_0 = \frac{KB^2}{2L}\frac{1+\alpha}{\alpha^2} - \frac{WL}{2} \tag{3}$$

Where:

- L = the distance of inland penetration of the saltwater wedge toe for a sharp − interface for a homogeneous and isotropic aquifer [L];
- $\alpha = \frac{\rho_f}{\rho_s - \rho_f} \approx 40$: density ratio based on Ghyben − Herzberg relation [−];

- K = aquifer hydraulic conductivity[1] [LT^{-1}];
- B = aquifer thickness [L];
- q_0 = freshwater discharge per unit of coastal length [L^2T^{-1}];
- W = natural recharge [LT^{-1}];

However, SWI is predominant during the non-rainy season when the rainfall recharge is almost zero $W \approx 0$. Therefore, equation (3) can be rewritten as follows and gives almost the same approximation for the toe location as equation (2):

$$q_0 = \frac{KB^2}{2L}\frac{1+\alpha}{\alpha^2}$$

$$L = \frac{KB^2}{2q_0}\frac{1+\alpha}{\alpha^2} \approx 0{,}0257\frac{KB^2}{2q_0} \tag{4}$$

The seawater wedge toe may be rigorously defined as the intersection of the freshwater-saltwater interface with the bottom of the aquifer [7]. From equations (2) and (4), it is evident that the extent of seawater penetration into the aquifer is highly dependent on the aquifer's hydraulic properties: it is proportional to aquifer conductivity and the square of aquifer thickness, but inversely proportional to freshwater discharge [1].

2.2 Dynamics of coastal aquifers

Under normal conditions, after infiltration, water slowly flows in the ground from locations of higher head (that is, higher potential energy) to locations of lower head (that is, lower potential energy) [5]. The well-known Darcy's law is usually applied to describe the fluid flow in a porous medium and is stated as follows, according to the level of idealisation of the medium [8]:

- 1D-flow in a homogeneous[2], isotropic[3] medium:

$$q = -K\nabla h \tag{5}$$

- 3D-flow in a homogeneous, isotropic medium:

$$\underline{q} = \begin{bmatrix} q_x \\ q_y \\ q_z \end{bmatrix} = -K\nabla h = -K \begin{bmatrix} \partial h/\partial x \\ \partial h/\partial y \\ \partial h/\partial z \end{bmatrix} \tag{6}$$

- 3D-flow in a heterogeneous, isotropic medium:

$$\underline{q} = \begin{bmatrix} q_x \\ q_y \\ q_z \end{bmatrix} = -K(x,y,z)\nabla h = -K\ x,y,z \begin{bmatrix} \partial h/\partial x \\ \partial h/\partial y \\ \partial h/\partial z \end{bmatrix} \tag{7}$$

- 3D-flow in a heterogeneous, anisotropic medium:

$$\underline{q} = \begin{bmatrix} q_x \\ q_y \\ q_z \end{bmatrix} = -\underline{\underline{K}}(x,y,z)\nabla h = - \begin{bmatrix} K_{xx} & K_{xy} & K_{xz} \\ K_{yx} & K_{yy} & K_{yz} \\ K_{zx} & K_{zy} & K_{zz} \end{bmatrix} \begin{bmatrix} \partial h/\partial x \\ \partial h/\partial y \\ \partial h/\partial z \end{bmatrix} \tag{8}$$

---

[1] By definition, the aquifer hydraulic conductivity K is the ability of the aquifer to transmit water. This propriety of the medium is the result of the interconnected pores (primary porosity) in the sediments and fractures in the consolidated rocks (secondary porosity) [6].

[2] Homogeneous/Heterogeneous medium: the physical properties are the same at all points/vary from point to point.

[3] Isotropic/Anisotropic medium: the physical properties at a point are independent/dependent on the direction.

Where:

- q=specific discharge (Darcy velocity) [LT^{-1}];
- K = aquifer hydraulic conductivity [LT^{-1}];
- ∇h=driving force of groundwater flow per unit weight of groundwater [–];

Therefore, in coastal discharge areas, it exists a natural hydraulic gradient towards the sea [3], as depicted by the arrows on the left in Figure 2-2. This natural movement of freshwater towards the sea prevents saltwater from entering freshwater coastal aquifers [9].

On the other hand, because of the mixing of freshwater and saltwater within the transition zone, a local circulation of saltwater is established in which some of the saltwater is entrained within the overlaying freshwater and return to the sea, which in turns causes additional saltwater to move landwards towards the transition zone, as depicted by the dashed arrows in Figure 2-2 [5].

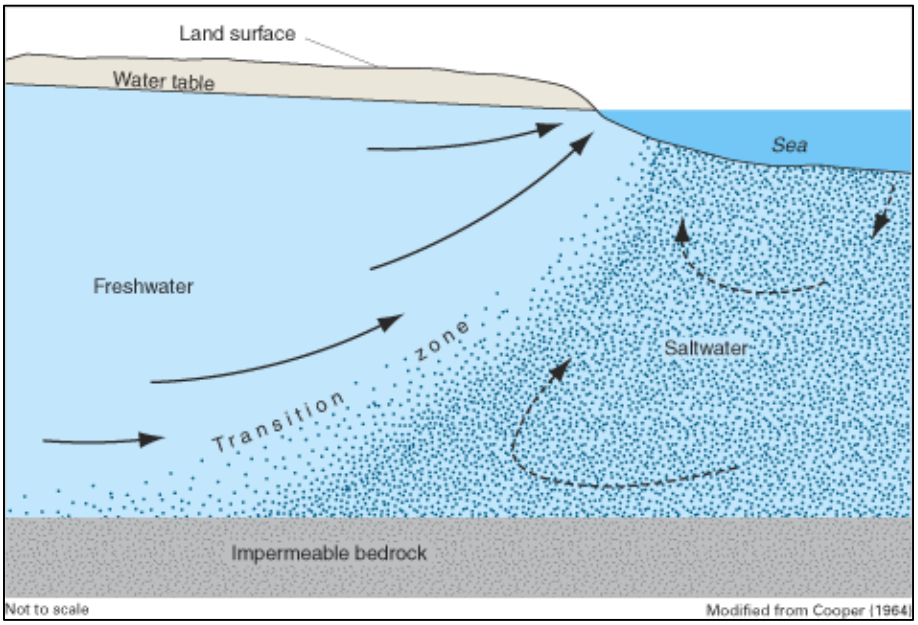

Figure 2-2: Groundwater flow patterns and the freshwater-saltwater transition zone in an idealized coastal aquifer [5]

Furthermore, this global system is not stationary but rather turns out to be in a state of dynamic equilibrium [2]: the transition zone fluctuates landwards ("natural" seawater intrusion) and seawards over time towards new dynamic equilibrium positions [1]. This is due to the fact that the boundary conditions are influenced by external natural forces and therefore they continuously change over time [7].

The main natural factors influencing the balance of the system are listed below:

- Climate variability: seasonal and annual variations in groundwater recharge;
- Long-term historic changes in SL due to eustatic and tectonic movements (transgression & regression);
- Climate hazards: flooding or tsunamis (saltwater intrusion);
- Tidal oscillations;
- Aquifer hydraulic properties;
- Land subsidence due to compaction processes or anthropogenic activities;

Some of these observed changes are taking place very slowly (long-term processes) and are only significant at a geological time scale. Others may proceed more quickly (episodic processes) [10]. In any cases, the time needed for the transition from one dynamic equilibrium stage to another is considerable, in the order of tens of years at least or even centuries [7]. Therefore, the saltwater intrusion process is most frequently in a transient state [2].

2.3 Problematic: human pressure

Table 2-1 gives a global overview of the distribution of water involved in the hydrological cycle around the globe. With $\pm$ 1.4 billion of cubic meters, water may be considered as the most widespread substance to be found in the natural environment [11]. However, the vast majority of water (97.5%) is in the form of saltwater in oceans, seas, bays and saline lakes and groundwater. Freshwater accounts for only 2.5% of the total volume of water. Among these 2.5%, a further breakdown shows that 70% is not accessible for human consumption because it is in the form of ice (ice caps, glaciers, permanent snow, ground ice, permafrost), in the form of vapour in the atmosphere or is part of the biosphere (biological water, soil moisture, swamp water) [7]. At the end, only the remaining 30%, representing 0.75% of the total water resource, can directly satisfy human needs. The vast majority of this accessible freshwater (99%) is stored in the ground in comparison to the freshwater stored in lakes and rivers (1%). All these results are summarized in Figure 2-3 and emphasize the importance of groundwater as a priceless resource for mankind.

Table 2-1: One estimate of global water distribution (percents are rounded, so will not add to 100) [12]

Water source	Water volume [km^3]	Fraction of freshwater [%]	Fraction of total water [%]
Oceans – Seas – Bays	1,338,000,000	-	96.5
Ice Caps – Glaciers – Permanent Snow	24,064,000	68.7	1.74
Groundwater	23,400,000	-	1.69
Fresh groundwater	10,530,000	30.1	0.76
Saline groundwater	12,870,000	-	0.93
Soil moisture	16,500	0.05	0.001
Ground Ice – Permafrost	300,000	0.86	0.022
Lakes	176,400	-	0.013
Fresh lakes	91,000	0.26	0.007
Saline lakes	85,400	-	0.006
Atmosphere	12,900	0.04	0.001
Swamp Water	11,470	0.03	0.0008
Rivers	2,120	0.006	0.0002
Biological Water	1,120	0.003	0.0001
Total	1,385,984,510	100.049	99.9681

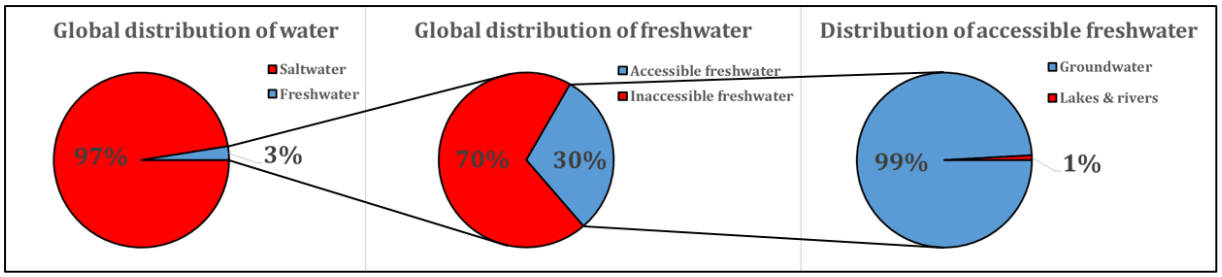

Figure 2-3: Distribution of Earth's freshwater

Historically, surface water has accounted for most of the human consumption, because it is easily accessible (with the exception of arid regions, where groundwater may be the only reliable source of water). However, modern development and population growth have greatly increased water demands in the last half century, leading to the depletion and to the contamination of surface water resources [7]. In this context, freshwater has become an alternative to surface water. As a source of water supply, groundwater has a number of essential advantages when compared to surface water: it is of higher quality, better protected from possible contamination, less subject to seasonal fluctuations and much more uniformly spread over large regions than surface water. These advantages have firstly resulted in a wide use of groundwater for public and domestic water supply (drinking water and sanitation). The use of groundwater has later been extended to other purposes (irrigation purposes, industrial supply, energy cooling and additional demands for tourism water consumption) [13], [2]. Nowadays, groundwater is the world's most extracted raw material with withdrawal rates currently in the estimated range of 982 km^3/year [14]. It is estimated (2010) to provide drinking water to at least 50% of the global population, to account for 43% of all the water used for irrigation and to ensure 20% to 40% of the industrial water needs [11], [15].

In particular, utilization of groundwater in the coastal zones is of even greater significance since coastal belts are among the most densely populated human settlements [11]. Indeed, almost two thirds of the world's population live within 400km of the ocean shoreline; just over half live within 200km, an area only taking up 10% of the earth's surface [16]. This concentration of the world's population in coastal areas have put the coastal aquifers under pressure [2], due to the subsequent economic growth, intensified agricultural/industrial development and loss of surface freshwater resources due to contamination [3]. As a consequence, the coastal aquifers are being overexploited, leading to the seawater intrusion in the aquifer [11].

Apart from groundwater over-abstractions[4], other anthropogenic stresses may affect the seawater-freshwater balance in coastal aquifers, such as the construction of drainage canals, the lower rates of recharge in urbanized areas or the climate change (i.e. induced by human activities) [5]. Among these, the climate change is expected to play a major role on seawater intrusion in the coming years, through two different mechanisms [3], [10]:

[4] Overconsumption of the fresh groundwater such that the rate of pumping exceeds the natural freshwater recharge, leading to the reversal of the natural seaward hydraulic gradient.

- the progressive reduction of the natural groundwater recharge: changes in climatic characteristics (i.e. increasing/decreasing of precipitations, temperatures and evapotranspiration patterns) will primarily affect the hydrological cycle and secondly groundwater by modifying recharge patterns, contributing to seawater intrusion in coastal groundwater;
- the sea-level rise (SLR): this expected effect of the global warming process, due to changes in atmospheric pressure, expansion of oceans and seas as they warm, and melting of ice and glaciers, could affect seawater intrusion in coastal areas by altering the position and morphology of the coastline;

However, the impact of assumed future climate conditions on groundwater is still a challenging study field today. Although these problems could affect a great number of coastal areas, the Fourth Report of the Intergovernmental Panel on Climate Change (IPCC) has reported that there "has been very little research on the impact of climate change on groundwater" and that "the few studies of climate impacts on groundwater for various aquifers show very site-specific results" [3].

2.4 Seawater intrusion description

With all these background information, one can now define more precisely the concept of seawater intrusion. Seawater intrusion (or saltwater intrusion, SWI) may be defined as the encroachment of saltwater into freshwater coastal aquifers due to the landward migration of the freshwater-saltwater interface [1]. Generally speaking, this process is in a state of dynamic equilibrium with the opposite seaward migration of the interface under the natural factors listed in the section 2.2. However, due to the anthropogenic externalities described in the section 2.3, this natural balance between freshwater and saltwater in coastal aquifers has been disturbed, exacerbating the SWI process. In this context, two situations must be distinguished: (1) as long as there is a net flow towards the sea, a reduction in flow due to water abstractions will result in an inland relocation of the seawater-freshwater interface towards a new dynamic equilibrium position; (2) in case of abstractions exceeding freshwater recharge (over-abstractions), the natural seaward hydraulic gradient is reversed and seawater is drawn actively into the aquifer replacing abstracted freshwater. This process will continue until either all freshwater is lost or a net seaward flow is restored [2]. Saltwater can contaminate a freshwater aquifer through two major pathways: (1) by lateral intrusion from the ocean due to SLR (see Figure 2-4 (b)) or due to freshwater abstractions (also known as saltwater up-coning, see Figure 2-4 (a)); (2) by upward intrusion from deeper, more saline zones of a groundwater system (i.e. relic saline and hypersaline groundwater) due to upwards hydraulic gradients imposed by anthropic activities (i.e. drainage systems, pumping wells) [5].

The problem related to SWI is not new. Back in 1845, incidents of SWI were detected on Long Island, New York [9]. Today, SWI has become a growing issue and affects a large number of coastal aquifers worldwide [3]. This considerable threat of SWI to water security on the global scale is well documented (large-scale reviews of SWI are available for North America [17], South America [18], Europe [19], Africa [20] and Australia [1]) and is mainly due to the scarcity of water salinity measurements for the management of SWI [21], [22].

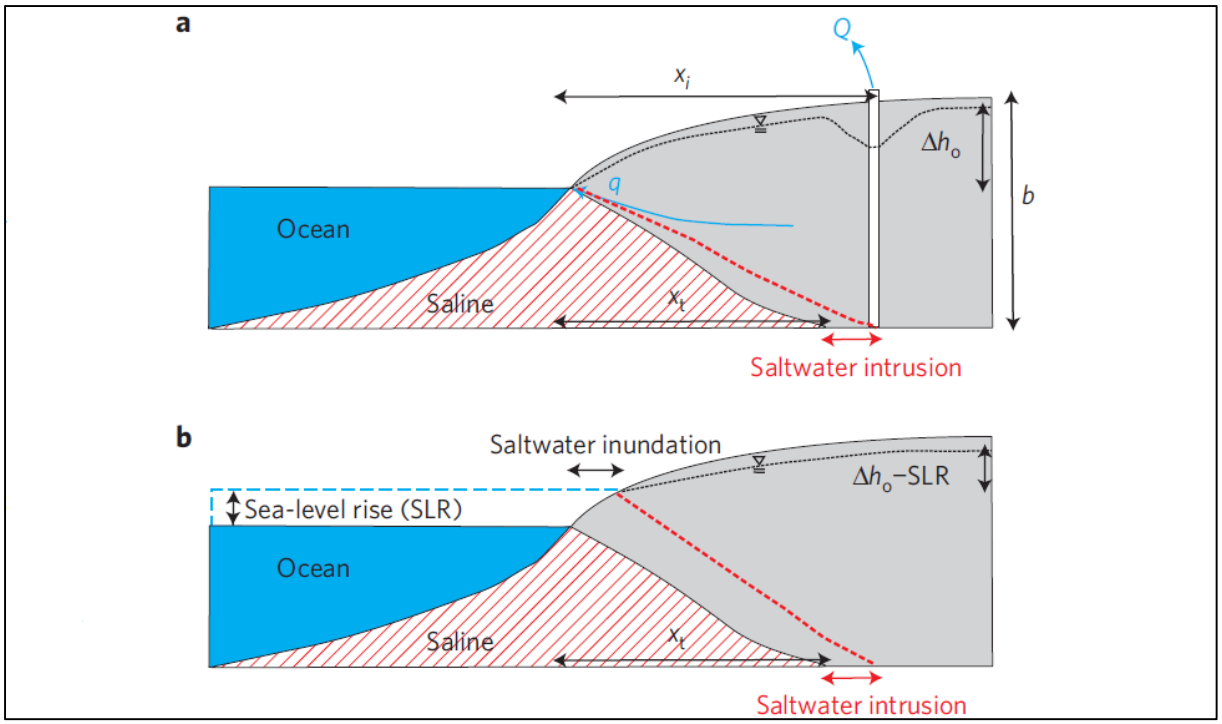

Figure 2-4: Conceptual model used for simulating the impact of groundwater extraction (**a**) and sea-level rise (**b**) [23]

The consequence of SWI and of its mixing with freshwater in coastal aquifers is the degradation of water quality [1]. Indeed saltwater is characterised by a high concentration of total dissolved solids (see section 3.2.1) and certain inorganic constituents which make it unfit for human consumption and many other anthropogenic uses [5]. In extreme cases, increase of salinity beyond a certain tolerance limit (drinking-water standards) leads to the abandonment of the bore-wells [11]. Subsequently, it has an impact on freshwater availability, population growth and all the related socio-economic activities (agriculture, industries…) [3].

For all these reasons, due to the significant cost of post-intrusion remediation and because of the priceless value of groundwater for humanity, considerable research effort spanning more than 50 years has been devoted to understand better coastal aquifer flow and transport processes and to improve the collection, storage and processing of relevant data [1], [7], [22].

This research has led to the development of a three-step approach which is commonly used nowadays to detect, manage and prevent SWI [5], [4]. This approach includes the following phases and is detailed more accurately in Chapter 3:

- Detection (monitoring phase): collection of data through the use of direct (drilling techniques, environmental tracers) and indirect (geophysical campaigns) field investigation methods in order to detect the occurrence of SWI [22];
- Modelling (conceptual description): simplification of the system based on the monitoring well data and on a series of assumptions (simplified aquifer geometry and boundary conditions…) in order to enable analytical or numerical solutions [2], [4];
- Prediction (solution phase): traditional analytical models have been slowly replaced by numerical models which enable investigations of more realistic coastal aquifer domains, taking into account the three-dimensional flow regime, heterogeneity, anisotropy… [7];

Such procedure only focuses on coastal individual aquifers at local scale because SWI remains challenging to measure and quantify at a larger scale, especially for three reasons [22]: (1) SWI is an invisible process, occurring in the subsoil and therefore difficult to delineate accurately [7]; (2) SWI is strongly dependent on local hydrogeological conditions which gives an inherent uniqueness to each real-world incidence of SWI [2], [22]; (3) SWI is a transient process which typically occurs very slowly [22]. These conditions make this approach particularly heavy and expensive (i.e. it is based on complex numerical models and requires intensive field data collection to reduce uncertainty) and therefore unlikely to be extended to large-scale problems [2].

However, management decision-making highly requires the development of qualitative and cost-effective methods for the rapid assessment of SWI over large areas. The role of these methods is (1) to detect the current and emerging risk areas, along with the key drivers of SWI in these areas [24]; (2) to prioritize areas requiring more detailed SWI investigations in the future [24]; (3) and to develop strategies ensuring a sustainable use of groundwater[5] for domestic consumption as well as industries and agricultural purposes [11]. In response to this, a number of risk and vulnerability assessment approaches have been developed during the last decade [22]. A short presentation of the most commonly used methods in proposed in Chapter 4.

[5] Maximum rate at which water can economically and legally be withdrawn from a particular source for beneficial purposes without bringing about some undesired results [5]

Chapter 3
Typical assessment method

3.1 Introduction

Actual coastal groundwater systems involving freshwater and saltwater are complex, as described in Chapter 2 [4]. Nowadays, a three-step approach is usually used to analyse such complex systems, involving: (1) the detection of SWI through a monitoring phase; (2) the conceptual description (modelling) of the study area; (3) and the analytical or numerical solution (simulation) of SWI processes. This approach to managing SWI (detection, modelling and simulation) would be beneficial anywhere to prevent further SWI and to ensure long-term sustainable rates of extraction from water resources [2], [4].

The monitoring phase includes direct and indirect methods. These methods consist of early-warning systems providing information about the location and the movement of saline water in coastal aquifers [5]. The direct methods are based on the data provided by the network of wells that are established in the study area [5]. Well monitoring in coastal aquifers started during the 50's and the 60's with the goal of providing a basis for understanding the complicated mechanisms behind SWI and that affect the shape of the saltwater-freshwater interface [7]. Today there are numerous of so-called direct investigation methods but this review only focuses on the main ones, namely the chemical analysis of groundwater samples (chloride, major-ions and environmental tracers) and head measurements. Those methods are introduced in the section 3.2.1. The indirect methods which consist of geophysical prospection techniques were developed later, and were found to provide more information faster than the drilling techniques [9]. Subsequently, they became more important for SWI monitoring [9]. Some of the major indirect methods are introduced in the section 3.2.2, namely the resistivity, electromagnetic and seismic methods.

Modelling approaches to calculate the position of the seawater-freshwater interface and to simulate SWI processes under various natural and man-made conditions include analytical and numerical methods [2]. Analytical methods (e.g. Glover 1964, Fetter 1972, Strack 1976) provide solutions for simplified conceptual models, based on simplified aquifer geometries and boundary conditions, and requiring only few input data [2]. They usually do not directly solve "real-world" problems but rather serve as tools for first-cut engineering analysis [2]. The section 3.4.2 provides a more detailed description of one of the most commonly used analytical models, namely the Strack method. On the other hand, numerical models enable investigations of more realistic coastal aquifer domains, taking into account one-to three dimensional, density dependent and transient flow regimes as well as heterogeneity or anisotropy [7]. They have the potential to simulate intrusion processes and are therefore especially suited to isolate the effects of the various factors influencing SWI, such as water well pumpage, rainfall or SLR [2], [4]. A non-exhaustive list of the main numerical models is proposed in the section 3.4.3.

3.2 Monitoring

3.2.1. Direct methods

Direct methods aim at measuring the location and movement of saltwater into freshwater aquifers [5]. They are based on the data provided by the network of wells that are established in the study area [5]. The most commonly used approach consists in collecting water samples from the wells to analyse their chloride content or in some cases, their total dissolved content or their specific electrical conductivity as proxies for salinity [5], [7]. It should be emphasized that the presence of elevated concentrations of chloride alone is not definitive proof of active SWI, because chloride concentrations are naturally elevated near the boundary between freshwater and saltwater [5]. SWI is indicated by an increase in the chloride concentration of water samples collected periodically over time, rather than by a single concentration measured at one point in time [5]. Another commonly-used approach consists of the analysis of the major-ion chemistry of water samples and of the comparison with the typical saltwater chemical composition through the use of diagrams. These two first methods consider seawater as the most obvious candidate to explain observed increases in groundwater salinity [22]. However, other sources and processes can contribute as well [22]. Therefore, techniques using environmental tracers and isotope geochemistry have been developed as diagnostic tools to establish the origin of saline water [5], [22]. Finally, water levels are also frequently measured at the monitoring wells to give information about the most likely direction of the seaward flow [5]. These four direct approaches, namely (1) chloride analysis, (2) major-ion analysis, (3) geochemical analysis and (4) head measurement are described below in more details.

Salinity analysis

The chemical composition of seawater (main cations and anions) is given in Table 3-1. In practice, water is often classified into a number of discrete classes according to its salinity level. This convenient macro-parameter gives a first characterization of water quality and is usually expressed through the use of proxies such as Total Dissolved Solids (TDS, in milligrams dissolved solids per litre of water), Chloride Content (in mg/L) or the Electrical Conductivity (EC, in μS/cm) [10]. Those three classifications are proposed below. Number and names of classes as well as numerical values of class limits may vary among the literature [10].

Table 3-1: Typical chemical composition of seawater [25]

Components		Concentration (mg/L)
Cations	Sodium (Na^+)	10,500
	Magnesium (Mg^{2+})	1,350
	Calcium (Ca^{2+})	410
	Potassium (K^+)	390
Anions	Chloride (Cl^-)	19,000
	Sulphate ($SO_4{}^{2-}$)	2,700
	Bicarbonate ($HCO_3{}^-$)	142
	Bromide (Br^-)	67
Total Dissolved Solids (TDS)		35,900

- Chloride concentration

Because of the very high concentration of chloride in seawater (typically 19,000 mg/L), the chloride concentration of groundwater samples is commonly used as an indicator of seawater occurrence and intrusion in coastal aquifers [5]. The classification of saltwater proposed by P.J. Stuyfzand (see [26]) is given in Table 3-2.

Table 3-2: Division in main types on the basis of chloride concentration (adapted from [26] & [27])

Main type of water	$[Cl^-]$ [mg/L]	$[Cl^-]$ [meq/L]
Very oligohaline	<5	<0.141
Oligohaline	5-30	0.141-0.846
Fresh	30-150	0.846-4.231
Fresh-brackish	150-300	4.231-8.462
Brackish	300-1,000	8.462-28.206
Brackish-salt	1,000-10,000	28.206-282.064
Salt	10,000-20,000	282.064-564.127
Hyper saline	>20,000	>564.127

- Total Dissolved Solids (TDS)

Total Dissolved Solids (TDS) is a measure of all constituents dissolved in water. The inorganic anions dissolved in water include carbonates, chlorides and sulphates while the inorganic cations include sodium, potassium, calcium and magnesium, as described in Table 3-1. The following classification, given in Table 3-3, is adopted by the USGS [25], [5]:

Table 3-3: Water salinity classification

Class name	TDS $[mg/L]$
Fresh water	0-1,000
Brackish water	1,000-20,000
Saline water	20,000-35,000
Brine	>35,000

- Electrical Conductivity (EC)

Electrical conductivity σ in $\mu S/cm$ is an intrinsic property of a material which characterizes its ability to conduct an electric current. It is the reciprocal of the electric resistivity ρ in $\Omega.m$ which quantifies how strongly a material opposes the flow of electric current [28]. Mathematically, the Pouillet's law is used to define those quantities:

$$R = \rho \times \frac{L}{S} = \frac{1}{\sigma} \times \frac{L}{S} \tag{9}$$

Where:

- R = the electrical resistance of a uniform specimen of the material $[L^2MT^{-3}I^{-2}]$;
- L = the length of the piece of material $[L]$;
- S = cross − sectional area of the specimen $[L^2]$;

The electric conductivity of water (and thus electrical resistivity) is function of its chemical composition (TDS content) and of its temperature [25]. Table 3-4 gives an overview of the electrical conductivity of water according to its quality (that is, its TDS content) for a temperature of 25°C.

Table 3-4: Electrical conductivity for diverse types of water at 25°C [25]

Type of water	Electrical conductivity σ [µS/cm]
Pure water	0,055
Distilled water	0,5
Mountain water	1
Running water	500-800
Maximum for drinking water	1,055
Seawater	56,000
Brine	100,000

Water salinity may be derived from its temperature and its electrical conductivity, using the empirical formula herebelow [25]. This formula is linear in terms of both the temperature and the electrical resistivity and this linear trend is presented graphically in Figure 3-1.

$$S = \ 0{,}72\sigma - 3{,}06 \ \times \left(1 + 0{,}02 \ T - 25 \ \right) \tag{10}$$

Where:

- S = salinity [ppm];
- σ = electrical conductivity [mS/cm];
- T = temperature [°C];

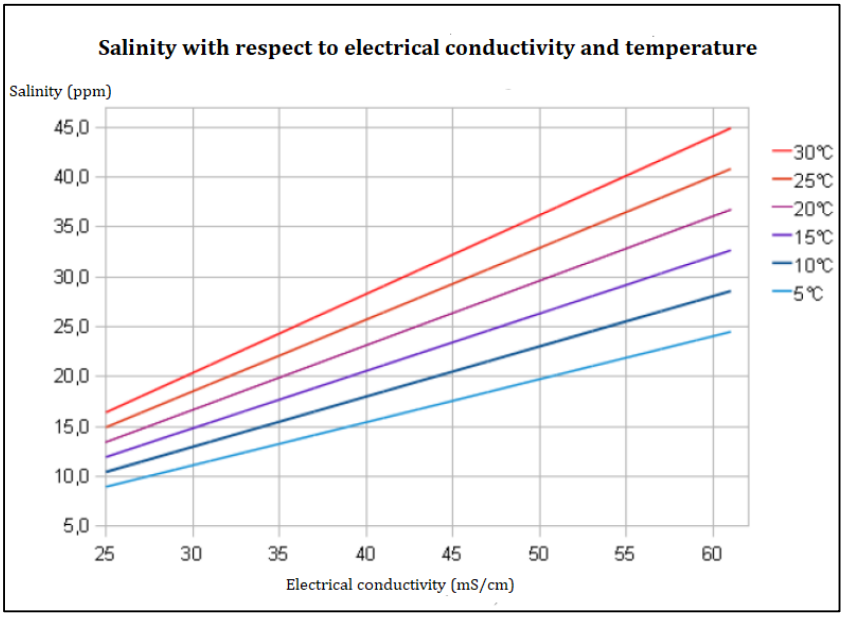

Figure 3-1: Evolution of the salinity as a function of the temperature and the electrical conductivity [25]

Major-ion analysis

Different visual approaches based on diagrams may be used to analyse the major-ion chemistry of water samples and to compare this content with the typical chemical composition of seawater, which was introduced in Table 3-1. Four different types of diagrams are introduced below:

- Piper diagram

The Piper diagram is a graphical representation of the chemistry of a water sample or samples [29]. It is composed of three parts, as shown in Figure 3-2: a ternary diagram in the lower left representing the relative abundance of cations ($Ca^{2+}, Mg^{2+}, Na^{+}, K^{+}$), a ternary diagram in the lower right representing the anions (SO_4^{2-},Cl^{-},HCO_3^{-}), and a diamond plot in the middle representing a projection of the two [30].

In the example given in Figure 3-2, the black dots indicate the chemical composition of the different water samples, the red curved arrow represents the typical path of SWI and the red dot indicates the chemical composition of seawater [25]. Therefore, this diagram provides a useful tool to analyse the phenomenon of SWI from a chemical point of view.

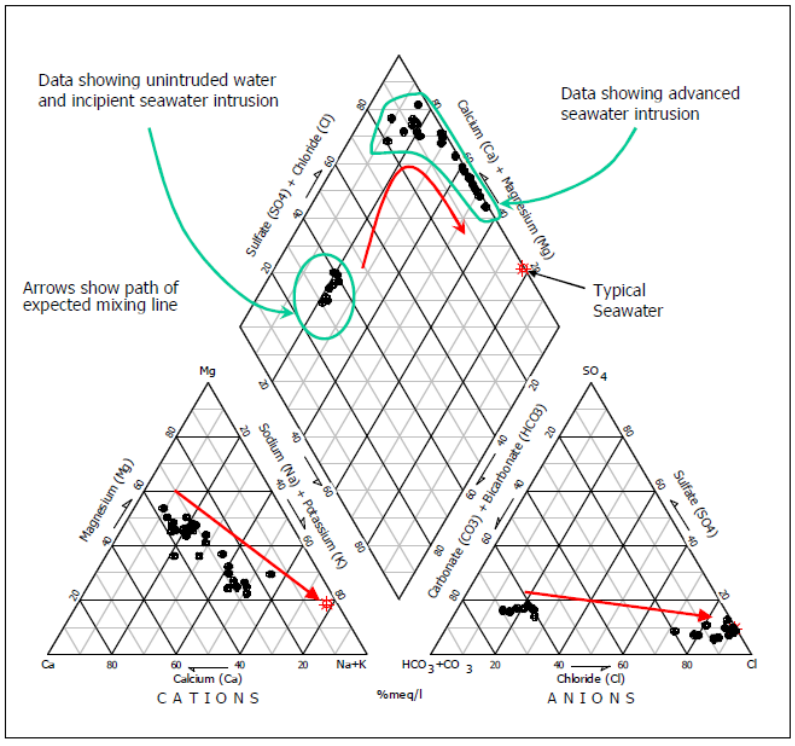

Figure 3-2: Example of a Piper diagram for a case study in La Pajaro Valley [25]

- Stiff diagram

A Stiff diagram is a graphical representation of chemical analyses, used to display the major ion composition of a water sample [31]. A polygonal shape is created from four parallel horizontal axes extending on either side of a vertical zero axis, as depicted in Figure 3-3 [31]. Cations

(Ca^{2+}, Mg^{2+}, Na^{+}) are plotted in milliequivalents[6] per litre (mEq/L) on the left side of the zero axis, one to each horizontal axis, and anions (SO_4^{2-}, Cl^{-}, HCO_3^{-}) are plotted on the right side [31]. Seawater intrusion is detected in this kind of diagram by an increasing chloride concentration coupled with a decreasing sodium concentration [25].

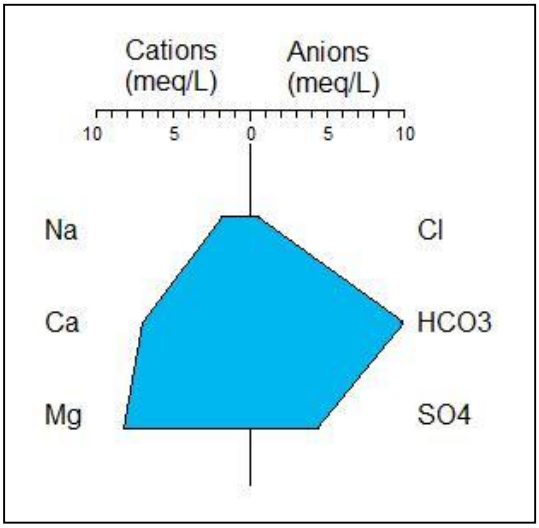

Figure 3-3: Example of a Stiff diagram [31]

- Durov diagram

The traditional Durov diagram is a composite plot similar to the Piper diagram [32]. It consists of 2 ternary diagrams where the cations of interest are plotted against the anions of interest [32]. Sides form a binary plot of total cation vs. total anion concentrations [32]. The expanded version includes TDS (mg/L) and pH data added to the sides of the binary plot to allow further comparisons [32]. Figure 3-4 shows an example of a Durov diagram.

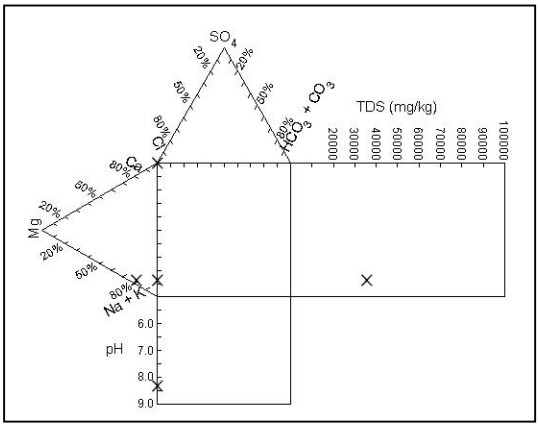

Figure 3-4: Example of a traditional Durov diagram [32]

[6] An equivalent (symbol: Eq) is a unit of equivalent weight representing the amount of anion or cation species needed to add or remove one mole of electrons from a system [32]. In practice, the amount of a substance in equivalents often has a very small magnitude, so it is frequently described in terms of milliequivalents (mEq), the prefix milli denoting that the measure has been divided by 0,001 [77]. Very often, the measure is used in terms of milliequivalents of solute per litre of solvent [77]. The following formula may be used to transform mg/L into mEq/L [32]:

$$\text{Concentration in mEq/L} = \frac{\text{Concentration in mg/L} \times \text{valence}}{\text{molar mass M of the ion in g/mol}}$$

➢ Schoeller diagram

A Schoeller diagram is a semi-logarithmic diagram of the concentration of the main ionic constituents in water $SO_4^{2-}, Cl^-, HCO_3^-, Ca^{2+}, Mg^{2+}, Na^+/K^+$ in milliequivalents per kg of solution mEq/kg [32]. Concentrations of each ion in each sample are represented by points on six equally spaced vertical lines and points are connected together by a line [32]. The diagram gives absolute concentration, but the line also gives the ratio between two ions in the same sample [32]. This technique also provides a visual comparison between different water samples, as shown in Figure 3-5 [25].

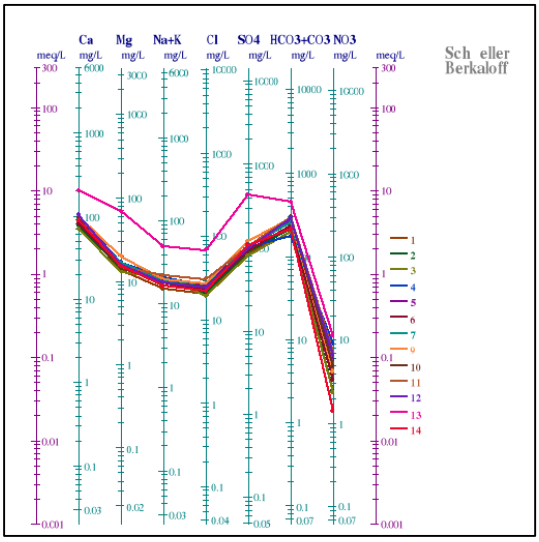

Figure 3-5: Example of a Schoeller diagram [25]

Environmental tracers

In addition to chloride analysis and major-ion chemistry, environmental tracers can be applied to identify the origin of salinity, especially detection of SWI as opposed to other salinity sources in coastal aquifers [7]. Generally speaking, environmental tracers may be defined as "natural or anthropogenic compounds or isotopes that are widely distributed in the near-surface environment of the Earth, such that variations in their abundances provide qualitative or quantitative information about the hydrological system, such as the source, the pathway or the timescale of environmental processes (Cook & Böhlke, 2000)" [33]. A non-exhaustive list of environmental tracers based on geochemical data (isotopes[7], trace elements[8], major ions[9]) is proposed here below.

➢ Cl/Br ratios

The Cl/Br ratio can be used as a reliable tracer to distinguish seawater (Cl/Br weight ratio=297) from relics of evaporated seawater ($Cl/Br < 297$ for hypersaline brines), from anthropogenic sources such as sewage effluents (Cl/Br ratios up to 800) and from agricultural-return flow (low Cl/Br ratios) [7].

[7] Isotopes are atoms of the same element that have different masses because of a difference in the number of neutrons in the atoms'nuclei [5]

[8] Chemical components which are present in very low quantities in seawater and are used to trace the origin or the pathway of the water [82]

[9] In geochemistry, major ions include the following anions (SO_4^{2-},Cl^-,HCO_3^-) and cations ($Ca^{2+}, Mg^{2+}, Na^+, K^+$) [83]

- Na/Cl ratios

Na/Cl ratios of SWI are usually lower than the marine values (i.e., <0.86, molar ratio) because Na often replaces Ca in the aquifer matrix during the early stages of salinization [7], [25]. Thus low Na/Cl ratios can be an indicator of the arrival of SWI, and are also distinguishable from the high (>1) Na/Cl ratios typical of anthropogenic sources like domestic waste waters [7].

- Ca/Mg, $Ca/(HCO_3 + SO_4)$ ratios

One of the most conspicuous features of SWI is commonly the enrichment of Ca over its concentration in seawater. High Ca/Mg and $Ca/(HCO_3 + SO_4)$ ratios (>1) are further indicators of the arrival of SWI. [7]

- O and H isotopes

The stable isotopes of O and H can also be used to describe mixing process between saline and freshwater. Fresh groundwater is generally depleted in both $\delta^{18}O$ and $\delta^{2}H$ (deuterium) relative to seawater. Linear correlations are expected from mixing of fresh and seawater while other water sources with high salinity (e.g. agriculture return-flows, sewage effluents) would result in different slopes due to variations in the isotopic composition. [7]

- Boron isotopes

The boron isotopic composition of groundwater can be a powerful tool to trace the origin of the salinity, in particular distinguishing seawater ($\delta^{11}B > 30‰$) from anthropogenic fluid such as domestic waste water $\delta^{11}B > 30‰$ [7].

Head measurements

In coastal aquifers, hydraulic head observations may be used to roughly approximate the depth of the freshwater-saltwater interface, based on the Ghyben-Herzberg relationship which was introduced in the first chapter (see equation (1)).

More generally, hydraulic observations may be used in any geographical context to infer groundwater flow directions and groundwater flow rates [8]. The main flow direction is obtained from the contour plot of the hydraulic heads in a map because it is normal to these contour lines [22], [9]. On the other hand, the flow rate is an application of Darcy's law (see equation (5)) which only requires estimates of hydraulic conductivity K and of the hydraulic gradient ∇h [8].

These approaches are rather straightforward but rely on strong assumptions, namely isotropy and homogeneity. Therefore the level of uncertainty, which arises from insufficient knowledge of hydraulic conductivity and heterogeneity and from complications due to anisotropy or large well spacing, is relatively high [8].

3.2.2. Indirect methods

Unlike direct methods, indirect methods do not directly determine characteristics such as salinity or lithology [7]. Instead, they rather measure the spatial distribution of physical properties of the earth such as bulk conductivity or seismic velocity [7]. These physical properties can then be related to hydrologic or geologic features, such as the distribution of water quality or the geometry, position and properties of geologic units [7]. The main advantages of indirect methods over the direct ones are their speed, their non-destructive nature and their cost which is usually lower [25]. On the other hand, they provide a result which is averaged over space and therefore more subjected to uncertainty and more difficult to interpret [25].

For coastal aquifers, the physical properties of principal interest are bulk conductivity and seismic velocity. Bulk conductivity is a macroscopic property of the fluid/matrix system [7]. For water-bearing geological formations, bulk conductivity, and its inverse, bulk resistivity, are solely controlled by the amount of connected pores in the aquifer (that is, the aquifer porosity) and by pore water conductivity (which was introduced in the section 3.2.1 as a function of the temperature and the TDS content) [5]. Increases in either porosity or fluid conductivity result in increases in the bulk conductivity [5].

Seismic velocity maybe defined as the rate at which a seismic wave travels through a medium, that is, distance divided by travel time [34]. Seismic velocity is dependent principally on the mechanical properties of a material, specifically the values of the elastic constants such as Poisson's ratio, Young's modulus, bulk modulus, and the shear modulus [7]. As a porous material becomes more compact, cemented, or lithified, grain-to-grain contacts increase, and mechanical strength and rigidity also increase, leading to an increase in seismic velocity [7].

The geophysical methods may be divided into three main categories, namely (1) the direct current (DC) resistivity method, (2) the electromagnetic (EM) method and (3) the seismic method. Those three methods are presented below. This chapter aims at presenting the most commonly used geophysical techniques without any ambition of writing the full inventory of all the existing techniques. A larger range of methods may be found on companies' websites, such as the following link: http://zonge.com/geophysical-methods/ [35].

Direct current (DC) resistivity method

The resistivity method is an electrical method which is usually used to locate brackish or saline waters, although it can yield some geologic information as well. This method is based on measuring the potentials between one electrode pair while transmitting DC between another electrode pair, as shown in the sketch of Figure 3-6 [36]. The most common measurement techniques are presented in Table 3-5. For all of them, the depth of penetration is proportional to the separation between the electrodes, in homogeneous ground, and therefore varying the electrode separation provides information about the stratification of the ground [36].

- 1D techniques

The work of introducing current into the ground for prospecting purposes started around a century ago in the 1920s with Conrad Schlumberger in Sweden and Wenner in the USA [36]. Data acquisition in these early studies was constrained to one dimensional (1D) surveys, either vertically with depth or laterally along a profile [22]. Profiling means moving a constant spacing electrode array along a line and plotting the variation against the profiled distance. Vertical electrical sounding (VES) involves increasing the electrode separations around a mid-point in order to find the layering of strata. Data acquisition was almost uniquely carried out manually till the 1980s, by moving two or four of the electrodes used, between each measurement, which was rather time consuming. [36]

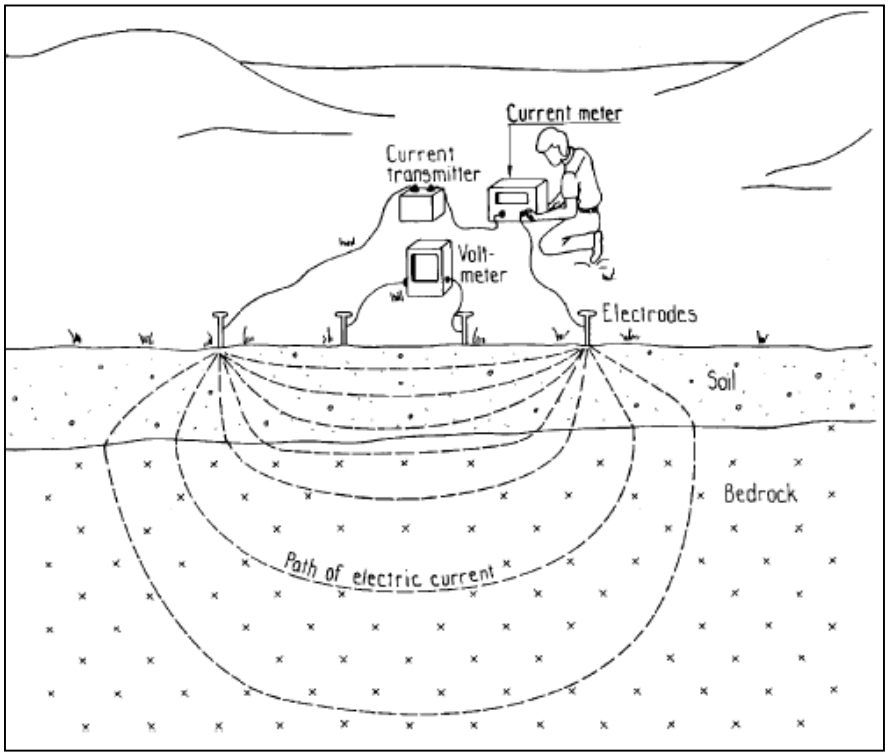

Figure 3-6: Sketch showing principle of DC resistivity measurement [36]

Table 3-5: Most common measurement techniques and expected investigation depth [adapted from [37]]

Measurement technique	L (=Span between the injecting electrodes)	Investigation depth	
		Roy and Apparao (1971) Roy (1972)	Barker (1989)
Wenner		0.11L	0.17L
Schlumberger		0.12L	0.19L
Dipole-Dipole		0.19L	0.25L
Pole-Pole	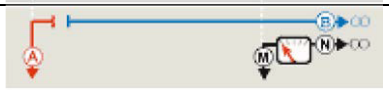	0.35L	/

- 2D techniques

Since the 1980s the use of automated multi-electrode systems for the data acquisition has allowed the development of electrical resistivity tomography[10] (ERT) which is the visualization of the subsurface resistivity distribution in 2D or 3D [22]. In 2D, 2 different acquisition methods are generally used, namely the multiple-electrode data acquisition and the towed array data acquisition. In both cases a cable with a number of electrodes is used, where one electrode pair is used for transmitting current while over several electrode pairs are used for measuring the potentials [36]. The difference is so that for the former method, sketched in Figure 3-7, the extension of the line is achieved through a roll-along technique, in which part of the layout is shifted for example, by a quarter of the total layout length before new measurements are performed [36]. By contrast the latter method, sketched in Figure 3-8, has been developed for marine as well as land-based application and provides a high speed of surveying through the use of an automated multi-electrode data acquisition system that is being towed behind a vehicle [36].

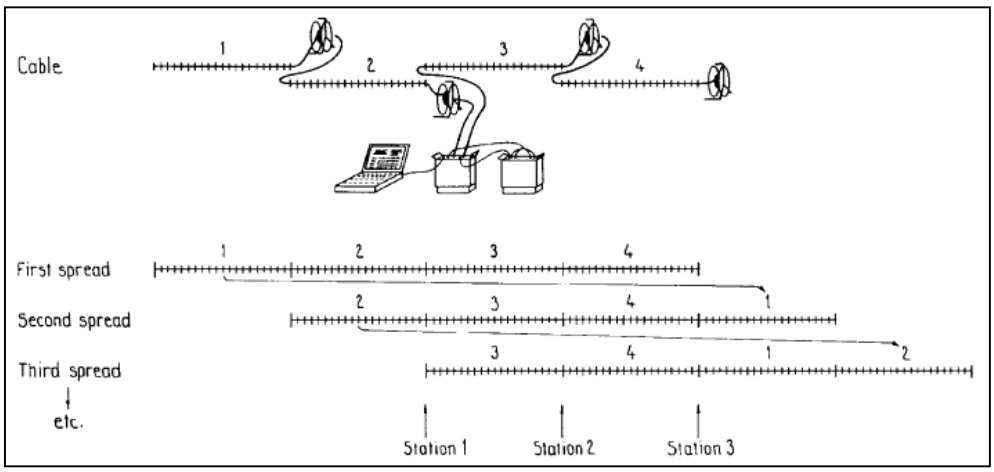

Figure 3-7: Sketch of a computer-controlled data collection system and of the principle of roll-along technique to move the cables [36]

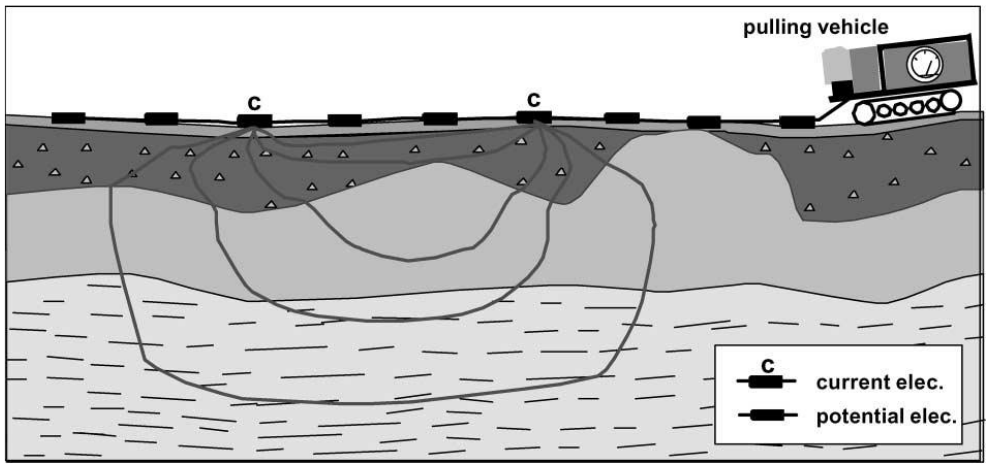

Figure 3-8: Sketch of pulled array system [36]

[10] Geophysical tomography refers to imaging by sections or sectioning. It is a technique that investigates a volume of the Earth through the use of numerous sources/receivers and any kind of penetrating wave. The three-dimensional distribution of velocity, reflectivity or resistivity is then reconstructed and displayed. There are several types of tomography in geophysics, including transmission tomography, reflection or seismic tomography, diffraction tomography or electrical resistivity tomography. [79], [80], [81]

- 3D techniques

In order to attain 3D information on the subsurface a grid of electrodes can be laid, and measurements taken with the electrodes aligned in different directions, as depicted in Figure 3-9. Thus the principles are the same as those for the 2D case, except that the demand on computational power is much higher due to the rapidly increasing number of independent electrode combinations that can be measured. [36]

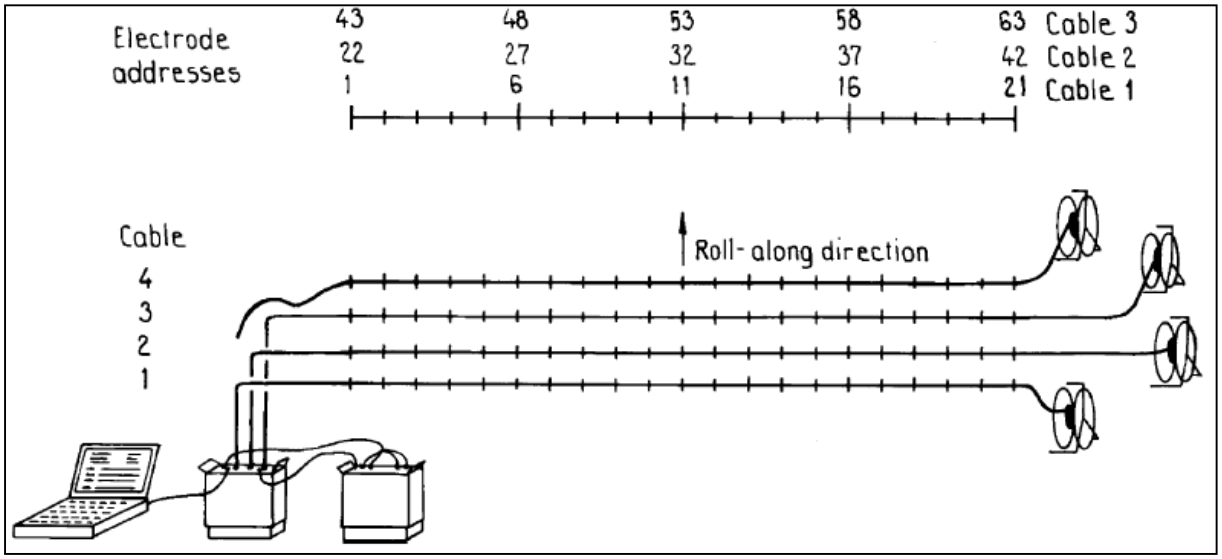

Figure 3-9: Sketch of 3D multi-electrode survey layout. By using more electrode cables than shown in figure, and connecting these sequentially to switching unit, measurements can be taken in both x and y direction for number of different electrode separations [36]

Electromagnetic (EM) methods

Like resistivity methods, electromagnetic (EM) methods have been used with considerable success to map groundwater salinity variations in coastal areas [22]. This paragraph introduces the most widely used methods namely (1) the time-domain electromagnetic (TDEM) method, (2) the frequency-domain electromagnetic (FDEM) method and (3) the ground penetration radar (GPR) survey method. Usually, EM methods are used in conjunction with resistivity methods as a cheap and rapid screening tool that helps to identify locations for more detailed ERT measurements [22].

- Time-Domain Electromagnetic (TDEM) method

The time-domain electromagnetic (TDEM), alternately called transient electromagnetic (TEM) method, is a commonly-used, non-intrusive, geophysical method for obtaining subsurface resistivity-conductivity data [35]. Because rock bulk conductivity is strongly correlated to rock properties, TDEM technique is an efficient way to map geological structure and therefore it may be used to delineate SWI [35].

This method requires very simple equipment, namely a transmitter loop, a receiver loop and a measurement device, as depicted in Figure 3-10, on the left. A time-varying direct current is firstly driven into the transmitter loop which is simply laid on the surface [35]. As a consequence, an EM field called primary field is generated and propagates into the subsurface [35]. At some

time (t_0) the current is cut off as quickly as possible [38]. Faraday's law of induction tells us that nearly identical currents, termed eddy currents, are then induced in the subsurface by an electromotive force to preserve the EM field produced by the original current [38], [7]. However, due to ohmic losses coming from the resistivity of the subsurface geological formations, these induced currents decay with time, with the ring of maximum current density moving downward and outward with increasing time (see Figure 3-10, on the left) [7]. As the transient decay occurs, the secondary attenuated EM fields are picked up at the surface by the receiver loop and the change in magnetic field with time is recorded [38], [35]. Therefore, the depth of investigation is principally a function of time with the first measurements being dominated by shallow units and the late measurements being dominated by deeper units [7]. The geological structure of the study area is finally build up based on the principle that the more conductive the earth, the stronger are the induced currents in the ground, and also the resulting output from the receiver loop [7].

This method doesn't require any contact between the measurement device and the ground surface, which has enabled the development of an airborne measurement system [22]. The equipment remains the same, namely a time-domain EM transmitter to drive an alternating current through an insulated electrical loop and a receiver which is installed in a towed "bird" [39]. The only difference is that the whole system is now attached to a helicopter, as shown in Figure 3-10, on the right. The main advantage of this technique is to allow for cost-effective mapping of the subsurface resistivity over large areas, and in areas that are inaccessible by ground-based vehicles [22].

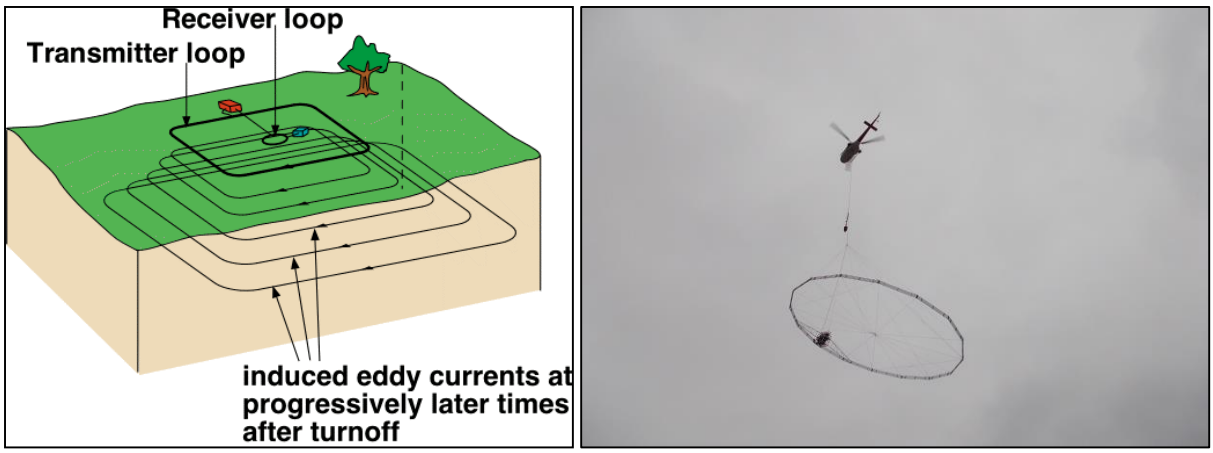

Figure 3-10: Principle of the time-domain electromagnetic method: land-based and airborne (GPRTEM) applications [35], [39]

- Frequency-Domain Electromagnetic (FDEM) method

The previous technique may also be conducted in the frequency domain and is then referred to as the frequency-domain electromagnetic (FDEM) method. The goal remains to measure the strength of secondary magnetic fields created by eddy currents in the ground induced by a time-varying primary magnetic field [7]. The only difference lies on this primary magnetic field which is this time produced by a frequency controlled AC current in the transmitter loop [7]. Therefore, the depth of investigation becomes a function of the frequency of the primary field rather than time, with lower frequencies having greater penetration [7].

Here again, this land-based method may be extended to an airborne system. To do so, the transmitter coils that induced electrical currents in the ground at different frequencies and the associated receiver coils that measure the EM produced by the induced currents are placed in a fiberglass casing called "bird" [5]. This bird is eventually attached to a helicopter, as shown in Figure 3-11.

Figure 3-11: Helicopter and equipment "bird" collecting electromagnetic geophysical data in Everglades National Park, Florida [5]

- Radar

Ground Penetration Radar (GPR) is the general term applied to survey methods employing high-frequency electromagnetic waves and exploiting contrasts in electromagnetic properties in order to map the geological structure of a study area [35], [40].

GPR equipment consists of a transmitter and receiver antenna set, as depicted in Figure 3-12 [7]. The transmitter antenna is used as a source (T_X) to focus high-frequency electromagnetic pulses (radiowaves) into the ground [35], [40]. The signal propagates and is then reflected by discontinuities or interfaces in soil materials [35]. It returns to the Earth's surface where its amplitude and travel time are measured by the receiver antenna (R_X) [40]. The device is then moved to another position and the procedure is repeated.

In practice, this process is continuous which allows for a very fast collection of data. These data from each pair (T_X-R_X) may finally be processed and displayed on a graphic recorder.

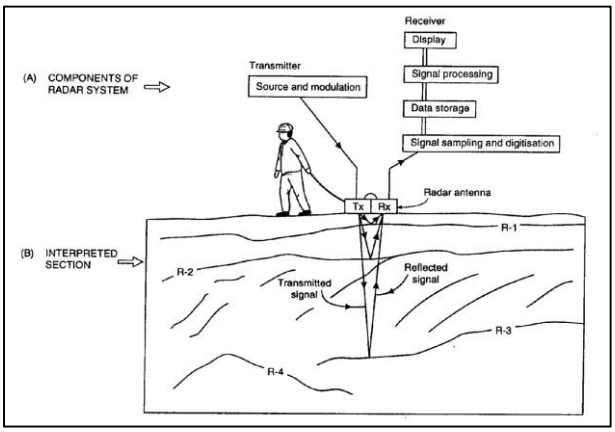

Figure 3-12: Principle of the Ground Penetration Radar method [40]

Seismic method

The seismic method is a classic geophysical method which utilizes differences in mechanical properties of geologic units, such as variations in seismic velocity, to delineate the location and geometry of the boundaries between geologic units, and to make some inferences about their lithology [7]. Therefore this method cannot be used to directly detect saltwater but it rather determines parameters which may affect the position and the movement of the saltwater interface [7]. The equipment is composed of three elements, namely a controlled shot of seismic energy (source), sensors to receive the energy (geophones), and a central data recorder (seismograph) connected via radio links or cabling [35].

The source, being a hammer blow or an explosive charge, generates a shock wave (elastic energy) which travels through the ground [35]. The sensors (geophones) are installed on the surface where they record the faint seismic energy that is returned from the subsurface discontinuities between materials with different seismic velocities (i.e. different densities) [40], [41]. At such boundaries there are two fundamental physical effects, namely reflection and refraction, and these two effects give rise to the two main techniques of applied seismology: reflection surveying and refraction surveying [40].

- Seismic refraction

A portion of the total seismic energy striking a density contrast is refracted into the underlying layer, as depicted in Figure 3-13 on the left [41]. Another portion is bent such that it travels along the interface between two subsurface materials, with some energy eventually returning to the surface [40]. This part of energy always represents the first arrival of seismic energy for the geophones located at a distance from the shot point [41].

- Seismic reflection

The remainder of the seismic energy impinging on an interface is bounced back, or reflected, towards the surface at the angle of incidence, as depicted in Figure 3-13 on the right [40]. Reflected seismic energy is never a first arrival for the geophones, and therefore must be identified in a generally complex set of overlapping seismic arrivals which requires a much higher processing time than for seismic refraction [41].

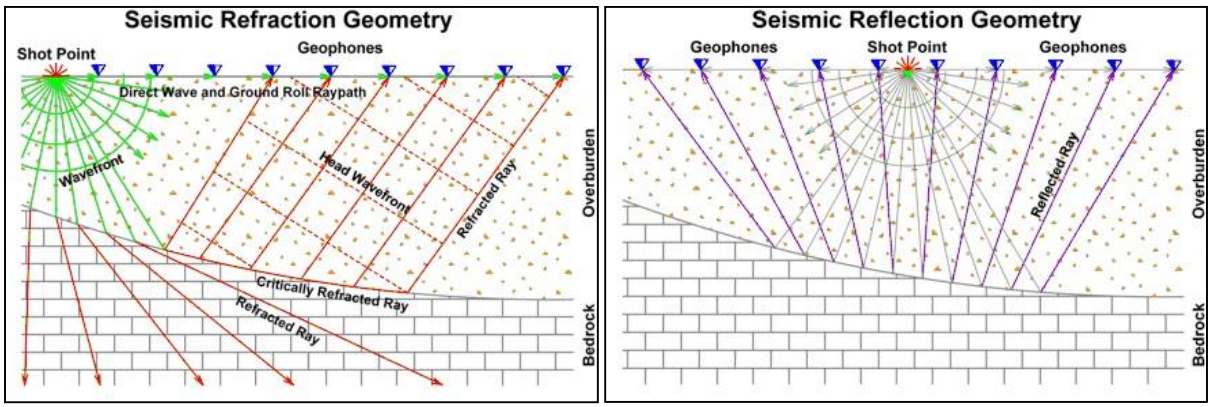

Figure 3-13: Seismic refraction (on the left) and reflection (on the right) principles [41]

3.3 Conceptual description

After the detection of SWI in an aquifer, the second step consists of a conceptual description of the study area. In other words, this step aims at collecting and presenting all the relevant information which may help to properly define, delineate and understand the system. These information will serve as the basis for the development of a numerical model which will be used to simulate SWI processes and make projections (see section 3.4.3). These information include, among others:

- The system boundaries

The delineation of the study area is based on the observations provided by the network of monitoring wells about the extension of the SWI process.

- The characterization of the subsoil [7]

The characterization of the study area consists of the description of the geologic structure of the subsoil and of the estimation of the main hydrogeological constants. Information on the geologic structure comes from borehole and geophysical prospecting and is collected during the monitoring phase (see section 3.2). The main hydrogeological constants include (1) the vertical hydraulic conductivity K_v, (2) the horizontal hydraulic conductivity K_h, (3) the specific yield S_y, (4) the longitudinal dispersivity α_L, (5) the transverse dispersivity α_T and (6) the porosity n. They are determined by pumping tests in the same boreholes or by lab experiments.

- Boundary conditions [7], [25]

This step requires the quantification of all the different input and output to the system and may be achieved by means of a groundwater balance, as depicted in Figure 3-14. This balance considers the main water bodies, namely the sea, one or several aquifers and the surface water bodies (rivers, lakes…) and aims at defining the links between these water bodies:

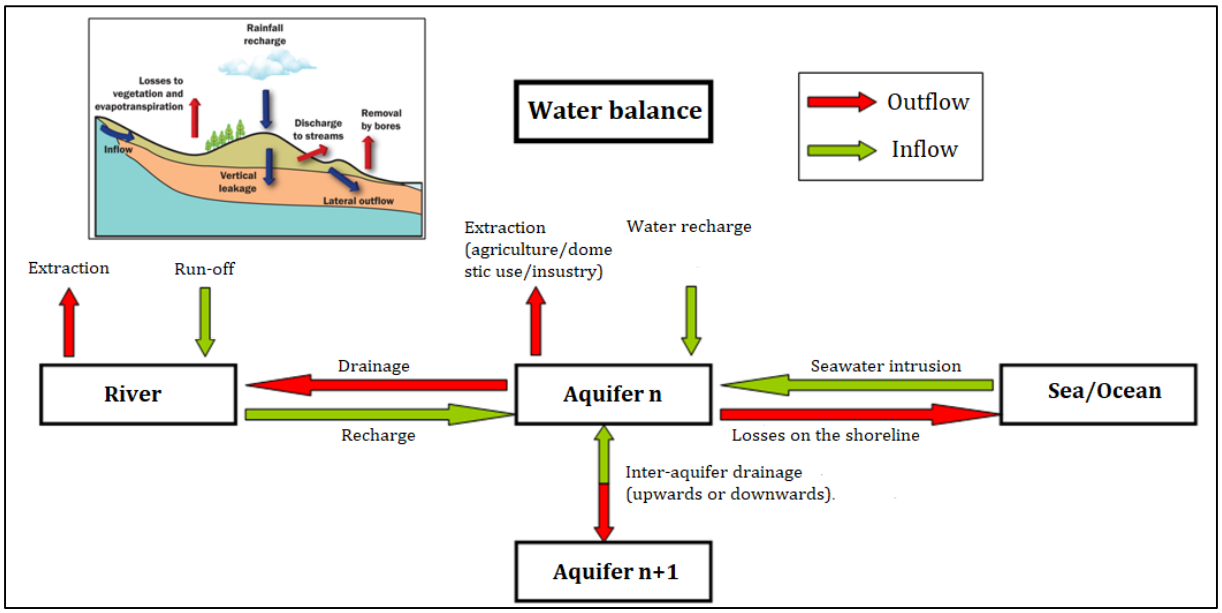

Figure 3-14: Conceptual diagram of water balance method [adapted from [42], [25]]

- Exchanges between the aquifer and the sea, considering SWI and the groundwater discharge towards the sea;
- Exchanges between the aquifer and the surface water bodies, through the mechanisms of drainage and recharge;
- Exchanges between different aquifers;
- Exchanges between the aquifer and the ground surface taking into account natural recharge, anthropogenic groundwater abstractions and soil artificialization/waterproofing;

These exchanges require the collection of the following information/data:

- The natural input into the groundwater system coming from natural recharge which is a function of time. This recharge is determined by the climate variables precipitation and evapotranspiration, by the soil moisture, by the vegetation and by the depth of the groundwater table;
- The piezometric levels as a function of location and of time. These levels may be used to infer groundwater flow directions and groundwater flow rates (inflow and outflow) and to roughly approximate the depth of the freshwater-saltwater interface;
- The rates and locations of the groundwater abstractions;

➢ Expected future stresses [7]

Estimations of the expected future threats are necessary to build future possible scenarios as the basis for the development of management strategies. As mentioned earlier in the section 2.4, these future stresses include (1) an increase in the water abstractions to match future water requirements and (2) the expected climate change affecting the natural recharge and potentially leading to SLR in coastal aquifers. These stresses are integrated in the model as boundary conditions or as internal source and sink terms [43];

➢ Initial conditions [43]

Since SWI is a transient process, initial conditions are complicated to estimate because they are rarely known with certainty and they can have a large effect on model predictions. Therefore a common procedure is to perform a steady-state simulation and then use the resulting salinity field as initial state for a subsequent transient simulation;

➢ Simplifying assumptions

All the above mentioned information are affected by a certain level of uncertainty. The major difficulty in the use of SWI models is to properly deal with the uncertainty associated to those input data. Indeed it has been shown that a sophisticated model without the support of reliable input data does not provide more accurate results [2]. Therefore a trade-off must be found between model complexity, data demand, uncertainty resulting from availability of input data and simplifications according to the scale and spatial resolution of the analysis [2]. The level of idealization (i.e. accuracy VS complexity VS time-demanding) has to be clearly established at this stage because it directly influences the type of numerical code that will be used later.

3.4 Solution

3.4.1. Types of models

Coastal aquifers are particularly difficult to simulate because the density of water varies substantially throughout the modelled area due to variation in salinity [22], [5]. There are two types of models which are generally used to simulate SWI: interface models and variable density models [22]. In interface models, the freshwater and saltwater zones are assumed to be immiscible (that is, they do not mix) and separated by a sharp interface [5]. In variable density models, the transition zone between freshwater and saltwater has a finite thickness along which the density of the water varies continuously [22]. SWI analytical solutions are predominantly based on the interface assumption, whereas variable density models are mainly solved using numerical methods [22].

3.4.2. Analytical solutions

Analytic interface modelling is a reasonable choice when reliable input data for sophisticated model are not available [24]. Indeed a sophisticated model without the support of reliable input data does not provide more accurate result [7]. Analytical solutions can also be used as a tool for first-cut engineering analysis to perform some rudimentary calculations before a large scale site investigation, or a comprehensive numerical modelling [7].

The usefulness of analytic models as instructional tools for providing insights into mechanical trend of the flow and steady-state interface location has been advocated by many researchers (e.g. Glover 1964, Fetter 1972, Strack 1976) [24]. The analytical solution described by Strack offers comprehensive coverage on interface approaches to SWI assessment [1]. It simplifies the SWI problem by: (1) assuming a sharp interface between the freshwater and saltwater (i.e. neglecting mixing processes); (2) assuming a stationary interface, with freshwater being mobile while seawater remains immobile; (3) adopting the Dupuit approximation (i.e. neglecting the vertical component of the groundwater flow); (4) adopting steady-state conditions. The steady-state interface position can then be estimated using the Ghyben-Herzberg relation (see equation (1), in Chapter 2). [24]

The Strack-Solution is defined for confined and unconfined aquifers. These aquifers are separated into two zones, a freshwater zone (zone 1) and a zone where freshwater exists on top of saltwater wedge (zone 2). The model representations of a confined and an unconfined aquifer are given in Figure 3-15 and the model variables are explained in Table 3-6. [2]

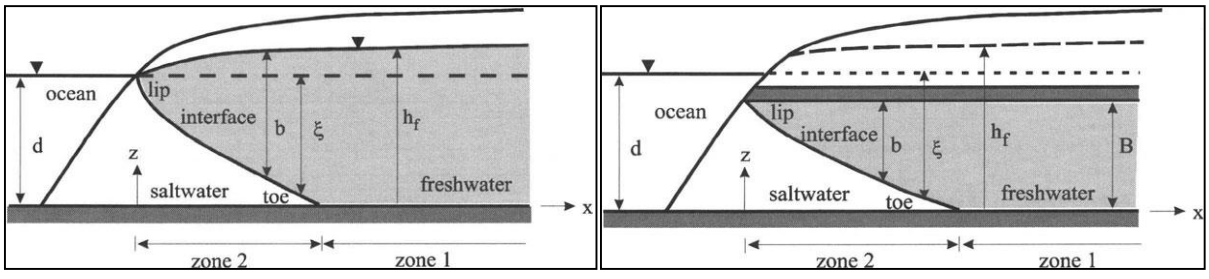

Figure 3-15: Model representation of an unconfined (on the left) and a confined (on the right) aquifer system [7]

Table 3-6: Variables of the analytical solution [2]

Variable	Description	Unit
b	Thickness of freshwater layer	[L]
d	Depth of lower confining layer b.m.s.l. (aquifer bottom)	[L]
z	Depth of saltwater interface b.m.s.l.	[L]
B	Aquifer thickness (confined aquifers)	[L]
L	Length of vertical cross section (perpendicular to coastline)	[L]
x	Position along cross section	[L]
h_f	Freshwater head	[L]
Φ	Potential	[L]
Φ_{Toe}	Potential at toe location	[L]
x_{Toe}	Toe location (location of interface between zone 1 and zone 2)	[L]
w	Recharge	$[L^3L^{-2}T^{-1}]$
q	Inflow	$[L^3T^{-1}]$
K	Hydraulic conductivity of aquifer	$[LT^{-1}]$
ρ_s	Density of saltwater (1.025)	$[ML^{-3}]$
ρ_f	Density of freshwater (1.000)	$[ML^{-3}]$

The position of the saltwater-freshwater interface and the thickness of the freshwater lens are calculated as follows [2]:

- The thickness of the freshwater lens b at each location x can be inferred from the following set of equations and from the Ghyben-Herzberg relation, written in the current notations (adaptation of equation (1)):

  For unconfined aquifers:

$$\begin{cases} \text{Zone 1:} & b = h_f \\ \text{Zone 2:} & b = h_f - d + z \end{cases} \tag{11}$$

  For confined aquifers:

$$\begin{cases} \text{Zone 1:} & b = B \\ \text{Zone 2:} & b = z - d + B \end{cases} \tag{12}$$

  Ghyben-Herzberg relation:

$$h_f - d = \Delta s z \tag{13}$$

  Where Δs is the density ratio of fresh- and salt-water, given by:

$$\Delta s = \frac{\rho_s - \rho_f}{\rho_f} = \frac{1}{\alpha} \tag{14}$$

- Potential functions are defined for confined and unconfined aquifers, depending on density difference, depth and thickness of the aquifer and the freshwater head.

  For unconfined aquifers:

$$\begin{cases} \text{Zone 1:} & \Phi = \frac{1}{2}\left[h_f^2 - (1+\Delta s)d^2\right] \\ \text{Zone 2:} & \Phi = \frac{(1+\Delta s)}{2\Delta s}(h_f - d)^2 \end{cases} \tag{15}$$

With the following condition of continuity at the interface: $\Phi_{Toe} = \frac{\Delta s(1+\Delta s)}{2} d^2$

For confined aquifers:

$$\begin{cases} \text{Zone 1:} & \Phi = Bh_f + \frac{\Delta s B^2}{2} - (1+\Delta s)Bd \\ \text{Zone 2:} & \Phi = \frac{1}{2\Delta s}[h_f + \Delta s B - (1+\Delta s)d]^2 \end{cases} \quad (16)$$

With the following condition of continuity at the interface: $\Phi_{Toe} = \frac{\Delta s}{2} B^2$

- Those potential functions (equations (15) & (16)) can be rearranged to solve the freshwater head h_f at any location x, assuming an analytical equation for the potential function $\Phi(x)$.

For unconfined aquifers:

$$\begin{cases} \text{Zone 1:} & h_f = \pm\sqrt{2\Phi(x) + (1+\Delta s)d^2} \\ \text{Zone 2:} & h_f = d \pm \sqrt{\Phi(x)\frac{2\Delta s}{(1+\Delta s)}} \end{cases} \quad (17)$$

For confined aquifers:

$$\begin{cases} \text{Zone 1:} & h_f = \frac{\Phi(x)}{B} - \frac{\Delta s B}{2} + (1+\Delta s)d \\ \text{Zone 2:} & h_f = (1+\Delta s)d - \Delta s B \pm \sqrt{2\Delta s \Phi(x)} \end{cases} \quad (18)$$

3.4.3. Numerical solutions

Governing equations

Numerical models are mathematical representations of groundwater systems in which the important physical processes that occur in the systems are represented by mathematical equations [5]. These processes include the groundwater flow and the movement of the salt [44].

- Groundwater flow equation

The description of the groundwater flow in an aquifer is obtained by applying the equation of motion and the equation of continuity to a control volume [44].

The equation of motion for three-dimensional (laminar) groundwater flow in an anisotropic non-homogeneous porous medium in the principal directions is described by the following equation which is a generalization to variable-density fluids of the Darcy's law which was introduced earlier through the set of equations (5) to (8) [45], [8]:

$$q_x = -\frac{k_x}{\mu}\frac{\partial p}{\partial x} \qquad q_y = -\frac{k_y}{\mu}\frac{\partial p}{\partial y} \qquad q_z = -\frac{k_z}{\mu}\left(\frac{\partial p}{\partial z} + \rho g\right) \quad (19)$$

With (state equation):

$$\rho(C) = \rho_f + \frac{\partial \rho}{\partial C}(C - C_0) \quad (20)$$

Where:

- q_x, q_y, q_z = Darcian specific discharges in the principal directions [LT^{-1}];
- k_x, k_y, k_z = principal intrinsic permeabilities [L^2];
- μ = dynamic viscosity of water at point x, y, z [$ML^{-1}T^{-1}$];
- p = pressure [$ML^{-1}T^{-2}$];
- g = gravitational acceleration [LT^{-2}];
- $\rho g = \gamma$ = specific weight [$ML^{-2}T^{-2}$];
- ρ_f = density of freshwater [ML^{-3}];
- C = mass fraction of total dissolved solids [−];
- $\frac{\partial \rho}{\partial C}$ = a constant value of density change with concentration [ML^{-3}];

The equation of continuity describes the non-steady three-dimensional mass flow in a small element of a saturated anisotropic, porous medium [45]:

$$-\left[\frac{\partial\ \rho_i q_x}{\partial x} + \frac{\partial(\rho_i q_y)}{\partial y} + \frac{\partial\ \rho_i q_z}{\partial z}\right] = \frac{\partial(n_e \rho_i)}{\partial t} + W'(x, y, z, t) \tag{21}$$

Where:

- t = time [T];
- n_e = effective porosity of the medium [−];
- $W'(x, y, z, t)$ = source or sink term, which describes the mass flux of the fluid into (negative sign) or out of (positive sign) the system (e.g. recharge, pumping, evapotranspiration) [$ML^{-3}T^{-1}$];

➢ Advection-dispersion equation

The advection-dispersion equation which describes the transport of a conservative[11] solute can be written as:

$$\frac{\partial C}{\partial t} = \frac{\partial}{\partial x_i}\left(D_{ij}\frac{\partial C}{\partial x_j}\right) - \frac{\partial}{\partial x_i}(CV_i) + \frac{(C - C')W}{n_e b} \tag{22}$$

Where:

- D_{ij} = coefficient of hydrodynamic dispersion [L^2T^{-1}];
- $V_i = q_i/n_e$ = effective velocity of the groundwater in the direction of x_i [LT^{-1}];
- C = concentration of the dissolved solids [ML^{-3}];
- C' = concentration of the dissolved solids in a source or sink [ML^{-3}];
- b = saturated thickness of the aquifer [L];
- n_e = effective porosity of the medium [−];
- $W(x, y, z, t)$ = general term for sources and sinks [LT^{-1}];

[11] A solute is conservative when no chemical reactions such as adsorption and radioactive decay are taking place.

The first term on the right hand side of this equation (22) represents the change in chemical concentration due to kinematic dispersion and diffusion since the two cannot be split up. The second term represents the effect of advective transport which means the movement of the fluid due to the movement of the water. The third term represents the contribution and removal of pollutant due to fluid sources and sinks. [44]

Solution of the equations

When studying any problem involving mass transport it is necessary to solve all the equations together. Several methods can be used to solve this so-called coupled system of equations. The two most common are finite differences and finite elements. In addition the advection-dispersion problem is sometimes solved using the method of characteristics. [44]

Those mathematical techniques are then implemented in computer codes which are relatively complicated and computationally demanding since the coupled system of equations is implicit [5], [22], [44]. Many codes exist for the simulation of SWI but none of them can outperform all the others in accuracy, efficiency, and ease of use, in a wide range of parameter values and problem settings [7]. Trade-offs always exist between model accuracy and run-times and at the end it is up to the users to select the most suitable code for their applications [22], [7]. A list of the most widely used codes is given in Table 3-7.

Table 3-7: Popular SWI codes [Adapted from [22]]

SWI codes	Basic model features[12]				
	FD	FE	S	SU	GUI
2D/3D FEMFAT		*		*	
FEFLOW		*		*	*
MOCDENS3D	*		*		*
SEAWAT	*		*		*
SUTRA	*	*		*	*

[12] FD=finite difference; FE=finite elements; S=saturated flow only; SU=saturated-unsaturated flow; GUI=dedicated graphical user interface available

Chapter 4
Vulnerability and risk assessment

4.1 Introduction

SWI is a complex process that involves variable-density flow, solute transport and hydrochemical processes which makes its characterisation relatively difficult and expensive, as described in Chapter 3. Therefore, there is a need for methods allowing a rapid assessment of SWI over large scales (regional, continental or global), such as the groundwater vulnerability and risk techniques [22]. These techniques aim at (1) detecting the current and emerging risk areas, along with the key drivers of SWI in these areas [24]; (2) prioritizing areas requiring more detailed SWI investigations in the future [24]; (3) assisting the development of groundwater protection strategies ensuring a sustainable use of groundwater for domestic consumption as well as industries and agricultural purpose [11], [46]. The vulnerability and risk assessment to SWI are mainly carried out using qualitative techniques which only consider a subset of the factors thought to impact SWI [24]. This Chapter 4 consists of a detailed literature review of these techniques.

Vulnerability assessment involves the mapping of coastline areas that are particularly vulnerable and is useful for those involved with coastal zone management (i.e. policy makers, local governments, environmental managers...) because it offers them a quick and cost-effective means to develop future groundwater protection or mitigation and remediation measures [46], [47]. The section 4.2 provides a general overview of the techniques that are commonly used to assess the vulnerability of coastal aquifers to both SWI and SLR.

Furthermore, vulnerability maps may be integrated into more complete assessments of groundwater risk [47]. While vulnerability assessments identify sensitive zones of a system based on hydrogeological criteria, risk assessments additionally consider the presence and the impact of external human activities, such as water over-abstractions or SLR due to human-induced climate change [3]. Up to now, only a few methods have been developed and applied for SWI risk assessment. These methods are presented in the section 4.3, through a review of the main study-cases proposed in the literature.

These two approaches are integrated with GIS environment in order to evaluate spatial changes more easily and quickly [46]. A Geographic Information System (GIS) may be defined as a computer-based tool that analyses, stores, manipulates and displays geographic data on a map [48]. By connecting data with geography, this gives people a geospatial perspective and helps them to more easily understand patterns and relationships [49], [48].

In this study, GIS technology is used to map out zones that are prone to further SWI by means of vulnerability and risk maps [3]. The idea of describing the degree of vulnerability/risk of groundwater to SWI by means of maps was conceived to show that the protection provided by

the natural environment varies at different locations and that it would be helpful to identify on maps areas where protection measures are most needed [13].

Finally, it is important to keep in mind that these specific thematic maps are not to be used as an alternate for detailed site-specific analysis, but rather as preliminary screening tools to identify sensitive areas where protection measures are most needed and to prioritize areas for further costly detailed site-specific analysis [47]. The further steps involve field-based investigations and the development of complex numerical models to predict future trends and to simulate different water management scenarios at local scale, as described in Chapter 3 [46], [24].

4.2 Vulnerability

4.2.1. Definition

The fundamental concept of groundwater vulnerability (which may be adapted to the groundwater vulnerability to SWI) is that some land areas easily contribute to groundwater contamination, and thus are more vulnerable, and others do not [13]. The term vulnerability in the field of hydrogeology was introduced by Albinet and Margat (1970) in France as "a degree of protection in the hydrological settings to tolerate against the ingress of pollutants to the aquifer" [46], [1]. Since then, "several definitions of vulnerability have been presented in the technical literature [50], but hydrogeologists have failed to reach a consensus" (Gogu and Dassargues, 1998) [1] meaning that a generally recognized and accepted definition of this term has not been developed yet [13]:

- Lobo-ferreira and Cabral (1991) defined the groundwater vulnerability to SWI as "the sensitivity of groundwater quality to an imposed groundwater pumping or SLR or both in the coastal belt, which is determined by the intrinsic characteristics of the aquifer" [46];
- Vrba and Zaporozec (1994) defined vulnerability in relation to groundwater systems as "the intrinsic properties of a groundwater system and its susceptibility to natural and/or human impacts" [1];
- According to Voice et al. (2006): "vulnerability is a function of exposure, sensitivity and adaptive capacity" [1];
- The IPCC (2007) defined vulnerability in the specific context of climate change as "the degree to which a system is susceptible to, or unable to cope with the adverse effects of SLR and groundwater extraction" [1];
- A definition of vulnerability used by the UNISDR (2010) is "the characteristics and circumstances of a community, system or asset that make it susceptible to the damaging effects of hazard" [1];
- According to Shirazi et al. (2013), the notion of vulnerability is based on "the assumption that certain areas are less protected by the geological system than others; as such, the less protected areas are more likely to be affected by contaminants" [47];

However, the most rigorous definition of vulnerability is given by Füssel (2007) who, after reviewing a broad range of vulnerability definitions and concepts developed a generally applicable framework of vulnerability that includes six dimensions. The first four dimensions are fundamental to describing any vulnerable situation while the two last dimensions are used to conceptualize vulnerability [1]:

- System: the system of analysis;
- Attribute of concern: the valued attributes of the vulnerable system that is threatened by its exposure to a hazard;
- Hazard: a potentially damaging influence on the system of analysis;
- Temporal reference: the point in time or period of interest (current, future, number of years into future…);
- Sphere: whether the vulnerability factors are internal to the system itself, and are therefore intrinsic properties of that system, or whether the factors are external to the system;
- Knowledge domain: the origin of the knowledge socioeconomic and/or biophysical factors;

The absence of a generally recognized and accepted definition of vulnerability may explain that no standardized approach to vulnerability mapping has been developed yet [13]. This may also be due to the fact that vulnerability of coastal aquifers to SWI is a relatively new issue and to the fact that hydrogeological environments are much too diverse for a standardized assessment [13]. In any cases, the main assessment approaches found in the literature are introduced in the following sub-sections.

The first method is the simplest and most popular one [47]. It consists of an overlay index, known as the GALDIT index (Chachadi and Lobo-Ferreira, 2001; Lobo-Ferreira et al., 2007) and is directly inspired by the traditional overlay indices used to assess groundwater vulnerability to pollution (DRASTIC, GOD...). This method is described in details in the sub-section 4.2.2. The GQI_{SWI}, developed by Tomaszkiewicz et al. (2014), consists of a second type of representative indices for SWI. It uses common water quality parameters indicative of SWI and it is presented in the sub-section 4.2.3 [46]. Other assessment techniques for coastal aquifer vulnerability are based on analysis of different coastal impacts, tending to focus on specific stresses, such as the CVI (Coastal Vulnerability Index) approach of Thieler and Hammar-Klose (1999) and the CVI(SLR) (Coastal Vulnerability Index–Sea-Level Rise) indexing method of Ozyurt (2007) [3]. Since this index solely focusses on the particular effect of SLR, it is not further developed in this report. A fourth approach was developed in Australia by Ivkovic et al. (2012) and consists of a qualitative evaluation of the factors which are thought to increase vulnerability to SWI [21]. Unfortunately this approach is not either developed in this report due to the difficulty to access the original paper.

4.2.2. GALDIT index

A range of vulnerability mapping approaches based on indices (DRASTIC, EPIK, SINTACS, GOD…) has traditionally been used to map the vulnerability of groundwater to contamination, by considering key factors that can influence the solute transport process [1], [3]. However, these classical groundwater vulnerability approaches are challenging to apply in the case of a SWI vulnerability investigation because the processes that lead to the migration of the freshwater-saltwater interface are different to those that lead to the migration of a contaminant from the land surface into an aquifer [1]. Therefore, the only example of a large-scale indicator-based approach for assessing coastal aquifer vulnerability to SWI is the GALDIT method which adopts simple indicators of the propensity for SWI to occur [3].

The GALDIT acronym is formed from these key factors that are presumed to control SWI [1], [3], [6]. These factors are listed below and represent measurable parameters for which data are generally available from a variety of sources without detailed examination.

- ***G***roundwater occurrence (aquifer type: unconfined, confined and leaky confined):

This basic nature of groundwater occurrence has an influence on the extent of SWI. In natural conditions, the unconfined aquifer is characterized with low pressure which makes it more vulnerable to seawater intrusions as compared to confined aquifer. However under pumping conditions, the confined aquifer becomes more vulnerable due to a larger cone of depression [51]. The data related to groundwater occurrence/type of aquifers can be obtained from analysis of pumping test data and/or lithological logs. [6], [46]

- ***A***quifer hydraulic conductivity:

The parameter aquifer hydraulic conductivity (introduced earlier in the section 2.2) is used to measure the rate of flow of water in the aquifer and hence to the sea. A coastal aquifer with a high hydraulic conductivity is associated with increased SWI risk, as it was described earlier by the two equations (2) & (4) in the section 2.1. The aquifer hydraulic conductivity can be estimated from pumping test data as well as from lithological logs. [6], [46]

- Depth to groundwater ***L***evel above the sea:

Height of groundwater level a.m.s.l. constitutes an important factor in the evaluation of SWI because it determines the hydraulic pressure eventually able to push back the seawater front. The groundwater level data with respect to mean sea elevation can be obtained by establishing the observation wells in the area. [6], [46]

- ***D***istance from the shore (distance inland perpendicular from shoreline):

The impact of seawater intrusion generally decreases as one moves inland at right angle to the shore and the creek. The maximum impact is witnessed close to the coast and creek. Data for this parameter can be computed using the topographical map of the area. [6]

- ***I***mpact of existing status of seawater intrusion in the area:

Groundwater is invariably under stress, and this stress has modified the natural hydraulic balance between seawater and fresh groundwater. The hydrochemical ratio $\frac{Cl^-}{HCO_3^- + CO_3^{2-}}$ is used to show the impact of existing status of SWI in the area. Chloride is the dominant ion in the seawater and it is only available in small quantities in groundwater while bicarbonate, which is available in large quantities in groundwater, occurs only in very small quantities in seawater. The information required for the above rating can be gathered from historical reports, inquiry from the local people, and chemical analysis data. [6], [46]

- ***T***hickness of the aquifer which is being mapped:

Aquifer thickness or saturated thickness of an unconfined aquifer plays an important role in determining the extent and magnitude of SWI in the coastal areas. It is well established as per equations (2) & (4) (see section 2.1) that the larger the aquifer thickness, the larger the extent of SWI and vice versa. The aquifer thickness in a given area can be obtained from lithological logs and can be deduced from carefully conducted vertical electrical sounding data. [6]

The identification of this set of indicators was achieved through extensive discussions and consultations with experts, academics, etc. and it is therefore recommended to keep those factors unchanged under normal circumstances. However, since the GALDIT-Index is an open-ended model, it allows for addition and deletion of one or more indicators under particular conditions, thus requiring the re-derivation of the weights and of the classification table that is presented hereafter (see Table 4-1). [52]

The system in itself contains three significant parts: weights, ranges, and ratings [6]. Each GALDIT factor is first assigned a weight ranging from 1 to 4, based on the relative importance of the factor to SWI with respect to the other factors [3], [6]. Then, each factor is assigned a numeric rating by using a scale of 2.5 to 10, based on the range of values for the area of investigation. Generally speaking, the lower the value of the weighting and rating, the lower is the influence of the factor [1]. The details of the weights and rating values for all the factors used in the computation of the GALDIT-Index are summarized in Table 4-1 [46]. The GALDIT-Index is finally obtained by multiplying each parameter weight by its rating, by summing all the six products and by dividing them by the total weight, as described by equation (23) below:

$$\mathrm{GALDIT-Index} = \sum_{\mathrm{i}=1}^{6} (\mathrm{W_i} \times \mathrm{R_i}) \,/\, \sum_{\mathrm{i}=1}^{6} \mathrm{W_i} \tag{23}$$

Where:

- $\mathrm{W_i}$ = weight of the $\mathrm{i^{th}}$factor;
- $\mathrm{R_i}$ = importance rating of the $\mathrm{i^{th}}$factor;

The "maximum GALDIT-Index" is obtained by substituting the maximum importance ratings of the indicators as shown below [6]:

$$Max = \frac{[10.W_1 + 10.W_2 + 10.W_3 + 10.W_4 + 10.W_5 + 10.W_6]}{\sum_{i=1}^{6} W_i} = 10.\frac{\sum_{i=1}^{6} W_i}{\sum_{i=1}^{6} W_i} = 10 \tag{24}$$

Similarly, the "minimum GALDIT-Index" is obtained by substituting the minimum importance ratings of the indicators as shown below [6]:

$$Min = \frac{[2.5.W_1 + 2.5.W_2 + 2.5.W_3 + 2.5.W_4 + 2.5.W_5 + 2.5.W_6]}{\sum_{i=1}^{6} W_i} = 2.5.\frac{\sum_{i=1}^{6} W_i}{\sum_{i=1}^{6} W_i} = 2.5 \quad (25)$$

Table 4-1: Summary of GALDIT parameter weights, rates, and ranges [46]

Factor	Weight	Rating			
		Very low 2.5	Low 5	Medium 7.5	High 10
G (aquifer type)	1	Bounded	Leaky-confined	Unconfined	Confined
A (m/day)	3	<5	5-10	10-40	>40
L (m)	4	>2	1.5-2	1-1.5	<1
D (m)	4	>1,000	1,000-750	750-500	<500
I (-)	1	<1	1-1.5	1.5-2	>2
T (m)	2	<5	5-7.5	7.5-10	>10

The range of minimum and maximum GALDIT-Index scores (i.e. 2.5 to 10) is divided into three classes: 2.5–5, 5–7.5 and 7.5–10 denoted, respectively, as low, moderate and high vulnerability [6], [46]. In a general way, the higher the index, the greater the vulnerability to SWI. By the way, the numerical values for the weights, ratings and class limits as well as the names and the number of classes are usually fixed but they may also vary slightly among the literature according to the properties of the investigation area.

By having a closer look to the scientific literature, it turns out that the GALDIT-Index is applied by most of the authors with the purpose of assessing the vulnerability of a given aquifer to SWI induced by water over-abstractions (art. [3], [1], [46], [53], [51], [54]). However it is also used by a minority of authors to study the impact of SLR on the coastal areas in terms of SWI (art. [6], [52], [55]). The final goal being in general to help local authorities with the management of the coasts by prioritizing the areas requiring more detailed investigations, by deciding where measures have to be taken or where money has to be invested. Finally it can be noted that the majority of the papers are dealing with unconfined aquifers with a variable spatial extent ranging from a few squared meters (art. [52]) up to several thousand squared meters (art. [51]).

This method has three major drawbacks: (1) it is subjective in terms of the applied ratings and weightings and therefore the index provides a relative tool rather than absolute answers [1]; (2) unawareness of the pumping effect on the SWI process: the rate of groundwater withdrawal relative to the amount of total freshwater recharge is not part the GALDIT assessment even if it is clearly a key driver of SWI [1], [46]; (3) Geochemistry prospecting techniques are required to determine the status of SWI into groundwater system [46].

Despite these limits, the GALDIT method is the most popular one due to its low cost and to its simplicity which makes it attractive for SWI vulnerability mapping [1], [46]. The main advantage of this method is the few and easy-to-collect, data required which makes it suitable for regional-scale assessments [46], [56]. Furthermore it gives relatively accurate results for extensive regions with complex geological structure, despite the absence of measurements of specific parameters that the most specialized methods would require [46].

4.2.3. GQI_{SWI} & Geo-statistics[13]

The groundwater quality index for seawater intrusion (GQI_{SWI}) was developed in 2014 by Tomaszkiewicz et al. [57] and is based on common water quality parameters indicative of SWI (hydro-chemical data) and on geostatistical techniques [58], [46]. It combines information from the Piper diagram and from the fraction of seawater (f_{sea}) and translates these information into a format that can be spatially analysed under a GIS framework [46]. Therefore this index allows for a rapid delineation of SWI into a particular aquifer and constitutes a helpful and robust visual tool for researchers and policy makers towards defining corrective or adaptive methods [46], [57]. The general steps behind the establishment of this index are detailed below:

- The first step consists in pixilizing the area of interest. In general, a grid of $20\text{m} \times 20\text{m}$ pixels is created [57];
- The parameters considered for the calculation of the GQI_{SWI} include levels of TDS, EC and major ions (Calcium (Ca^{2+}), Magnesium (Mg^{2+}), Sodium (Na^{+}), Potassium (K^{+}), Bicarbonate (HCO_3^-), Chloride (Cl^-) and Sulfate (SO_4^{2-})) [58], [46], [57]. The second step consists in collecting those data through the use of a spatial and temporal groundwater sampling program from the wells available in the study area (field investigations and laboratory analyses) [58]. A database is established to store and manipulate all the data.
- In practice, it is costly and hardy possible to obtain sufficient water quality samples that are densely distributed across the study area. Therefore, geo-statistical methods (kriging) are used to interpolate data at unmeasured points in the study area based on the measured concentration values in the neighbourhood of those unmeasured points [58], [57]. Every collected value (measured or predicted) is then assigned to a particular pixel of the study area and a database is established to store and manipulate all the data.
- The fourth step consists in evaluating the fraction of seawater (f_{sea}) for each pixel. This fraction represents the percentage of seawater in a freshwater sample and may be estimated based on the concentrations of Cl^- (m_{Cl}) in meq/L, as expressed in equation (26) [57], [58]. From this equation (26) an index may be easily derived, reflecting the level of

[13] According to [84], geo-statistics is the generic name for a family of techniques which are used for mapping of surfaces from limited sample data and the estimation of values at unsampled locations.

Geo-statistical estimation is a two stage process:

i. Studying the gathered data to establish the predictability of values from place to place in the study area; this study results in a graph known as a semi-variogram which expresses the spatial dependence between neighbouring observations;

ii. Estimating values at those locations which have not been sampled. This process is known as “kriging”. The basic technique “ordinary kriging” uses a weighted average of neighbouring samples to estimate the 'unknown' value at a given location. Weights are optimized using the semi-variogram model, the location of the samples and all the relevant inter-relationships between known and unknown values.

SWI in the aquifer. This index, given by equation (27), has a range of values between 0 and 100 [57].

$$f_{sea} = \frac{m_{Cl}(sample) - m_{Cl}(freshwater)}{m_{Cl}(seawater) - m_{Cl}(freshwater)} \quad (26)$$

$$GQI_{f_{sea}} = (1 - f_{sea}) \times 100 \quad (27)$$

- The fifth step consists in plotting the different collected data on the Piper diagram. The Piper diagram was introduced in the section 3.2.1 as a graphical representation of the chemistry of a water sample or samples [29]. It is composed of three parts, as it was shown in Figure 3-2: a ternary diagram in the lower left representing the cations ($Ca^{2+}, Mg^{2+}, Na^{+}, K^{+}$), a ternary diagram in the lower right representing the anions (SO_4^{2-}, Cl^-, HCO_3^-), and a diamond plot in the middle representing a projection of the two [30]. Water samples shown on the Piper diagram can be grouped in hydrochemical facies [29]. In particular, the diamond field may be divided into six different domains as shown in Figure 4-1 [57]. Two indices are introduced to define those six domains: (1) the $GQI_{Piper\ mix}$ (equation (28)) which describes the mixing between freshwater (domain I) and saline water (domain II) and (2) the $GQI_{Piper\ dom}$ (equation (29)) which makes the distinction between the four other domains (III, IV, V and VI). The ranges (from 0 to 100) of the $GQI_{Piper\ mix}$ and of the $GQI_{Piper\ dom}$ and the six corresponding hydrogeochemical domains are presented in Table 4-2 [57].

$$GQI_{Piper\ mix} = \left[\frac{Ca^{2+} + Mg^{2+}}{\text{Total cations}} + \frac{HCO_3^-}{\text{Total anions}}\right] \times 50 \text{ (in meq/l)} \quad (28)$$

$$GQI_{Piper\ dom} = \left[\frac{Na^{+} + K^{+}}{\text{Total cations}} + \frac{HCO_3^-}{\text{Total anions}}\right] \times 50 \text{ (in meq/l)} \quad (29)$$

Table 4-2: Hydrogeochemical domains related to the $GQI_{Piper\ mix}$ and the $GQI_{Piper\ dom}$ [46]

Domain	Hydrogeochemestry	$GQI_{Piper\ mix}$	$GQI_{Piper\ dom}$
I	$Ca - HCO_3$	50-100	25-75
II	$Na - Cl$	0-50	25-75
III	mixed $Ca - Na - HCO_3$	25-75	50-75
IV	mixed $Ca - Mg - Cl$	25-75	25-50
V	$Ca - Cl$	25-75	0-25
VI	$Na - HCO_3$	25-75	75-100

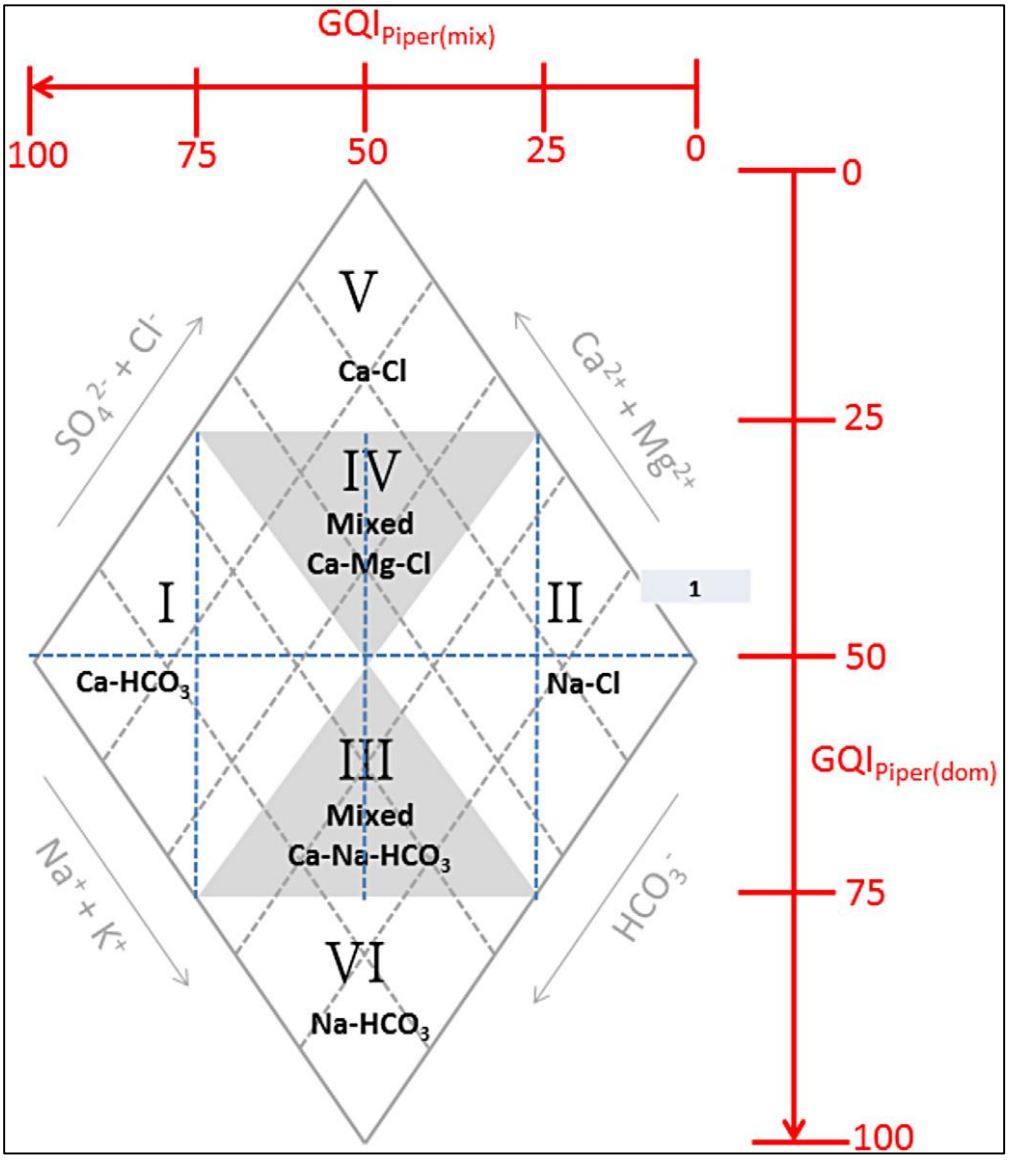

Figure 4-1: Development of the $GQI_{Piper\ mix}$ and $GQI_{Piper\ dom}$ resultant domains [46]

- A seawater intrusion groundwater quality index (GQI_{SWI}) is finally obtained for each pixel by combining values of $GQI_{f_{sea}}$ and $GQI_{Piper(mix)}$, as described by equation (30) [57], and imported into the GIS environment to produce the vulnerability map of the study area.

$$GQI_{SWI} = \frac{GQI_{f_{sea}} + GQI_{Piper\ mix}}{2} \tag{30}$$

To conclude, it is important to address two of the main limitations related to this approach. On the one hand, its application requires a minimum of geochemical and groundwater head data and in many cases the rarity or absence of data constitutes a real difficulty for the use of this approach [46]. On the other hand, seawater intrusion entails complex hydrogeochemical processes that cannot be fully captured through the use of the GQI_{SWI} [57]. It is therefore recommended to use this approach for preliminary assessments, as a complementary tool to verify, discuss and compel the shortcoming of the GALDIT model [46].

4.3 Risk

4.3.1. Definition

According to Dentoni (2012) [3], the risk may be widely defined as "the probability of harmful consequences or expected losses (e.g. disruption of economic activity or environmental damage), in a certain area and in a certain period of time, resulting from interactions between natural or human-induced hazards and vulnerable conditions" [3].

Based on this general definition, the risk of SWI in the particular field of coastal hydrogeology may be specified more precisely as a function of:

- The natural vulnerability of the aquifer system to SWI (which is function of its intrinsic properties);
- The hazards due to human activities (groundwater over-abstraction or human-induced climate change leading to SWI);

The term vulnerability was introduced in the section 4.2 hereabove. The word hazard has been defined in general terms by the UNISDR as "a dangerous phenomenon, substance, human activity or condition that may cause loss of life, injury or other health impacts, property damage, loss of livelihoods and services, social and economic disruption, or environmental damage" [1]. In particular, an environmental hazard may be defined as "an event, or continuing process, which if realized, will lead to circumstances having the potential to degrade, directly or indirectly, the quality of the environment" (Royal Society (London) Study Group, 1992) [3]. In the context of groundwater contamination, a hazard is defined more precisely as "a potential source of contamination resulting from human activities taking place mainly at the land surface" (Zwahlen, 2004) [3]. In the field of saltwater contamination, the potential source of contamination is saltwater which intrudes from the sea; this phenomenon can be exacerbated, from one side, by natural and climate change possible impacts, and on the other hand from human activities such as overpumping [3].

These concepts being clearly established, it makes it easier to understand the difference between pollution risk and vulnerability. Pollution risk due to seawater mixing depends not only on vulnerability but also on the existence of hazards in the proximity of the coast (i.e. significant groundwater pumpage or SLR or both). It is possible to have high aquifer vulnerability but no risk of SWI, if there is no significant groundwater pumpage or SLR in the proximity of the coast; and to have high pollution risk in spite of low vulnerability, if the groundwater pumpage or SLR is exceptional. It is important to make clear the distinction between vulnerability and risk. This is because risk of SWI is determined not only by the intrinsic characteristics of the aquifer, which are relatively static and hardly changeable, but also on the existence of intensive activities of groundwater pumpage or SLR along the coast, which are dynamic factors. [59]

In the same way as for vulnerability assessment, risk mapping may be used as a tool for decision makers and groundwater managers. However no standard method has been developped yet. A literature review of the main assessment approaches is proposed in the next sub-sections, based on real case-studies.

4.3.2. Aquifer vulnerability and seawater intrusion risk using GALDIT, GQI_{SWI} and GIS: case of a coastal aquifer in Tunisia [46]

In this paper [46], Trabelsi et al. propose an integrated approach to investigate SWI in semiarid regions due to water over-abstraction. The study area is the Sfax basin which is located in the eastern part of Tunisia. This coastal aquifer is under tremendous stresses due to the increase in population and due to agricultural activities and therefore SWI has become a serious concern in this region. The method built in this paper aims at assessing SWI risk through the integration of the GALDIT model, the GQI_{SWI} approach and GIS. This assessment produces three types of maps (vulnerability, hazard and risk) which may help to spotlight the areas threatened by SWI. This way it provides a useful decision-making tool for groundwater management. [46]

For vulnerability assessment, two types of maps are built, the first one using the classical GALDIT approach (which was described in the sub-section 4.2.2) and the second one using the groundwater quality index for SWI (GQI_{SWI}, which was introduced in the sub-section 4.2.3). The authors suggest the use of the GQI_{SWI} as a complementary methodology to the GALDIT one to verify, discuss and compel the shortcomings of the GALDIT model. [46]

For hazard assessment, an index is firstly derived based on the spatial distribution of the pumping wells active in the time of investigation. The general idea behind the construction of this index is that the higher the number of pumping wells over an area, the larger the volume of extracted water and therefore the larger the hazard. This index shows three ranges of hazard: low (2 wells/km^2), moderate (2-4 wells/km^2) and high (7-12 wells/km^2). The hazard map is then constructed by plotting the index distribution over the investigation area. [46]

Finally, the SWI risk map of the Sfax aquifer is simply obtained through the combinaison of the vulnerability and hazard maps. Indeed, referring the definition provided in the sub-section 4.3.1, the risk was found to be dependent on two elements: (1) the hazard due to human activities, represented in this study by heavy consumption and pumping rates; (2) and the intrinsic vulnerability of the system to SWI which is computed here using the GALDIT index. [46]

4.3.3. Risk Analysis and Mitigation of Seawater Intrusion for the Gaza Strip Coastal Aquifer under Climate Induced Changes [3]

In this Ph.D. dissertation [3], the main objective is to elaborate a framework for a risk assessment methodology by considering both impacts of potential climate changes in hydrological processes (changes in groundwater recharge, SLR) and human induced impacts (over-pumping) that could affect SWI. This methodology is applied to the Gaza Strip hydrogeological basin, located in the Palestinian Territories, in which the problem of SWI is so exacerbated that corrective measures are needed to properly manage the groundwater and to restore it. [3]

The approach of the proposed SWI Risk Analysis methodology is based on the origin-pathway-target model, in which the three elements are: (1) the origin of SWI, which is the seaside boundary of the aquifer; (2) the pathway, which is the horizontal and vertical groundwater flow in the aquifer; (3) the target, which is the water pumped from the wells. Figure 4-2 provides a schematic overview of this model. The risk of groundwater contamination due to SWI thus depends on the

hazard (origin), the vulnerability of the system (pathway) and the potential consequences of a saltwater contamination event, i.e. its impact on the groundwater extracted from wells (target). [3]

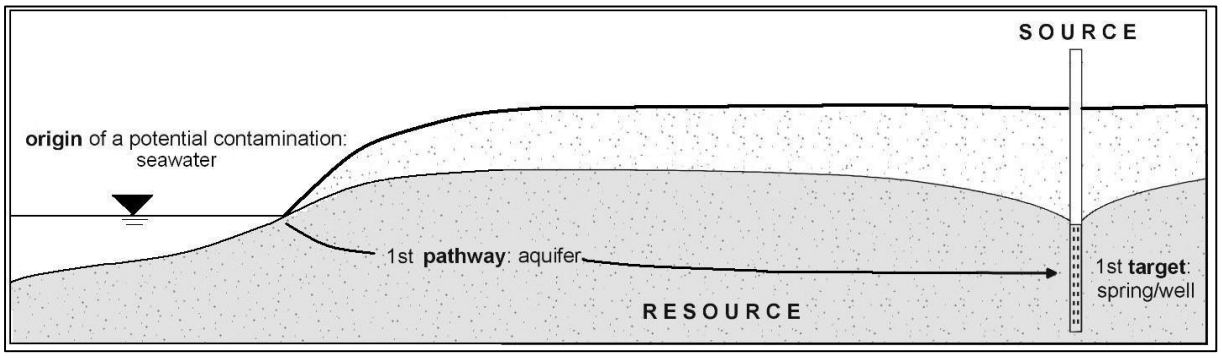

Figure 4-2: Origin-pathway-target model for saltwater intrusion risk methodology [3]

In this study, the Hazard (H) to SWI is obtained by identifying areas where salt concentration is higher than a fixed level in a certain time period; thus, hazard is calculated by the means of a 3D hydrogeological model, allowing to simulate coupled problems of variably saturated flow and contaminant transport in groundwater, in the presence of a fluid phase of variable density, and to assess possible future scenarios of how groundwater system can evolve under climate induced changes conditions and SLR. The Vulnerability (V) to SWI is calculated using the classical GALDIT approach, which was introduced in the sub-section 4.2.2. The possible consequences of a contamination are evaluated on the wells (elements, E) by considering their use (agriculture, industrial, drinking purposes) and their operational pumping values. The Elements rating is based on the radius of the relative 'influence' circular area centred in each pumping well, which is a function of pumping rates. In this study, a simplified configuration of Elements rating is adopted and illustrated in Table 4-3. [3]

Table 4-3: Elements rating [3]

Pumping Wells		Radius	Pumping rate	Elements
Purpose	Level	(m)	(m^3/y)	map colour
Drinking	Very High	700	>1,000,000	Red
		600	500,000 - 1,000,000	
		500	100,000 - 500,000	
		300	<100,000	
Agriculture/Drinking	High	300	<100,000	Orange
Agriculture	Moderate	100	<100,000	Green
Different uses (only sporadic)	Low	100	<50,000	Blue

As the scope of the methodology is to map out zones that are prone to further SWI, the spatial overlay principle is applied to the three thematic maps coming from the three elements described above, namely the hazard map (H), the vulnerability map (V) and elements map (E). The procedure is finalized by the means of simple risk matrix techniques. In a first step, the aggregation of the hazard and vulnerability indices provides a "Risk intensity map", based on the matrix given in Table 4-4. In the second step, this "Risk intensity map" is aggregated within Elements map in a "Total Risk map", according to the matrix set out in Table 4-5. [3]

Table 4-4: Risk intensity map matrix [3]

		Hazard			
		Very High	High	Medium	Low
Vul.	High	Very High	Very High	High	Medium
	Moderate	Very High	High	Medium	Low
	Low	High	Medium	Low	Low

Table 4-5: Total risk map matrix [3]

		Elements			
		Very High	High	Medium	Low
Risk Intensity	Very High	Very High	Very High	High	Medium
	High	Very High	Very High	High	Medium
	Medium	High	High	Medium	Low
	Low	High	Medium	Low	Low

4.3.4. Saline intrusion: a screening tool for the assessment of risk to coastal aquifers in Scotland [60]

This report, commissioned by the Scottish Environment Protection Agency (SEPA), proposes a simple methodology to assess the risk of SWI caused by the construction of new abstraction boreholes close to the coast in Scotland. This methodology, translated into a GIS-based format, relies on very basic level information and is to be used as an initial screening tool for decision-making by SEPA non-technical staff. The role of the maps is to indicate, in broad terms, which boreholes can clearly be excluded from any further investigation and which ones are perceived to be at risk to warrant more-detailed, individual assessment by SEPA hydrogeologists. Therefore, those maps should help to minimise the amount of time specialists have to spend on routine abstraction applications. [60]

The paucity of reliable data on aquifer properties (porosity, permeability, fracture patterns…), on hydraulic gradients or on the rates of recharge for the Scottish coastal aquifers means that a sophisticated method could not be used to construct meaningful maps assessing the risk of SWI for the whole coastline. Therefore risk assessment is based on the four basic and widely available parameters described below [60]:

- Bedrock/superficial aquifers

This distinction is made in order to distinguish between dominantly fracture flow and intergranular flow aquifers. The former is characterized by a higher risk of SWI due to the potential presence of fractures linking the borehole directly to the margins of the freshwater aquifer. By contrast, the latter is less exposed to SWI due to a higher freshwater content provided by the interconnected porosity, which prevents the rapid penetration of saline water towards the borehole. [60]

- Groundwater elevation

This factor is used as a proxy to identify the coastal sites where there is likely to be a flatter gradient present. Generally speaking, flatter hydraulic gradients towards the coast are associated with a higher risk of SWI and tend to be found under low-lying areas, such as raised beaches. Therefore, DEM are used to subdivide the Scottish coastal regions between low (0-30m) and high ground (>30m). [60]

- Abstraction rate

The general trend is that a higher rate of groundwater abstraction leads to a greater risk of SWI. Two situations must be distinguished, as it was discussed earlier in the section 2.4: (1) as long as there is a net flow towards the sea, a reduction in flow due to water abstractions will result in an inland relocation of the seawater-freshwater interface towards a new dynamic equilibrium position; (2) in case of abstractions exceeding freshwater recharge (over-abstractions), the natural seaward hydraulic gradient is reversed and seawater is drawn actively into the aquifer replacing abstracted freshwater. In this study, four ranges of abstraction rates ({<50, 50-100, 100-500, >500} m^3/day) have been chosen accordance with the SEPA abstraction licensing regulations.

- Distance from the coast

In general terms, the greater the distance from the coast, the lesser the risk of SWI for boreholes. It is assumed that no SWI will occur if the source (the well) is located at more than 4 km from the coast. In this study, this reference distance is divided into five bands ({<100, 100-200, 200-500, 500-1000, 1000-4000}m). [60]

The last step consists of the building of the risk assessment maps based on the matrixes given in Table 4-6 and Table 4-7. Two matrixes are considered due to the fact that a distinction must be made between bedrock aquifers and superficial aquifers.

Table 4-6: Risk map matrix for new boreholes in all types of aquifers except superficial aquifers

Abstraction rate (m^3/day)	Distance from coast (m)									
	<100		100-200		200-500		500-1,000		1,000-4,000	
	Low Ground	High Ground	Low Ground	High Ground	Low Ground	High Ground	Low Ground	High Ground	Low Ground	High Ground
<50	Risk	Risk	Risk	No Risk	No Risk	No Risk	No Risk	No Risk	No Risk	No Risk
50-100	Risk	Risk	Risk	Risk	Risk	No Risk	No Risk	No Risk	No Risk	No Risk
100-500	Risk	Risk	Risk	Risk	Risk	Risk	Risk	Risk	No Risk	No Risk
>500	Risk	Risk	Risk	Risk	Risk	Risk	Risk	Risk	Risk	Risk

Table 4-7: Risk map matrix for new boreholes in superficial aquifers

Abstraction rate (m^3/day)	Distance from coast (m)									
	<100		100-200		200-500		500-1,000		1,000-4,000	
	Low Ground	High Ground	Low Ground	High Ground	Low Ground	High Ground	Low Ground	High Ground	Low Ground	High Ground
<50	Risk	No Risk	No Risk	No Risk	No Risk	No Risk	No Risk	No Risk	No Risk	No Risk
50-100	Risk	Risk	Risk	No Risk	No Risk	No Risk	No Risk	No Risk	No Risk	No Risk
100-500	Risk	Risk	Risk	Risk	Risk	Risk	No Risk	No Risk	No Risk	No Risk
>500	Risk	Risk	Risk	Risk	Risk	Risk	Risk	Risk	No Risk	No Risk

4.3.5. Large scale screening of SWI risk in Europe: methodological development and pilot application along the Spanish Mediterranean coast [2]

In this paper, Wriedt and Bouraoui propose a simple screening methodology for large-scale assessment of SWI risk in coastal areas, focussing on potential impacts of water abstractions and using generally available data and simple modelling approaches. This method is based on a two-tiered procedure: (1) Tier 1 consists of an easy-to-use general assessment of SWI risk based on the balance of groundwater recharge and water abstractions; (2) Tier 2 provides a quantitative characterization of SWI for standardized aquifers based on an analytical modelling approach (the Strack solution, introduced in the sub-section 3.4.2). The integration of these two tiers in a GIS environment provides useful maps whose primary goal is to support policy making and water management at larger level. A pilot application was carried out along the Spanish Mediterranean coast to demonstrate the potential capabilities of the methodology and to explore the limitations related to data availability and challenges in data processing.

A schematic outline of the 2-tiered assessment approach is presented in Figure 4-3. The simple Strack analytical solution used in Tier 2 was previously introduced in the sub-section 3.4.2. Therefore, in this sub-section 4.3.5, we focus our attention only on the left part of Figure 4-3, namely the general risk assessment method developed in Tier 1. This assessment first requires the definition of a certain number of assessment points distributed regularly along the coastline. A calculation of abstractions and recharge is then carried out at each assessment point for a set of virtual aquifer domains of different spatial extent ({2.5-5-10-20-40}km). The core issue of the proposed methodology is the use of the local recharge-abstraction balance as a risk indicator. Two general risk classes are defined for this purpose: (1) the transient intrusion class if the net recharge is positive and (2) the over-abstraction class if the net recharge is negative. The risk indicator is finally provided at each assessment point by the number of aquifer domains falling into a specific risk class and it is subdivided into three categories: high risk (>0.66), medium risk (0.33-0.66) and low risk (<0.33). The computations of the assessment points, the recharge and abstractions are further detailed below:

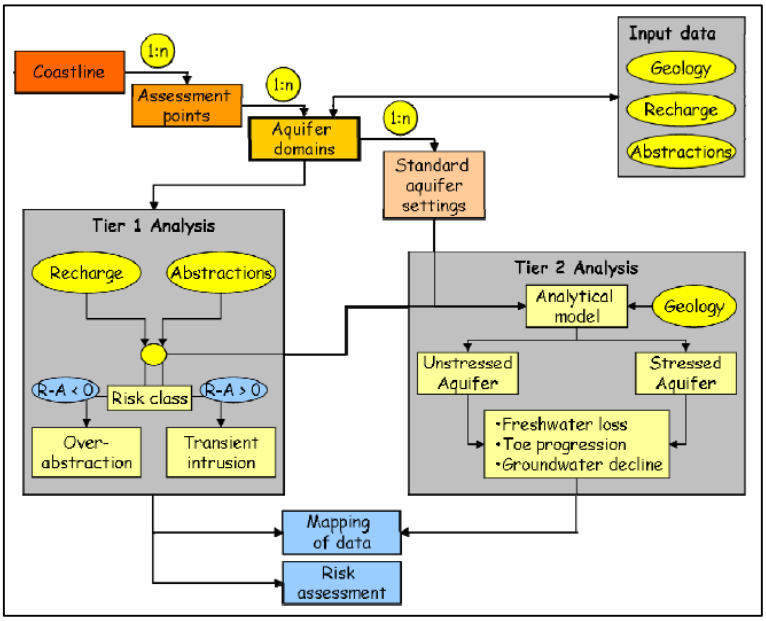

Figure 4-3: General outline of the two-tiered assessment approach [2]

- Assessment points and aquifer domains

The delineation of assessment points and aquifer domains along the coastline is carried out through the following procedure: (1) a centreline is created keeping a constant distance of 2500m from the coastline; (2) all points of a 2500m raster falling within a certain distance of the centre-line (tolerance of 880m) are selected as assessment points; (3) a set of circular-shaped virtual aquifer domains is created around each assessment point (radius: {2.5-5-10-20-40}km); (4) the basic input data, namely groundwater recharge and water abstractions, are defined for each aquifer domain as the average values over the domain. This procedure is illustrated in Figure 4-4.

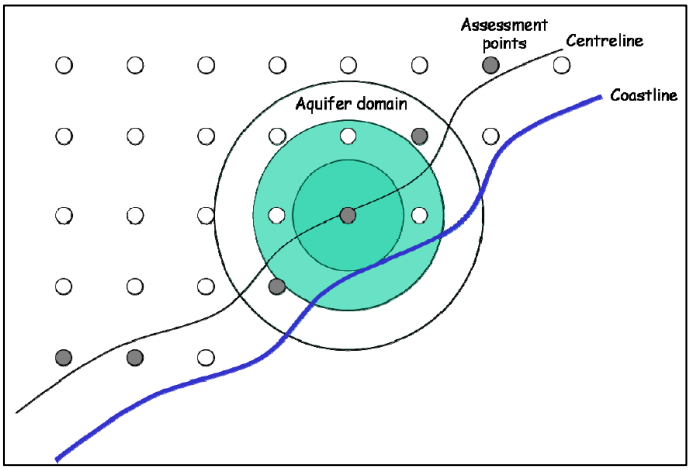

Figure 4-4: Delineation of assessment points and aquifer domains [2]

- Groundwater recharge

Groundwater recharge is estimated through a tentative, very simple three-step approach using the climatic data provided by the MARS-Database in a 50X50km raster. The first step consists in computing monthly water balances, based on equation (31):

$$\mathrm{WBal_M} = \sum_{\mathrm{d}} (\mathrm{P_d} - \mathrm{ETP_d}) \tag{31}$$

Where:

- $\mathrm{WBal_M}$ = water balance of month m [mm];
- P = precipitation [mm];
- ETP = potential evapotranspiration [mm];
- M = month index;
- d = day index;

From there, the annual water surplus is computed as the sum of positive water balances:

$$\mathrm{WSurplus_A} = \sum_{\mathrm{M}} \mathrm{WBal_M}\,, \qquad \mathrm{M}|\mathrm{WBal_M} > 0 \tag{32}$$

Where:

- $\mathrm{WSurplus_A}$ = annual water surplus [mm];
- A = year index;

The final step of the modelling is to provide an estimation of groundwater recharge by separating water surplus into groundwater recharge and surface runoff. This estimation is given by equation (33) which constitutes a decrease of groundwater recharge with increasing slope and limits groundwater recharge in flat areas:

$$GWR_A = WSurplus_A . \left[1 - \frac{WSurplus_A}{MaxWS}\right]^{0.5} . \left[1 - \frac{Slope}{100}\right]^2 \quad (33)$$

Where:

- GWR = groundwater recharge [mm];
- Slope = slope [%];
- MaxWS = maximum water surplus (= 2,000mm in Europe);

➢ Water abstractions

Generally speaking, ground- and surface water sources may be used to meet water demands and water may be transported over large distances. Therefore it is almost impossible to trace back the exact origin of the water. The pilot study along the Spanish coast proposes a general attempt to assess groundwater abstractions in this area. In this study, groundwater abstractions are defined as the sum of agricultural abstractions, industrial abstractions and public and domestic abstractions while abstractions for electricity cooling in thermal and nuclear power plants are assumed to be taken from surface waters only. The idea is to use the European database EUROSTAT to collect information about abstractions on national level. Then this information is disaggregated to a local level (raster data set of 100m resolution) based on the spatial distribution of suitable proxy measures, as depicted in Figure 4-5. It is important to point out that the final raster data sets reflect the locations of water uses rather than of water abstractions.

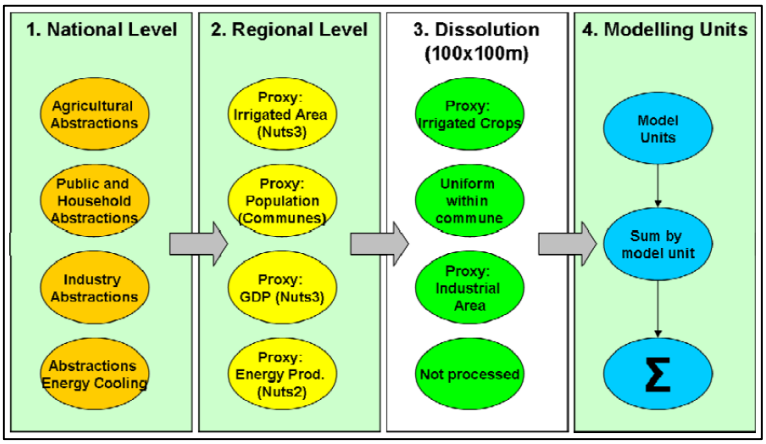

Figure 4-5: Scheme for disaggregation of water abstraction data [2]

In conclusion, it should be reminded that this risk analysis does not predict real occurrences of SWI nor can be used for quantitative assessment of real-world intrusion problems, as the approach is not applied and validated to real aquifers. Moreover, it combines optimistic recharge estimation with worst case estimation of abstractions and therefore future improvement is necessary concerning the assessment of the input data. Anyway, this methodology is relatively simple, robust and promising, allowing assessment of future intrusion risks (scenario analysis) based on climate change, land use changes and changes in water demand.

Chapter 5
The Emilia-Romagna coastal area

5.1 Geographical location

The study area is located in the north-eastern part of Italy (see Figure 5-1) and consists of a small portion of the huge Po River plain that stretches between the Southern Alps and the Northern Apennines.

More precisely, the study area covers the four coastal provinces (Ferrara, Ravenna, Forli-Cesena and Rimini) of the Emilia-Romagna region - that is, an area of approximately 7730km^2 (see Table 5-1). It is delimited by the following physical boundaries:

- In the north: the Po di Goro, i.e. one of the Po River branches;
- In the east: the Adriatic Sea with a coastline of about 135km [61];
- In the south: the promontory of Gabicce where the Apennines mountains meet the Adriatic Sea;
- In the south-west: the Northern Apennines;
- In the west: the administrative boundaries of the Ferrara and Ravenna provinces;

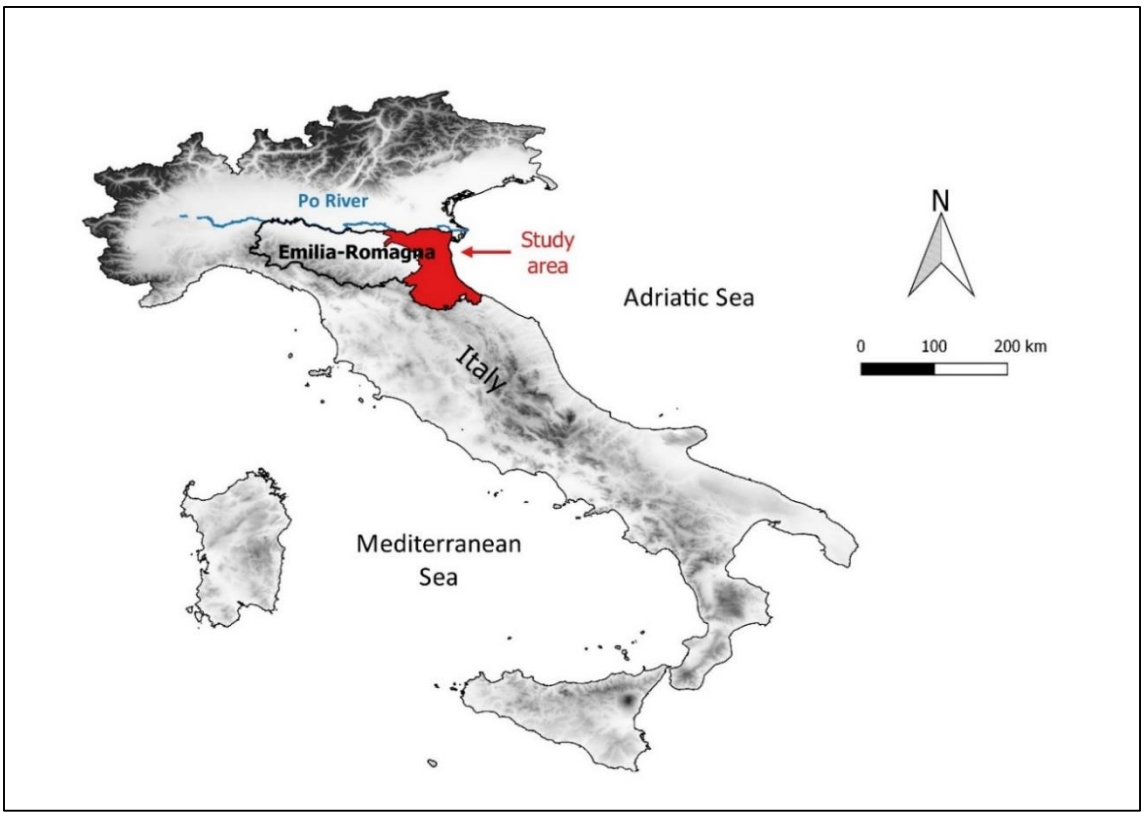

Figure 5-1: Location of the study area

Table 5-1: Emilia-Romagna - Administrative divisions [62]

Province	Code	Population	Area (km^2)
Piacenza	PC	284,885	2,589
Parma	PR	431,419	3,449
Reggio-Emilia	RE	517,374	2,293
Modena	MO	686,104	2,689
Bologna	BO	973,255	3,702
Ferrara	FE	357,471	2,632
Ravenna	RA	383,945	1,858
Forli-Cesena	FC	387,200	2,377
Rimini	RN	325,219	863
Total	EMR	4,346,872	22,446

5.2 Climate

The climate of the study area is Mediterranean and characterized by warm summers and mild winters: the average annual temperature is 13-14°C as depicted in Figure 5-2 (on the top), but varies from -5°C to 10°C in the winter period and from 20°C to 35°C in the summer months [63].

The average annual rainfall is comprised between 600 and 800mm/year (see Figure 5-2 in the bottom) but is evenly distributed throughout the year: it is usually concentrated in the spring and autumn months whereas the summer season is very dry [63], [64].

Finally aquifer recharge from precipitation surplus is minimal due to a reference evapotranspiration rate of about 650mm/year. This recharge mainly occurs during the winter months. [64]

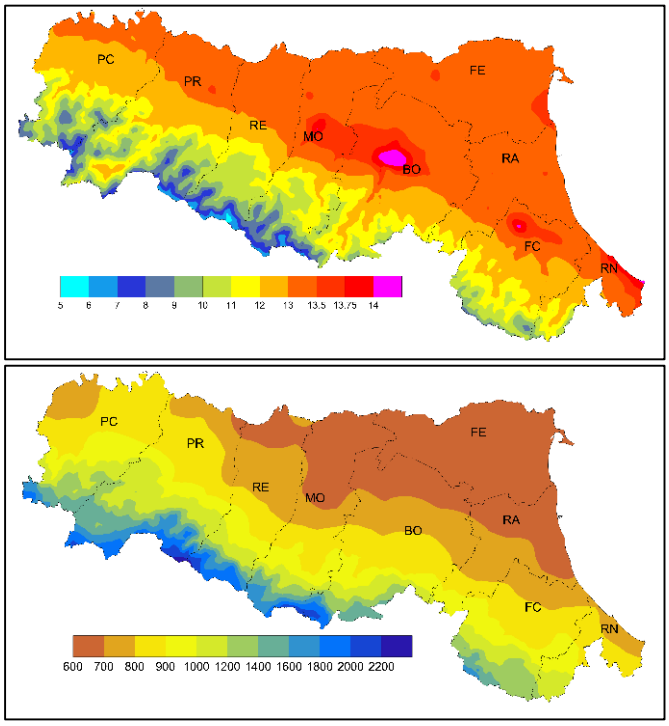

Figure 5-2: Annual average temperature (on the top) and rainfall (on the bottom) for the Emilia-Romagna region and based on a long-term database (1961-2015) [65]

5.3 Geological evolution

The large sedimentary basin (about 46,000km^2) of the actual Po River originates from the pit grown up between Oligocene (34 – 23.5mya) and Miocene (23.5 – 5.3mya), due to the emergence of the Apennines and the presence of the Alps already almost fully emerged [66]. Since then, the region has experienced several marine transgressions[14] and regressions[15] due to eustatic and climatic fluctuations. This has led to a stratigraphic architecture that is depicted in Figure 5-3.

This Figure 5-3 shows a cross-section of the upper 700-800m of the sedimentary sequence from the Apennine foothills to the Emilia-Romagna coastline. It can be seen the alternation of continental and marine sedimentation leading to the development of a multiaquifer freshwater system. This system is divided into two major confined hydrostratigraphic units known as A and B, each of them being characterized by a number of high-permeable interconnected layers (named respectively A1 to A4 and B1 to B4). For the sake of completeness, it should be pointed out that this multiaquifer system is covered by a thin surface layer called A0 (not represented in Figure 5-3) that stands for the phreatic aquifer. [67]

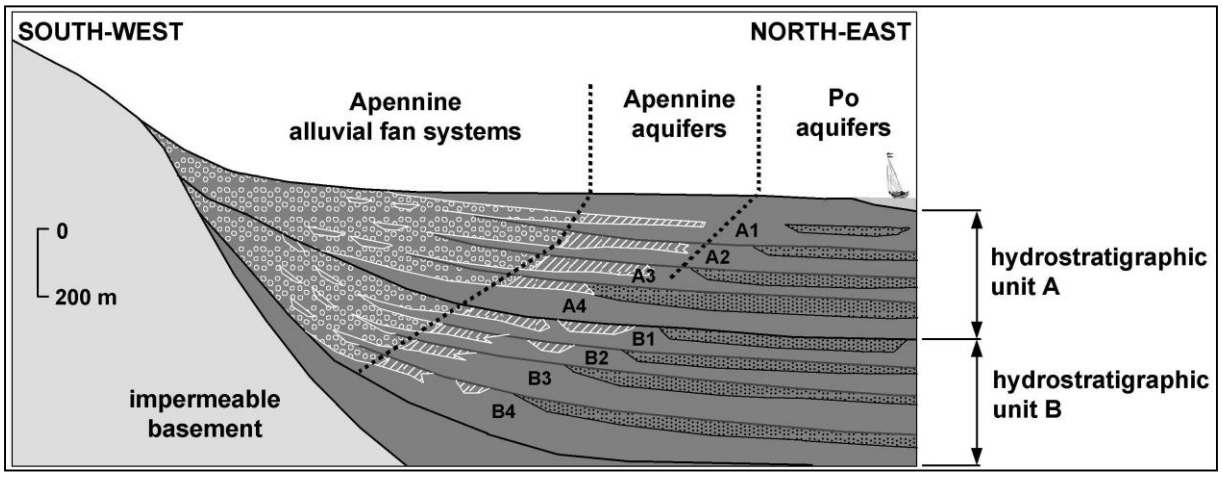

Figure 5-3: Schematic lithological section showing the main formations of the multiaquifer system underlying the Emilia-Romagna coastland [67]

Among all these layers, solely the aquifers A1 to A4 are of practical interest and may be exploited for the extraction of freshwater, the others being too deeply confined. The scope of this work is therefore limited to the study of the aquifer body A (including the phreatic part A0). In order to better understand the structure of this aquifer, a more detailed description of its geological evolution is provided herebelow. For the sake of clarity, the description is limited to the sallow part of the aquifer, namely the phreatic aquifer body A0 and the first confined aquifer body A1, but similar processes may be assumed to be behind the formation of the deeper layers (i.e. A2 to A4).

This shallow part of the aquifer was controlled by two main transgression-regression depositional cycles that occurred during the late Quaternary and formed a sequence of sand and silty clay units, as shown in Figure 5-4 [68]:

[14] A marine transgression is a geologic event during which sea level rises relative to the land and the shoreline moves towards higher ground, resulting in flooding [85]

[15] Marine regression is a geological process occurring when areas of submerged seafloor are exposed above the sea-level [86]

During the Pleistocene (1.8mya – 12kya) → formation of the confined aquifer body A1

- The Eemian interglacial period (130 – 115kya)
- The Würm glaciation (115 – 12kya)

This period occurring during the last years of the Pleistocene was the most recent glacial period and is commonly known as the Ice Age. It was firstly composed of a regression system tract (FRST) in the period 115 - 30kya, characterized by a high lowering of SL, i.e. about 120m below the present level and by a shift of the paleoshoreline 250km South-East of its current position [66], [64]. During the following stage, i.e. a lowstand tract (LST) over the period 30 - 12kya, the north Adriatic area became a sedimentation floodplain with wide and little carved valleys [66]. In the stratigraphic sequence, the roof of the Würmian continental silty-clay formation is at a depth varying from 20m in the western part to 30m at the present shoreline [69].

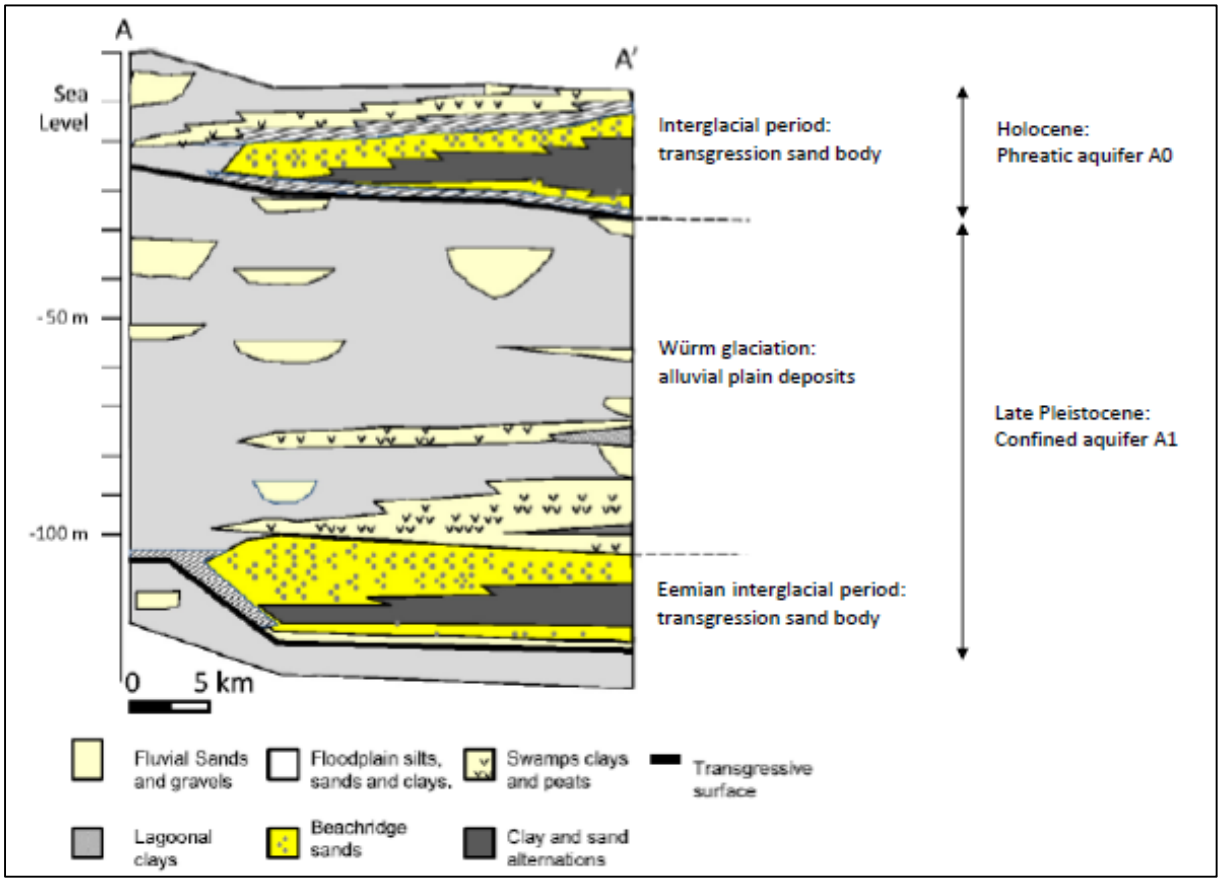

Figure 5-4: Stratigraphic cross-section of the phreatic aquifer body A0 and the first confined aquifer body A1 (modified from [27])

During the Holocene (12kya to present) → formation of the phreatic aquifer body A0:

- The Holocene interglacial period

This period was firstly composed of a transgressive system tract (TST), known as the Flandrian transgressive phase, which occurred over the period 15 - 5.5kya, brought back the seawater into the North Adriatic Sea and drowned the continental deposits [70]. During the optimum climatic period, approximately 5.5kya, the paleoshoreline was located 20-30km westwards compared to

its current position [64]. The sedimentation of this period consists of beach sands with interspersed fine-grained deltaic deposits and is organised as followed from top to bottom [69]:

- at the surface, a thick medium-grained sand unit ranging from 0 to -10m b.m.s.l.;
- at the bottom, a second thinner fine-grained sand unit laying above the Pleistocene alluvional-plain deposits with a thickness of 0 to 5m;
- in between, a clayey-silty and sandy-silty unit ranging from -10 to -21m b.m.s.l.;

The last phase, i.e. highstand system tract (HST), transformed the sedimentation from marine to continental in the study area [63]. It started 2000 years ago and corresponds to a strong progradation of the Po delta, due to a greater contribution of river sediments and increase erosion combined with subsidence [66]. This predominant progradational trend led to the formation of a series of coastal sandy bodies composed of marsh-lagoonal (delta plain) clays, beach-ridge (delta front) sands and shallow-marine (prodelta) clay-sand alternations [69], [70].

This general sedimentation sequence of the modern Po delta is depicted in Figure 5-5, where 8 minor cycles coming from small positive/negative SL fluctuations have been identified [66], [70]. It can be seen that the coastal aquifer is generally unconfined except in its western part where some thin layers of continental alluvial deposits (mostly silt and clay deposited in marshes and lagoons) overlay the aquifer sands and tend to make the aquifer semi-confined [64], [70].

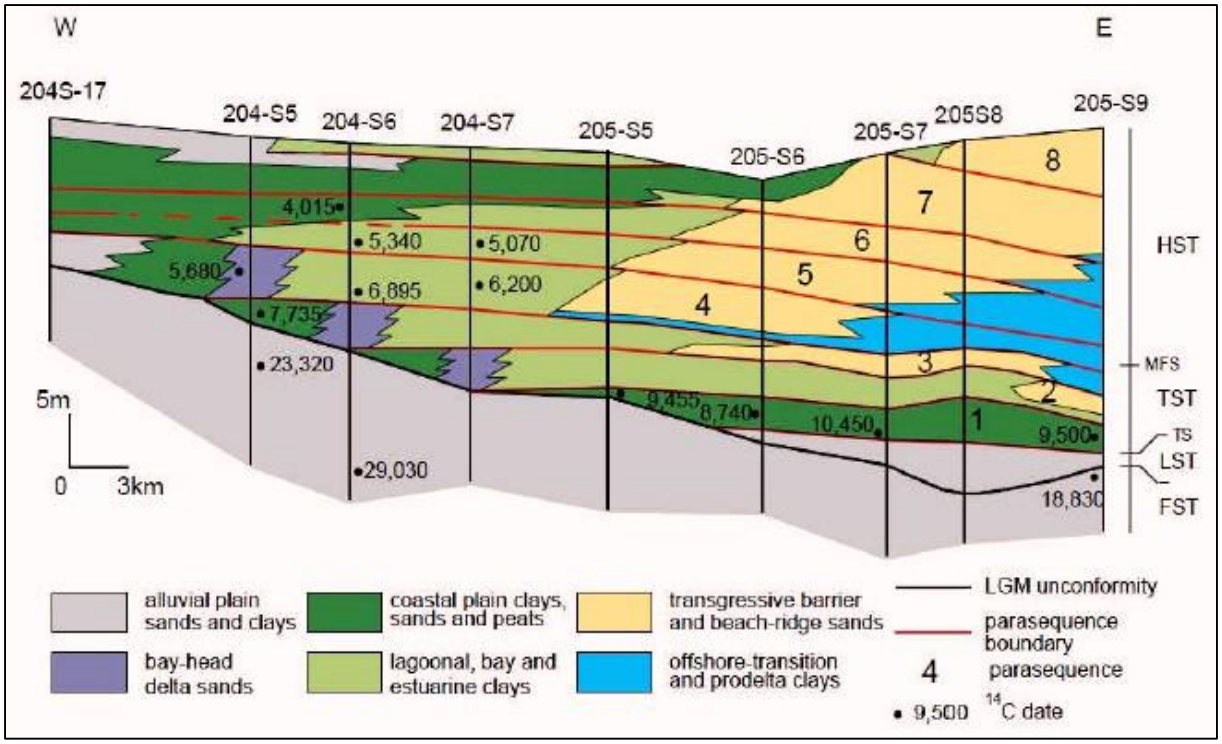

Figure 5-5: Section of the phreatic aquifer A0 of the Southeast Po valley, with the transgressive-regressive sequence subdivided in 8 minor cycles [66]

5.4 Land use

From Figure 5-6, it can be seen that the land use in the coastal area is mostly composed of three different types of environments:

- Urban areas (cities, industries, urbanized coastline for touristic activities…);
- Natural areas (pinewoods, surface water bodies such as wetlands or lagoons…) [27], [66];
- Agricultural areas which represents the largest portion of the study area. A large part of this cultivated surface is equipped with irrigation systems and consists of horticultural crops (vineyards, orchards…) or extensive crops (barley, wheat, maize…) [63];

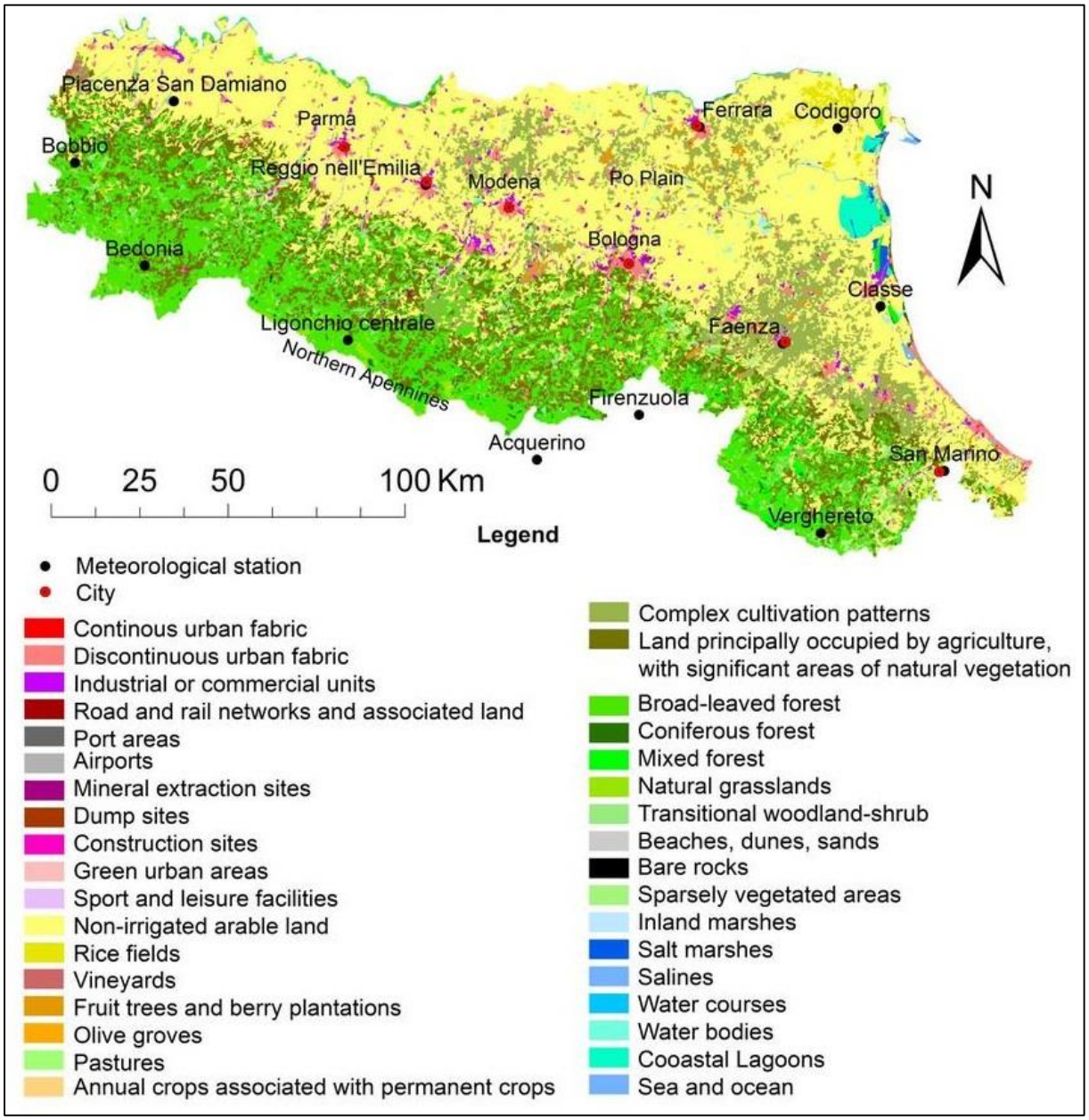

Figure 5-6: Land cover and land use of the Emilia-Romagna region [71]

5.5 Topography and subsidence

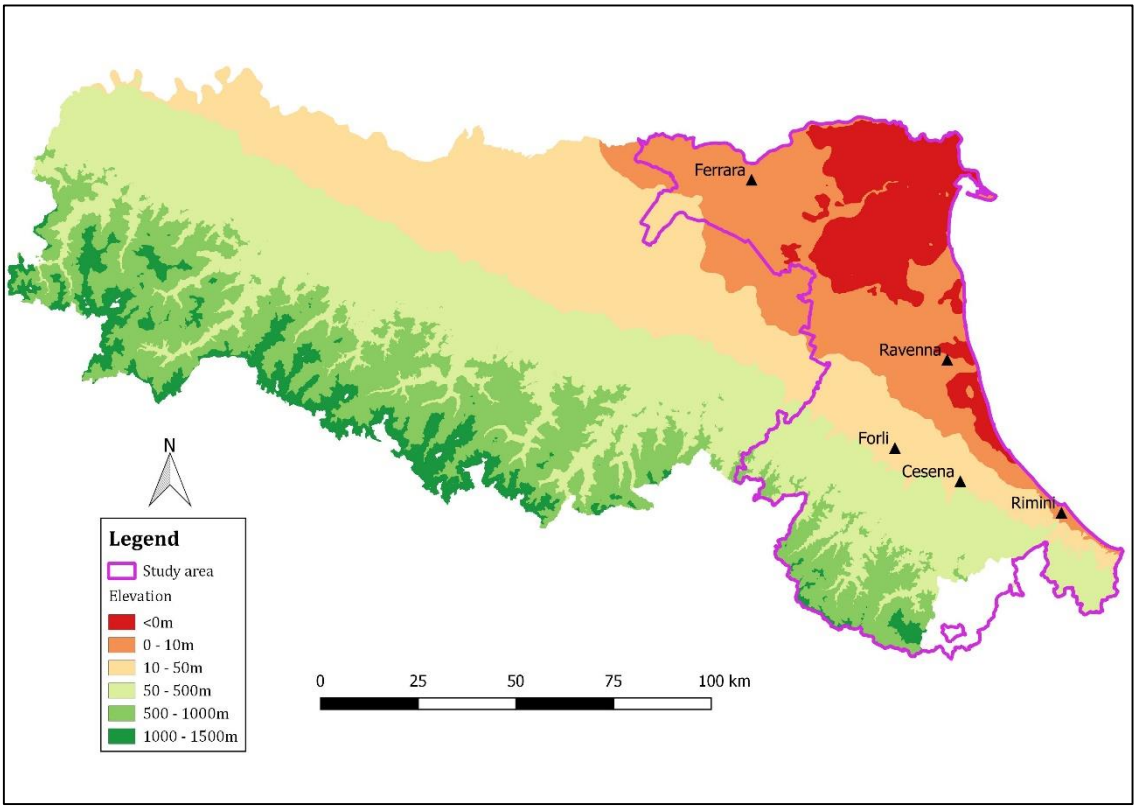

Figure 5-7: General topography of the study area

From Figure 5-7, it can be seen firstly that the study area presents a relatively flat topography in the north, with a large part of the coastline located below SL or only a few meters above SL. The topography is then slowly increasing in the NE-SO direction towards the Apennines.

This general pattern in the topography may be explained by the fact that the study area has been experiencing a natural subsidence over the entire Quaternary due to the compaction of alluvial deposits [69], [66]. The average speed of subsidence is approximately 1-3mm/year [66].

However, during the last century and more particularly during the rapid industrialization of the area after World War II these rates of natural subsidence were dramatically emphasized by anthropogenic factors to values up to ten times larger [66], [67]. The main anthropogenic factors responsible for this alarming subsidence are known to be [72]:

- Groundwater and hydrocarbons extraction (main cause);
- Land reclamation for agriculture leading to embankment interventions and to the control of watercourses, consequently reducing sedimentary supply in the coastal area [66];
- Urban loading;

Consequently those phenomena have dropped a large proportion of the coastline b.m.s.l. [69]. Today the subsidence still continues over a few-kilometre-wide coastal strip at a rate that is larger than the natural one but has been significantly reduced thanks to the construction of new public aqueducts (i.e. CER=Canale Emiliano-Romagnolo, see the next section 5.6) in the 1970s and 1980s using surface water rather than groundwater [69].

5.6 Hydrology

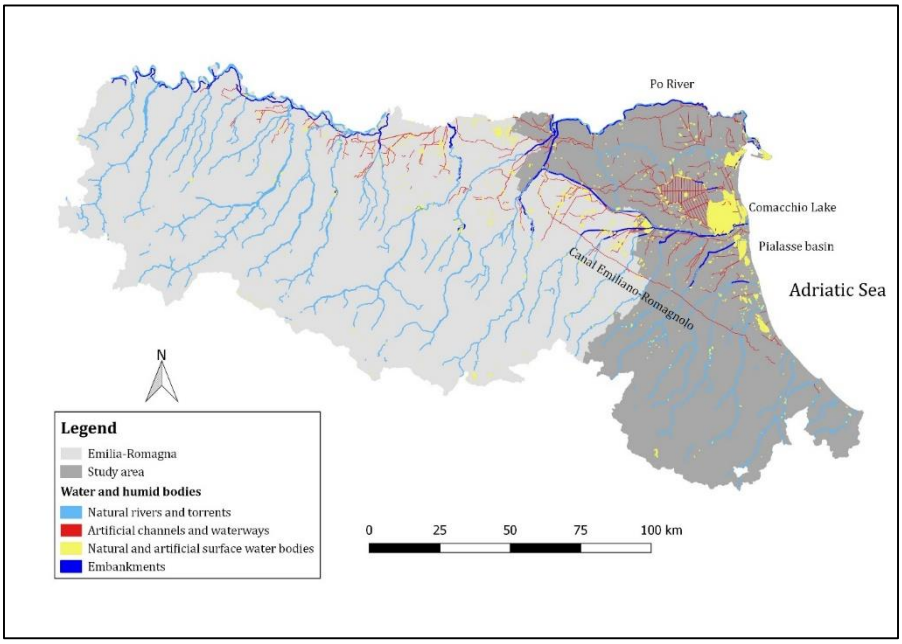

Figure 5-8: General hydrology of the study area

The hydrological system of the study area is extremely complex because it is constituted by numerous natural and non-natural water bodies, as depicted in Figure 5-8 [66], [64]:

- Extensive drainage network (in red in Figure 5-8)

The construction of the extensive land reclamation drainage system started more or less 150-200 years ago and was conducted in order to lower the phreatic level and to keep the land dry to allow for urban and industrial settlements as well as for agricultural activities [68], [63]. This drainage system consists of a dense network of canals organized around pumping stations that are typically located inland, several kilometres from the shoreline [68], [63].

These channels are used in different ways according to the climate: in winter, they are used to drain the area and to collect rainfall water that is then lift into a main canal by the pumps and conveyed to the sea [66], [68]. By contrast in the summer season, the same channels are kept filled with water to ensure irrigation of the surrounding agricultural areas [66].

- Natural rivers (in blue in Figure 5-8)

The natural hydrological network of the study area is composed of the Po River, its tributaries and some other natural rivers flowing from their sources in the Apennines towards the Adriatic Sea. Some of these rivers, pointed out in dark blue in Figure 5-8, underwent multiple actions of rectifications and embankment during the land-reclamation works in the last century [63].

Furthermore most of the rivers in the study area are characterized by water flows that are mostly derived from surface runoff rather than from sources [66]. As a consequence their regimes are directly influenced by the variable rainfall pattern described in the section 5.2, with highly reduced discharges during the dry summer season, that maintain average annual values relatively low [66].

Until some decades ago the main source of irrigation water was groundwater from the phreatic and confined aquifers, but the increase of subsidence rates forced to change the water supply from groundwater to surface water [63]. Therefore those rivers are also tapped for irrigation during the summer period [63].

- The Emiliano-Romagnolo Channel

The Emiliano-Romagnolo Channel (i.e. Canale Emiliano-Romagnolo CER) represents one of the most important hydraulic works of all Italy and is active since 1960 in Emilia-Romagna to deal with the problem of water scarcity during the summer period [66]. Indeed during this period, there is not enough water in the minor rivers crossing the study area (see previous paragraph) and therefore some additional water is taken from the Po River by means of the Canal Emiliano-Romagnolo and is brought into the irrigation systems via the same channels that are used for drainage in the winter [63]. This artificial channel has a length of 135km between the Po River and the Uso River and diverts an average of 7 million m^3 per year [73].

5.7 Problematic: salinization

Anthropogenic aquifer salinization in the study area is due to the combination of two main drivers – land subsidence and extensive mechanical drainage – and may be divided into two main classes (the same as the ones that were introduced in the section 2.4) [27], [63]:

- Seawater intrusion from the coast

A significant part of the study area has dropped b.m.s.l. over the last decades due to large rates of subsidence caused by anthropogenic activities, as described in the section 5.5. As a result, those areas don't have a hydraulic head able to stop the hydraulic gradients of seawater imposed by the Adriatic Sea, therefore leading to the intrusion of large volumes of seawater [63], [70].

- Upwelling of relic saline and hypersaline groundwater

The phreatic aquifer in the study area is affected by relic saline and hypersaline groundwater [64]. This water originates from the Holocene period when it was contained in vast coastal lagoons connected to the sea [64]. Those lagoons were buried during the Holocene interglacial period keeping a high degree of salinity in pore-water [64]. Since then this SW has not been flushed completely by freshwater due to the very low natural rate of recharge of the aquifer (see section 5.2) [68]. As a consequence, the aquifer is now threaten by the up-coning of such highly saline groundwater due to the hydraulic gradients induced by the drainage system and by the pumping wells [64], [27].

In this context the next step naturally consists in applying the GALDIT-Index to the Emilia-Romagna coastal area in order to give a qualitative overview of the vulnerability of this area to SWI. This analysis (the general procedure was introduced in the sub-section 4.2.2) will be limited to the phreatic aquifer body A0 and the confined hydrostratigraphic unit A as described here-above in the section 5.3. Finally it is important to note that the GALDIT-Index doesn't take into account the SWI due to the upwelling of relic saline water.

Chapter 6
Results and discussion

6.1 General approach

In order to quantify this general problematic of salinization that is affecting the Emilia-Romagna coastal area, the next step would naturally consist in applying one of these methods that were introduced in Chapter 4. In this thesis, it is the GALDIT approach that has been chosen due to its capacity to provide relatively quickly a general overview of the vulnerability of a region to SWI. It has also been decided to limit the analysis to the two shallowest aquifer bodies that were described in the section 5.3 of Chapter 5, namely the phreatic aquifer body A0 and the confined hydrostratigraphic unit A. For these two bodies, the same general approach has been followed and is conceptually described in Figure 6-1. Finally it is important to keep in mind that the GALDIT-Index only takes into account the SWI from the coast, but not the one due to the upwelling of relic saline water.

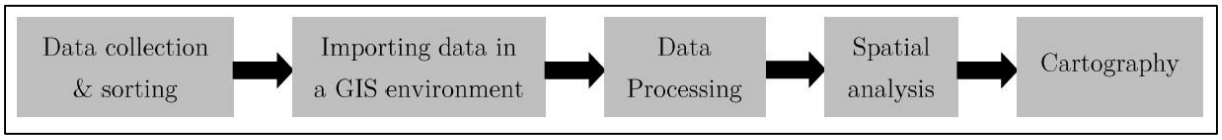

Figure 6-1: Conceptual model for the vulnerability analysis

The methodology for this work includes the collection, processing and spatial analysis of data and is based on the procedure that was described in the sub-section 4.2.2:

- Data collection and sorting

Data are collected for every monitoring network, using various sources [54]: (1) direct field data (geographical coordinates of the monitoring wells, distance from the shore, depth, groundwater level etc.); (2) results of laboratory analysis of water samples (chemical parameters); (3) secondary data (geological sections, map of hydraulic conductivity, DEM). All those data are then sorted and solely the relevant parameters that are necessary to derive the GALDIT-Index are kept and assembled in an EXCEL spreadsheet.

- Importing of the data in a GIS environment

The data are integrated within a GIS environment, thanks to the geographical coordinates of each well. A Geographic Information System (GIS) was defined in Chapter 4 as a computer-based tool that analyses, stores, manipulates and displays geographic data on a map [48]. By connecting data with geography, this gives people a geospatial perspective and helps them more easily understand patterns and relationships [48], [49]. In this project, the free, open source software QGIS© has been used while the coordinate reference system (CRS) has been fixed to [ETRS89 / UTM zone 32N - EPSG: 25832].

- Data processing [74], [75]

Because of high cost or limited resources, data collection is usually conducted only in a limited number of selected point locations (i.e. at the location of the wells). The purpose of data processing is then to rasterize the compiled database (i.e. to create a raster surface covering an entire area) by using interpolation techniques that estimate values for all raster cells based on a limited number of sample data points (i.e. vector points with known values). QGIS© offers several interpolation techniques, among which the most widely used are kriging, the Inverse Distance Weighted (IDW) method and the Triangulated Irregular Network (TIN) method. Briefly, kriging is an advanced tool based on geo-statistics and that was presented in the section 4.2.3; IDW interpolation gives weights to sample points, such that the influence of one point on another declines with distance from the new point being estimated; TIN interpolation uses sample points to create a surface formed by triangles based on nearest neighbour point information. In this project it is the IDW method that has been selected to produce the maps that give the spatial distribution (i.e. the range) of the 6 parameters.

- Spatial analysis [75]

Spatial analysis is used to manipulate the 6 newly created maps in order to extract new information. Ratings (R_i) are assigned to each parameter layer (i.e. to each pixel) based on the range of values of the parameter and then equation (23) is implemented in the 'Raster Calculator' tool of QGIS© (i.e. data layers are overlaid and weighted) in order to produce the final GALDIT map.

- Cartography

This final step consists in improving the layout of the maps by adjusting properties and adding features such as a title, a legend, a colour scale, a scale bar or labels in order to provide clear, high-quality maps. All these steps can be achieved by using the 'Print Composer' tool of QGIS© which finally allows to export the final maps to image formats. All the relevant maps related to the phreatic and confined aquifer bodies are presented and discussed in the next sections 6.2, 6.3 & 6.4. It has been decided to adopt the same unique resolution for all the maps, namely 100m × 100m. This resolution has been chosen as a trade-off between accuracy and computational burden.

6.2 Ravenna phreatic aquifer

6.2.1. Monitoring network

As described in Section 5.3, the phreatic aquifer body A0 is generally unconfined on its coastal side and becomes semi-confined when moving westwards where it is overlaid by thin layers of continental alluvial deposits (mostly silt and clay deposits). This situation is depicted in Figure 6-2 (on the left) which gives an overview of the general extent of the phreatic aquifer body, considering the outcropping part and the semi-confined part.

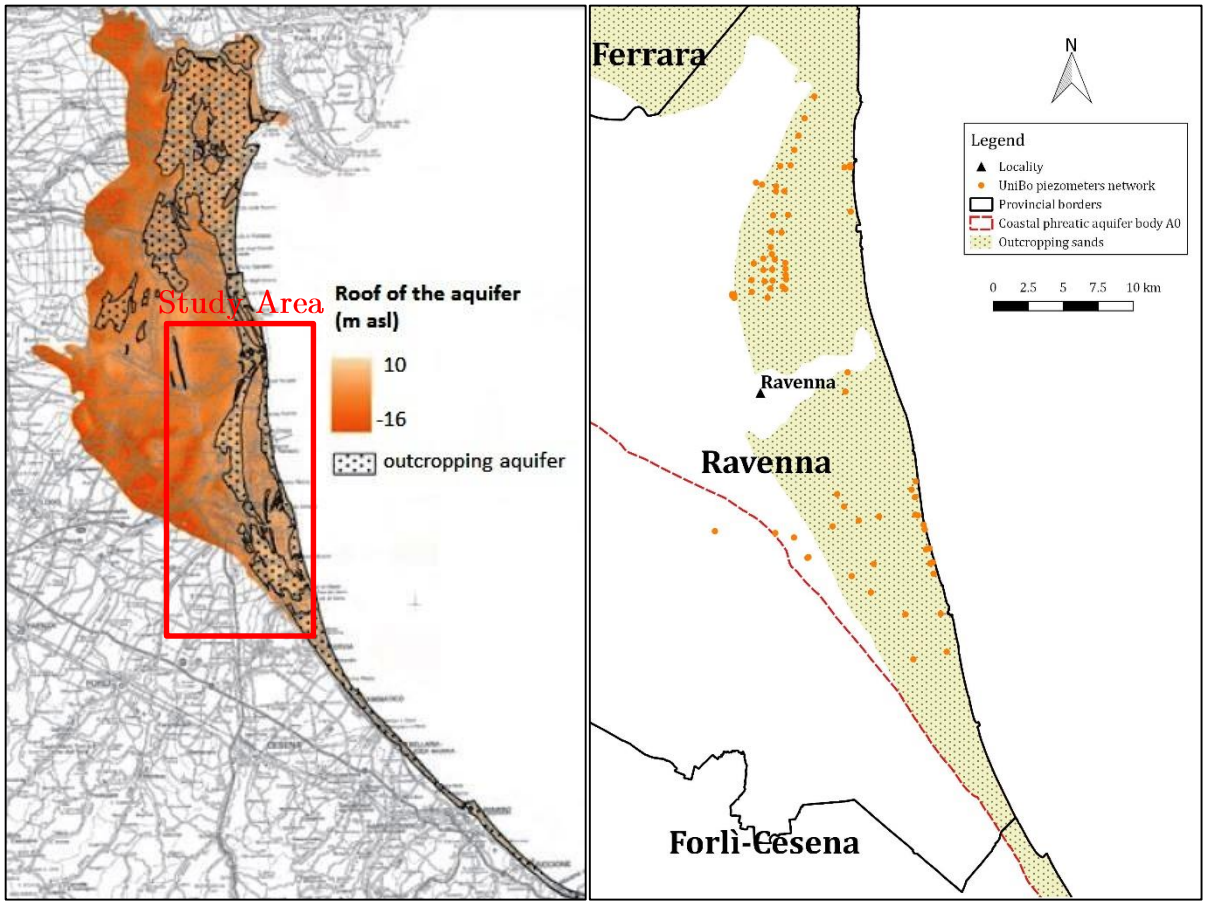

Figure 6-2: Description of the extent and the Emilia-Romagna coastal phreatic aquifer A0 (on the left, modified from [66]) and monitoring network of piezometers from the University of Bologna (on the right)

To study the impact of SWI on the coastal phreatic aquifer in the province of Ravenna, a network of 78 piezometers has been implanted (See Figure 6-2, on the right). This network is the result of an agreement between the University of Bologna (UniBo), ENI and the Municipality of Ravenna and it is part of the "Coastal Salt Water Intrusion Project". [66]

In this context, a lot of different parameters were measured, recorded, collected or processed during the monitoring programme in June 2010, regarding the wells' characteristics (depth, geographical location, distance from the coastline), the aquifer structure and properties (thickness, hydraulic conductivity) and the groundwater properties (groundwater table, chemical and isotopic analysis on samples, temperature profiles, salinity, electrical conductivity). A table summarizing only the relevant information for this particular case study is provided in Appendix A.

Because of this abundance of data, the application of the GALDIT index to the Ravenna phreatic aquifer is rather straightforward and the results relatively easy to derive. This first base case is therefore used as a reference for the validation of the GALDIT procedure as well as the results that are presented in the next section 6.3 for the whole Emilia-Romagna phreatic aquifer.

From Figure 6-2 (on the right), it can be seen that most of the monitoring piezometers are located in the outcropping sands (i.e. the part of the phreatic aquifer that is not semi-confined) beside eleven of them. For this reason, the extent of the study area will be limited to this zone of outcropping sands around the city of Ravenna.

6.2.2. Mapping of the parameters

- Groundwater occurrence

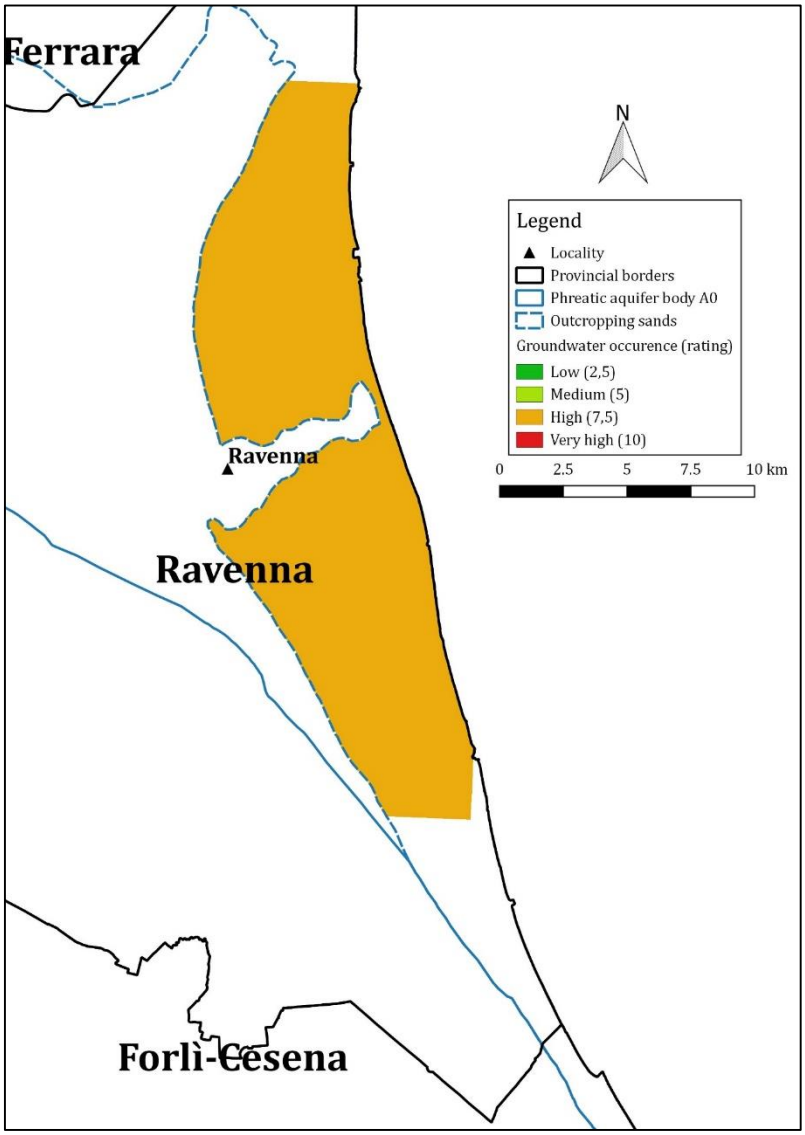

Figure 6-3: Groundwater occurrence (G) - rating

As mentioned hereabove, the analysis focuses on the part of the aquifer that is mainly unconfined (i.e. the outcropping sands) and therefore the rating for the groundwater occurrence corresponds to 7.5 (see Figure 6-3).

- Aquifer hydraulic conductivity

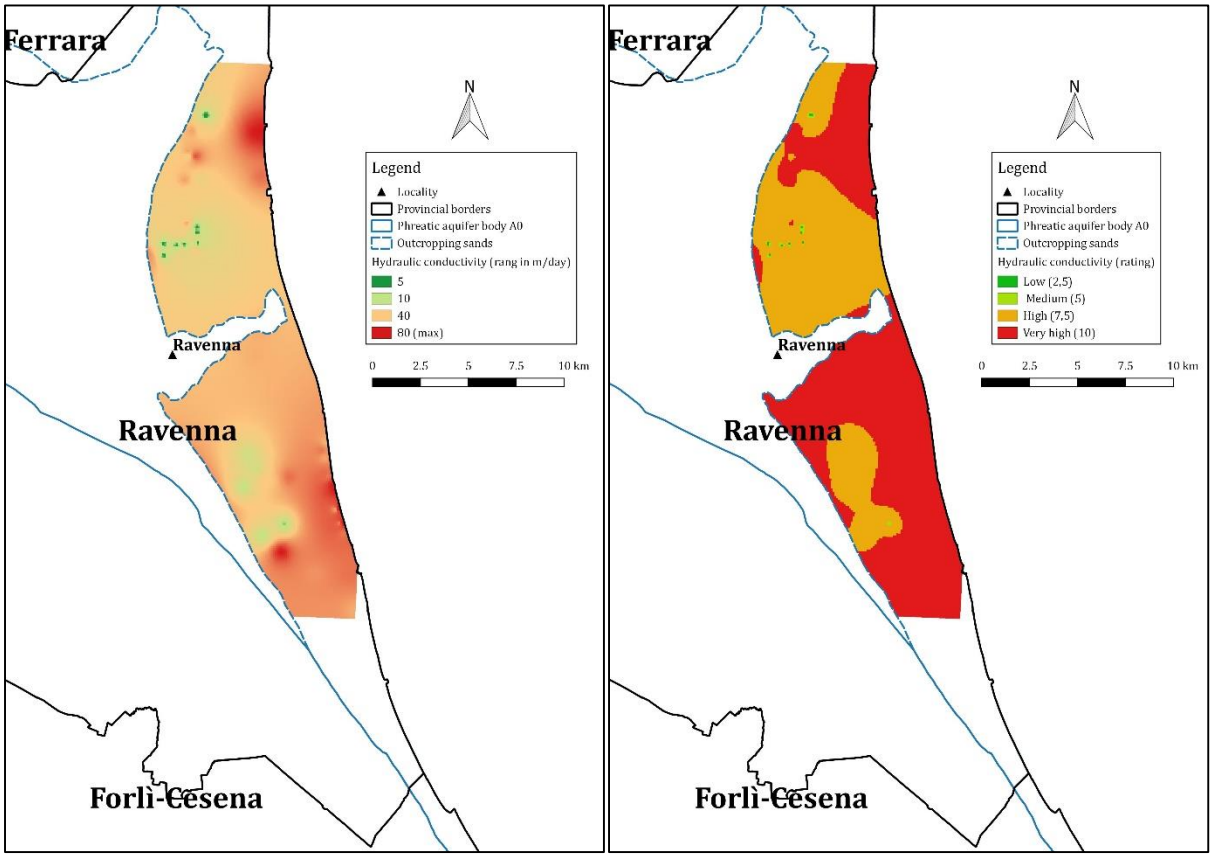

Figure 6-4: Aquifer hydraulic conductivity (A) - range (on the left) and rating (on the right)

The hydraulic conductivity data (A) were extracted from pumping tests conducted on the network of 79 piezometers that covers the whole study area (see the table in Appendix A). The IDW method was then used to produce the map depicted in Figure 6-4 (on the left) by interpolating those known values over the whole study area.

It can be seen that the hydraulic conductivity varies from a minimum value of 2.9m/day to a maximum value of 80m/day. This range of values was finally classified into four main classes, according to Table 4-1 and rated from 2.5 to 10 to generate Figure 6-4 (on the right). From this Figure 6-4 (on the right), it can be seen that the hydraulic conductivity is “high” or “very high” over the major part of the study area which means that the hydraulic conductivity acts as an important contributor to SWI.

Finally it is important to underline that the information related to the depth at which the hydraulic conductivities were measured are missing.

- Height of groundwater *L*evel a.m.s.l.

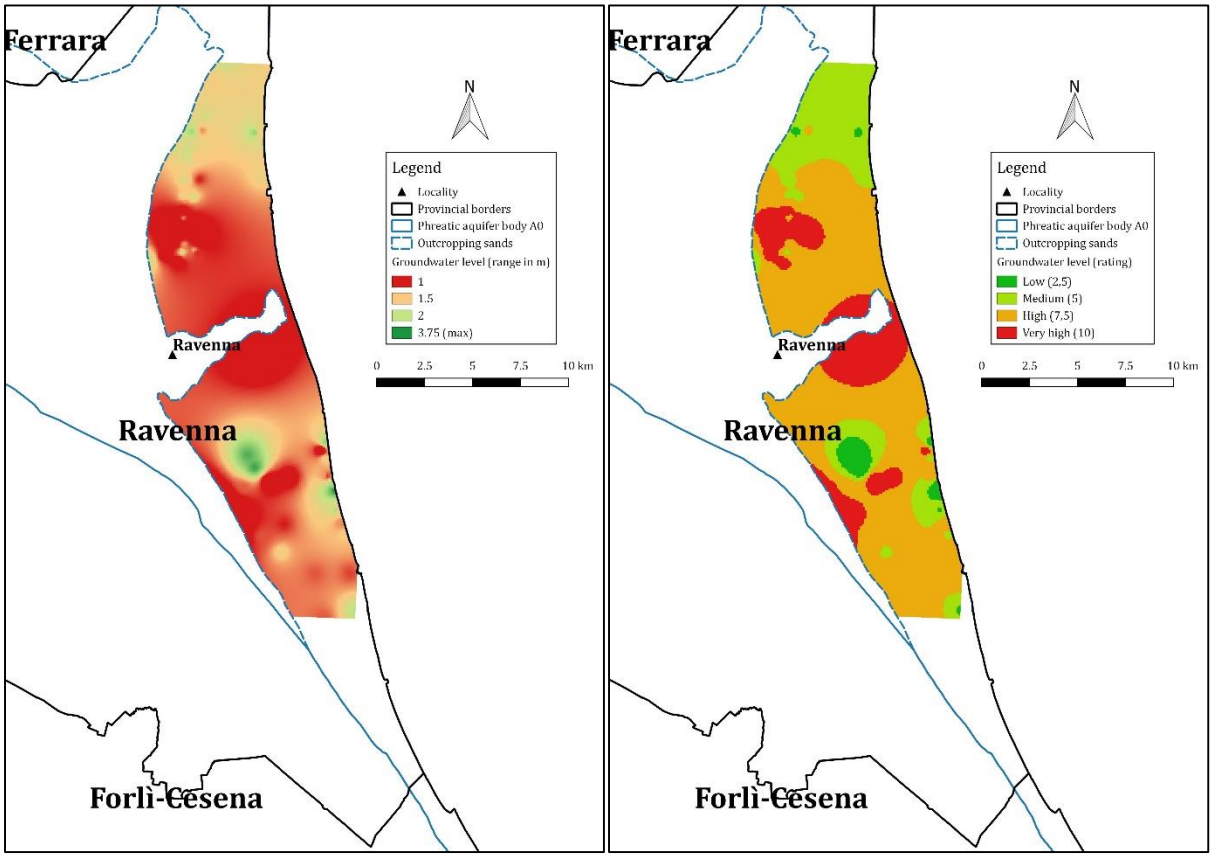

Figure 6-5: Height of groundwater level a.m.s.l. (L) - range (on the left) and rating (on the right)

The height of groundwater level a.m.s.l. (L) was calculated from the measurements that were conducted in June 2010 over the whole network of 79 piezometers that covers the study area (see the table in Appendix A). The IDW method was secondly used to produce the map depicted in Figure 6-5 (on the left) by interpolating those known values over the whole study area.

It can be seen that the groundwater level varies from a minimum value of -1.7m b.m.s.l. to a maximum value of 3.75m a.m.s.l. Those values were finally classified into four main classes, according to Table 4-1 and rated from 2.5 to 10 to generate Figure 6-5 (on the right).

It can be seen from the orange and red areas in Figure 6-5 (on the right) that the groundwater level is mostly lower than 1.5m a.m.s.l. over the study area, indicating a “high” to “very high” vulnerability to SWI due to the very low hydraulic pressure that those areas oppose to the inland motion of the seawater front. Those results are in line with the general topography of the area depicted earlier in Figure 5-7 and that shows that most of the region around Ravenna is located b.m.s.l. or only a few meters a.m.s.l.

Finally it is important to keep in mind that the groundwater level is a dynamic parameter that is characterized by a seasonal and annual variability. It is generally recommended to consider the minimum groundwater levels a.m.s.l. since this would provide the highest possible vulnerability risk. For this case study, solely the data recorded during the summer 2010 are available and were therefore used for the analysis.

- *D*istance from the shore

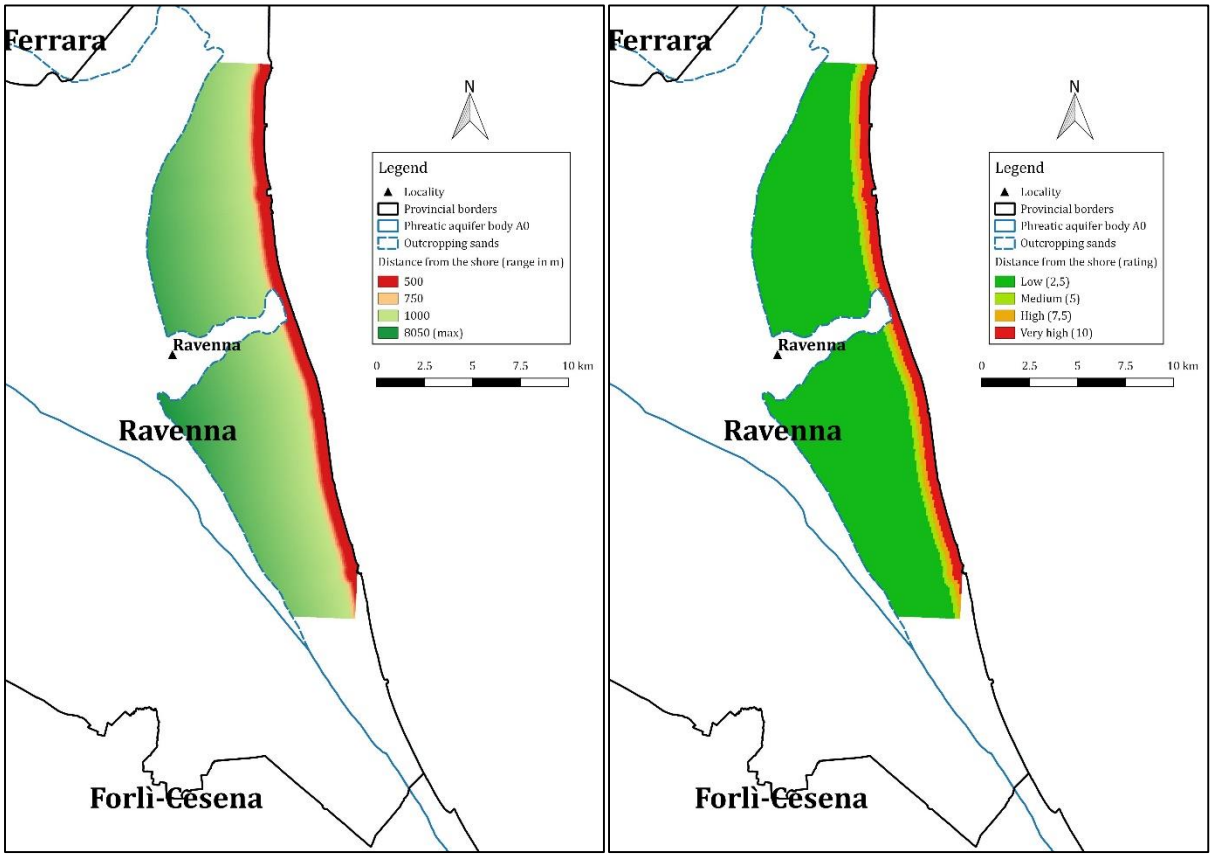

Figure 6-6: Distance from the shore (D) - range (on the left) and rating (on the right)

The distance from the shore (D) was estimated for every point of the study area by using the "Distance Matrix" tool of the software QGIS© (see the table in Appendix A). The Figure 6-6 (on the left) was then obtained by plotting the results while considering three different reference distances perpendicular to the coastline (i.e. 500, 750 and 1000m).

All the values were secondly classified into four main classes, according to Table 4-1 and rated from 2.5 for a distance higher than 1000m to 10 for a distance lower than 500m (see Figure 6-6, on the right). Indeed the impact of SWI decreases when moving perpendicularly from the shore towards the land. The further away the groundwater is from the shore, the lesser the pressure from seawater to infiltrate. [46]

At this point an important remark concerns the presence of brackish surface water bodies (such as the Pialasse basin that is shown in Figure 5-8) in the study area. In theory those water bodies have the same effect in terms of SWI in the area as those of the coastal zone and should therefore be treated as such. In this study, it has however been decided to only consider the SWI coming from the sea.

- *I*mpact of existing status of SWI in the area

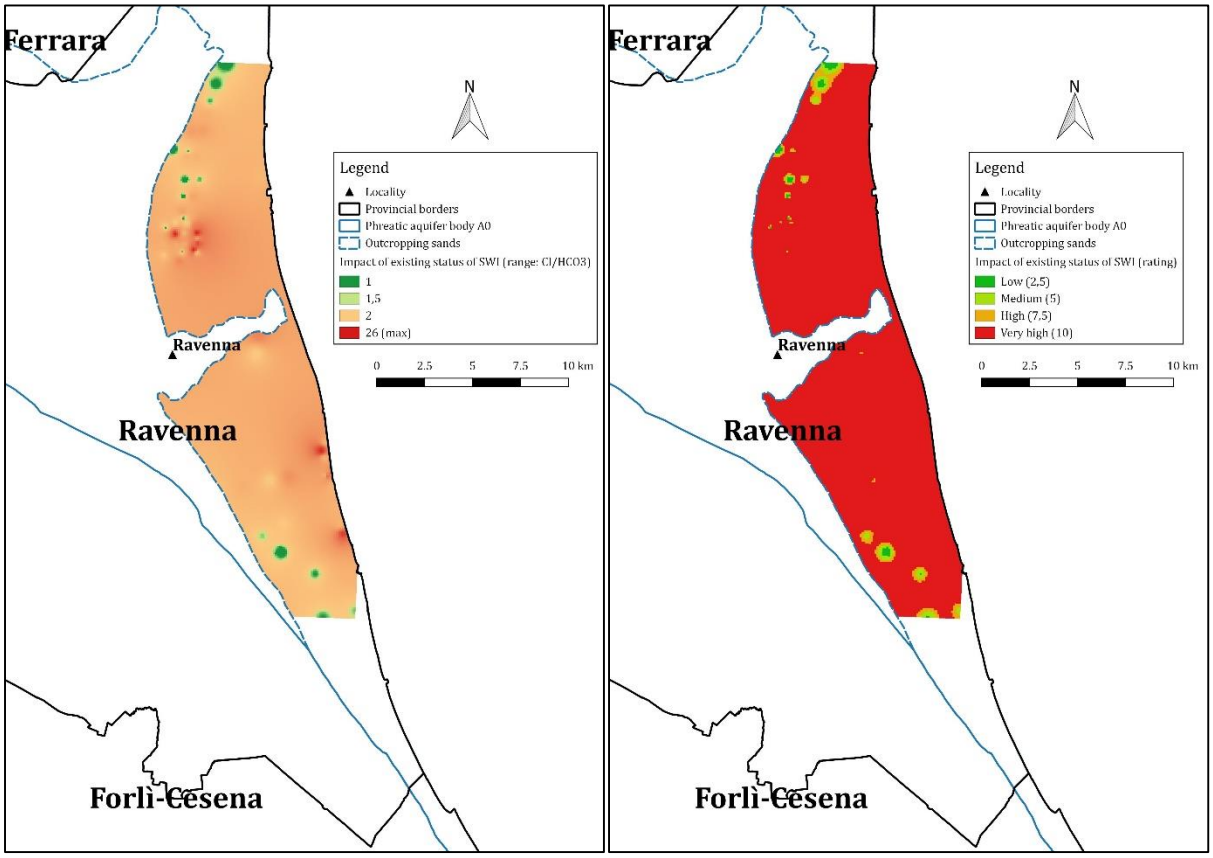

Figure 6-7: Impact of existing status of SWI in the area (I) - range (on the left) and rating (on the right)

To evaluate the impact of existing status of SWI in the study area (I), it is recommended to consider the ratio $\frac{Cl^-}{HCO_3^-}$ rather than the ratio $\frac{Cl^-}{HCO_3^- + CO_3^{2-}}$ when the contribution of CO_3^{2-} is unknown. This is the approach that has been adopted here.

The ratio $\frac{Cl^-}{HCO_3^-}$ was obtained from the chemical analyses that were performed in June 2010 on the water samples that were extracted from the 79 piezometers that cover the study area (see the table in Appendix A). The IDW method was secondly used to produce the map depicted in Figure 6-7 (on the left) by interpolating those known values over the whole study area.

It can be seen that the ratio varies from a minimum value of 0.125 to a maximum value of 25.57. Those values were finally classified into four main classes, according to Table 4-1, and rated from 2.5 to 10 to generate Figure 6-7 (on the right). From this Figure 6-7 (on the right), it can be seen that most of the study area shows a ratio greater than 2 indicating that this area is already "highly" affected by SWI.

At this point it is important to note that the impact of existing status of SWI in the study area (I) is a second dynamic parameter (after the groundwater level) and that the ratio is characterized by a seasonal and an annual variability. It is generally recommended to consider the maximum ratio since this would provide the highest possible vulnerability risk. However for this case study, solely the data recorded during the summer 2010 are available and were therefore used for the analysis.

- Thickness of the aquifer

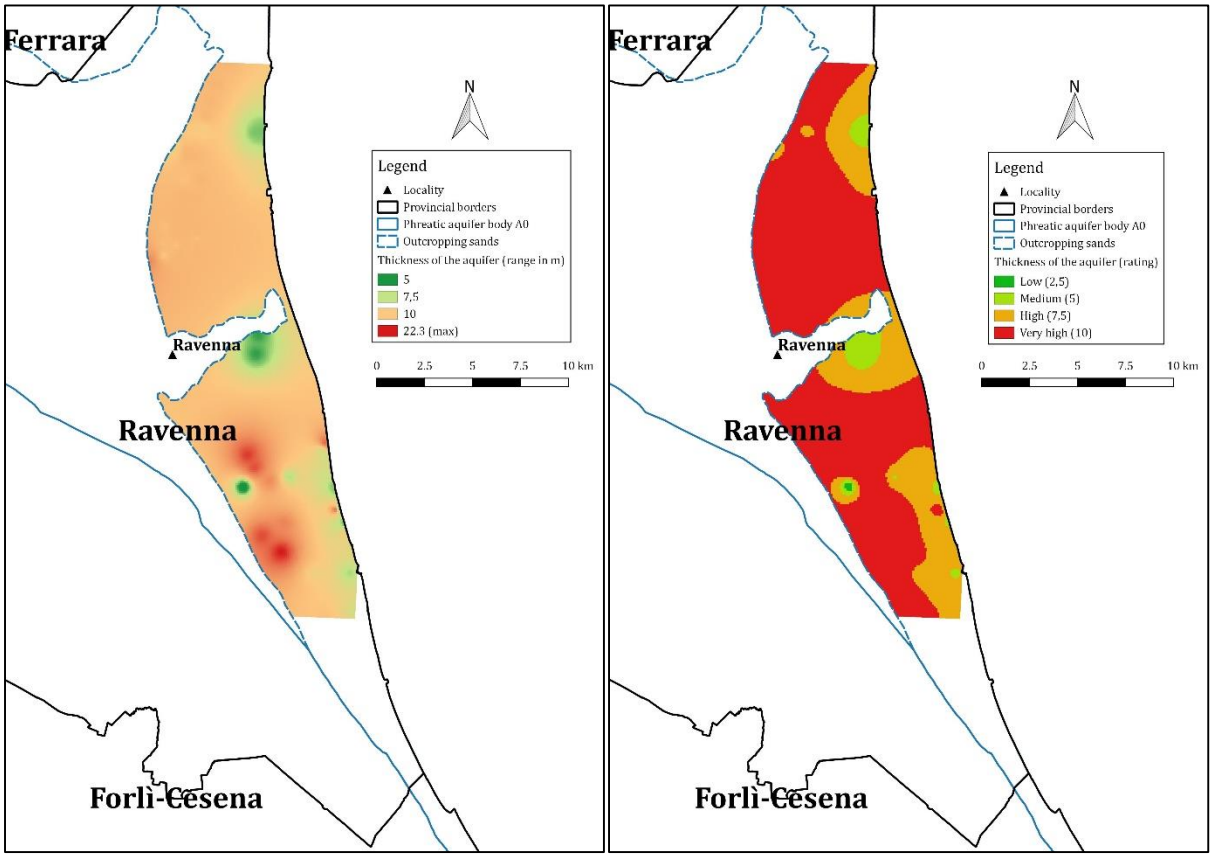

Figure 6-8: Thickness of the aquifer (T) - range (on the left) and rating (on the right)

The thickness of the aquifer (T) was calculated from the data extracted from the network of 79 piezometers that covers the study area (see the table in Appendix A). The IDW method was secondly used to produce the map depicted in Figure 6-8 (on the left) by interpolating those known values over the whole study area.

It can be seen that the thickness of the aquifer varies from a minimum value of 1.9m to a maximum value of 22.3m. Those values were finally classified into four main classes, according to Table 4-1, and rated from 2.5 to 10 to generate Figure 6-8 (on the right).

It can be seen from the orange and red areas in Figure 6-8 (on the right) that the thickness of the aquifer is larger than 7.5m over the major part of the study area, indicating that this parameter has a “high” to “very high” contribution to SWI.

At this point an important remark concerns the fact that in theory the GALDIT procedure requires to solely consider the saturated thickness of the unconfined aquifer. However in this work it has been assumed for simplicity purposes that the whole thickness of the phreatic aquifer was saturated.

6.2.3. GALDIT vulnerability assessment

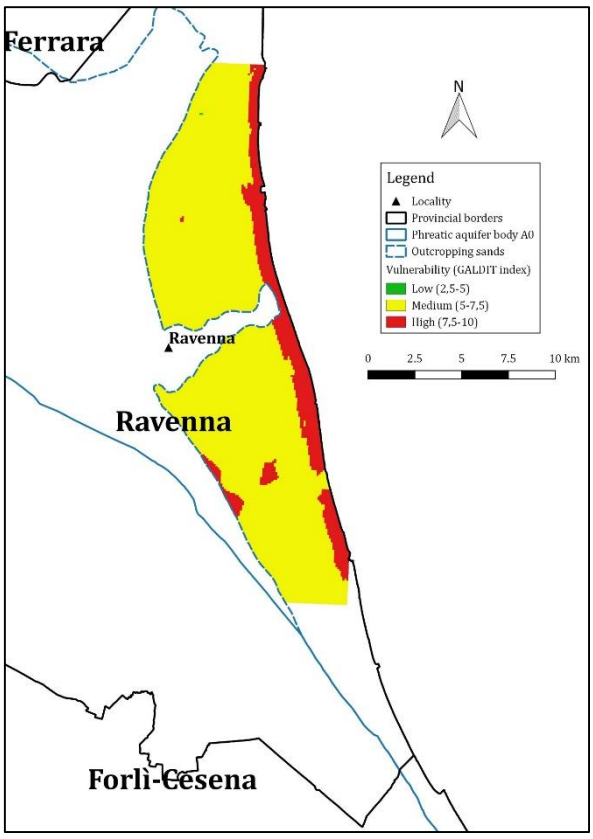

Figure 6-9: GALDIT vulnerability assessment for the phreatic aquifer around Ravenna

Figure 6-9 gives an overview of the spatial distribution of the GALDIT-Index in the study area. It has been prepared by applying equation (23) to the 6 parameter layers that were presented in the previous section 6.2.2.

The range of the GALDIT-Index scores (i.e. 2.5 to 10) is divided into three classes: 2.5–5, 5–7.5 and 7.5–10 denoted, respectively, as low, moderate and high vulnerability. Generally speaking, the higher the index, the greater the vulnerability to SWI. The use of this index therefore enables to highlight the areas that are likely to be more susceptible to SWI.

From Figure 6-9, it can be seen that all the study area presents at least a moderate vulnerability to SWI. The general trend is the following: the most vulnerable area consists of a narrow buffer zone along the coast on the eastern side of the study area and then the vulnerability tends to decrease while moving landwards. This may be explained by the fact that those highly vulnerable zones are characterized by a high proximity to the sea and by a low elevation (i.e. a low height of the groundwater table) and those two factors (i.e. L and D) turn out to be the most significant ones when deriving the GALDIT-Index (see the weights in Table 4-1).

In the study area some other isolated parts, characterized by a low level of the groundwater table (see Figure 6-5), are also highly vulnerable to SWI. This decrease in the level of the groundwater table may be interpreted by a drop in the topographic level that may be due to local subsidence.

Finally from a statistical point of view, the percentage distribution between moderate and highly vulnerable zones is 86 and 14% respectively.

6.3 Emilia-Romagna phreatic aquifer A0

6.3.1. Monitoring network

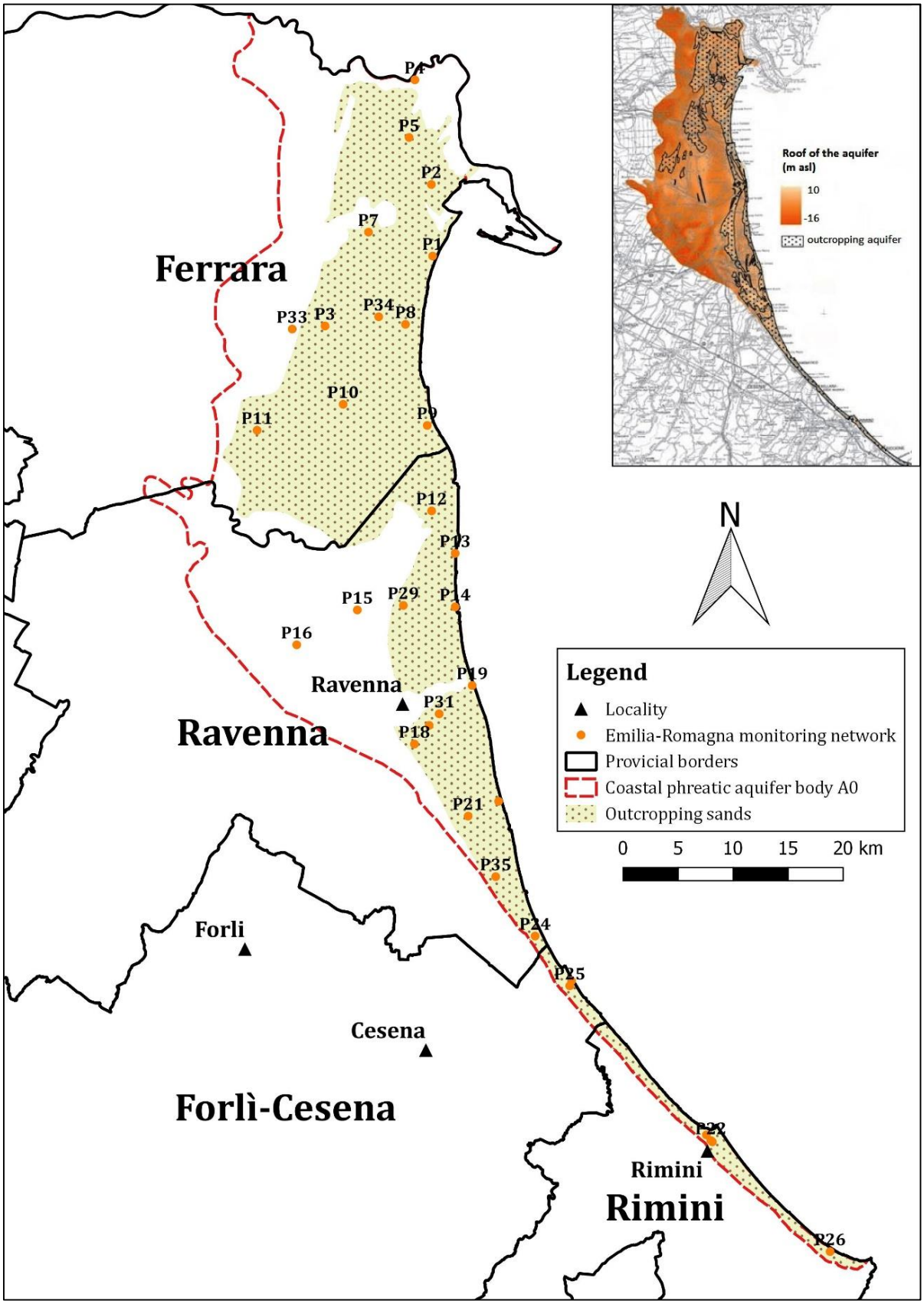

Figure 6-10: monitoring network of piezometers from the Emilia-Romagna region

As described in Section 5.3, the phreatic aquifer body A0 is generally unconfined on its coastal side and tends to widen towards west where it is buried by thin layers of continental alluvial deposits (mostly silt and clay deposits). This situation is depicted in Figure 6-10 which gives an overview of the general extent of the phreatic aquifer. It can be seen that the phreatic aquifer is properly in the southern sector where it is also very thin, while in the central and northern parts it is free near the coast and becomes semi-confined when proceeding westwards. [66]

Since 2009, the Geological, Seismic and Soil Survey of Emilia-Romagna, i.e. Servizio Geologico, Sismico e dei Suoli (SGSS), has been undertaking a study project in order to create an updated knowledge framework, outlining the physical characteristics, the dynamics and possible fragility of the coastal phreatic aquifer [66]. As a part of this project, a quali-quantitative monitoring network of piezometers was implemented over the study area with the purpose of providing a distribution of the data that is as homogeneous as possible [66]. This monitoring network is composed of 32 wells, of which 12 are located in the province of Ferrara, 14 in Ravenna, 2 in Forli-Cesena and 4 in Rimini, as depicted in Figure 6-10.

Each piezometer measures the depth of the groundwater table and the trend, with respect to the depth, of the specific electrical conductivity EC (mS/cm), of the temperature T (°C), and of the content of Total Dissolved Solids TDS (g/L). Those parameters are recorded every meter and on a regular basis with a multiparameter probe. A monography summarizing all the measurements as well as the technical characteristics and the precise location (provided by GPS) was finally prepared for each piezometer. An example of such monography is provided in Appendix B (B.1) for the piezometer P1. [66]

In order to overcome the lack of information required for the derivation of the GALDIT-Index, secondary data were collected from the literature (maps showing the hydraulic conductivity, the top and the bottom of the phreatic aquifer, see Appendix B (B.2)) in addition to the direct field data. A table summarizing all the relevant information for this particular case study is provided in Appendix B (B.3).

From Figure 6-10, it can be seen that most of the monitoring piezometers are located in the outcropping sands (i.e. the part of the phreatic aquifer that is not semi-confined) beside two of them in the province of Ravenna. For this reason, the extent of the study area will be limited to this zone of outcropping sands.

6.3.2. Mapping of the parameters

- Groundwater occurrence

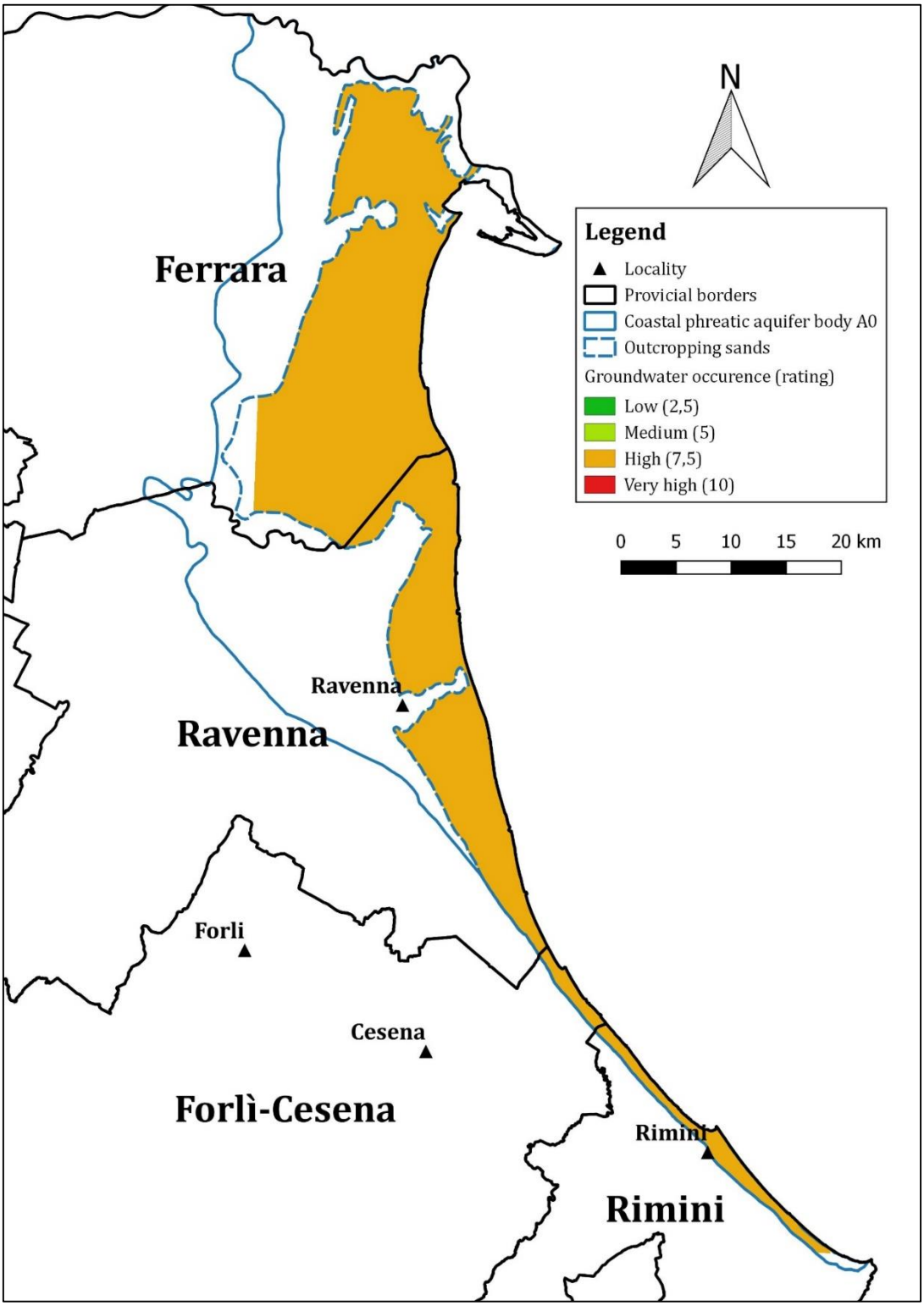

Figure 6-11: Groundwater occurrence (G) for the phreatic aquifer A0 - rating

As mentioned hereabove, the analysis focuses on the part of the aquifer that is mainly unconfined (i.e. the outcropping sands) and therefore the rating for the groundwater occurrence corresponds to 7.5 (see Figure 6-11).

➢ Aquifer hydraulic conductivity

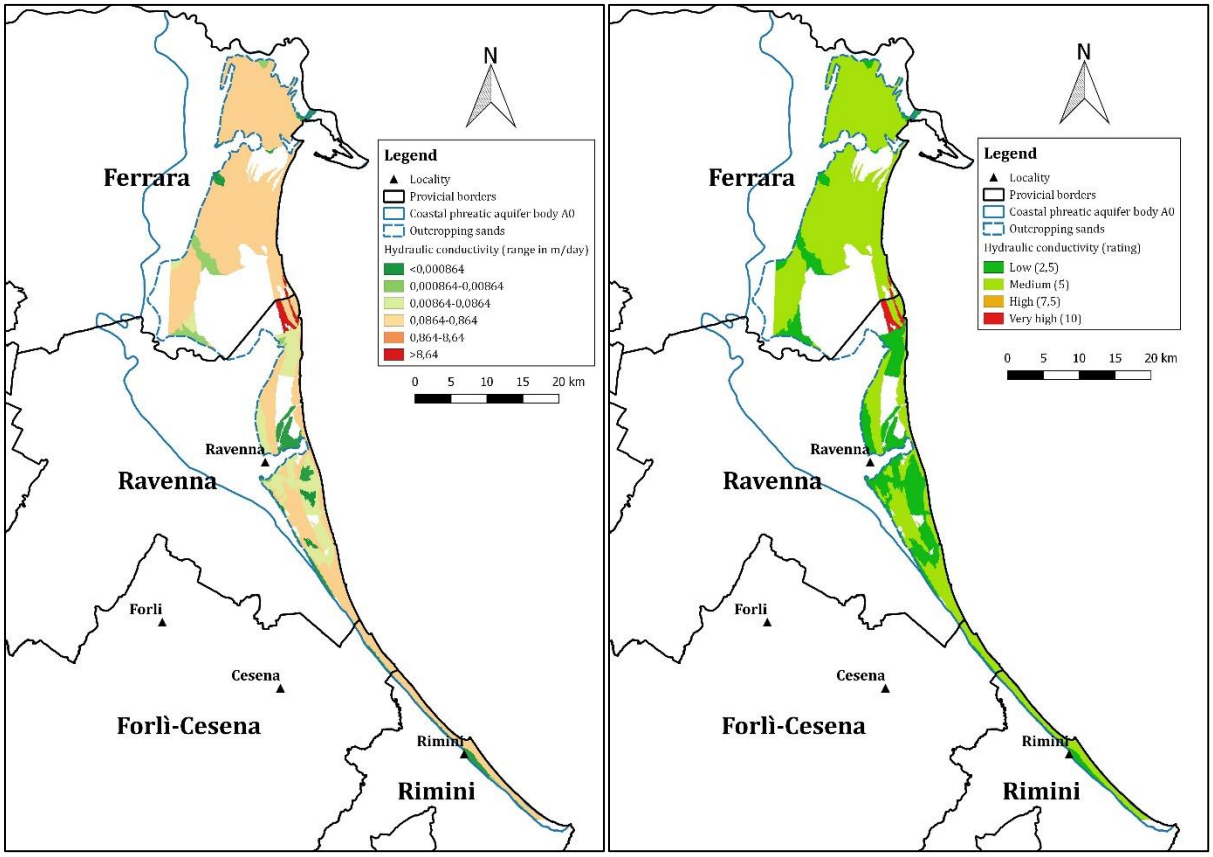

Figure 6-12: Aquifer hydraulic conductivity (A) for the phreatic aquifer A0 - range (on the left) and rating (on the right)

The data for the hydraulic conductivity (A) were extracted from the map depicting the saturated hydraulic conductivity of the whole Emilia-Romagna region (see the map in Appendix B (B.2)). This map was downloaded from the website of the Emilia-Romagna region (http://ambiente.regione.emilia-romagna.it/geologia/temi/suoli/proprieta-fisico-idrologiche-suoli).

The saturated hydraulic conductivity is characterized by a high degree of variability with a total range covering more than 4 orders of magnitude between the extreme values, as depicted in Figure 6-12 (on the left). However the major part of the study area is characterized by low values of saturated hydraulic conductivity that mainly vary between 0,0864m/day and 0,864m/day. In terms of rating, this means that the hydraulic conductivity act as a “low” to “moderate” contributor to SWI (see Figure 6-12, on the right).

At that point it is important to keep in mind two limitations that are related to the use of this map of hydraulic conductivity: (1) data are missing at the level of the surface water bodies; (2) the information about the depth of measurement of the hydraulic conductivity was not mentioned on the website. This second limitation may partly explain the significant difference between these results and the results that were presented earlier in Figure 6-4 for the phreatic aquifer of Ravenna, namely that the hydraulic conductivities behind Figure 6-12 and Figure 6-4 were measured at different depths (i.e. directly at the surface of the ground for the former and more deeply for the latter).

- Height of groundwater *L*evel a.m.s.l.

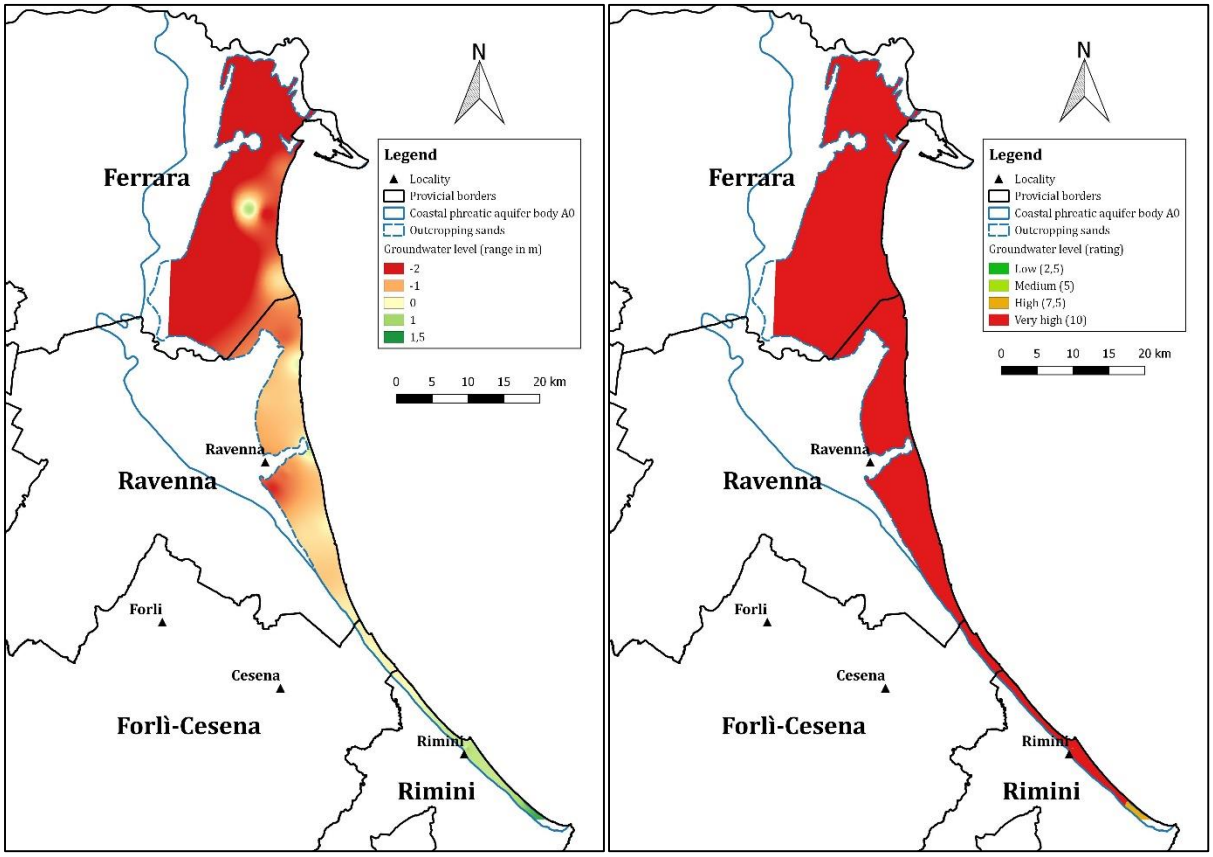

Figure 6-13: Height of groundwater level a.m.s.l. (L) for the phreatic aquifer A0 - range (on the left) and rating (on the right)

The height of groundwater level a.m.s.l. (L) was computed from the measurements that have been conducted since 2009 over the whole network of 32 piezometers that covers the study area. Among the sequence of data that is available for each well (see the example in Appendix B (B.1)), only the lowest value of the groundwater table level was kept. Those extreme values are summarized in the table in Appendix B (B.3). This approach aims at considering the worst-case scenario (i.e. the highest possible vulnerability risk) rather than the annual or seasonal variability in the vulnerability assessment. The IDW method was secondly used to produce the map depicted in Figure 6-13 (on the left) by interpolating those extreme values over the whole study area.

It can be seen that the groundwater level is located b.m.s.l. in most of the study area, with a minimum value of -3m b.m.s.l. in the province of Ferrara and a maximum value of 1.4m a.m.s.l. in the south of the province of Rimini. Those levels were finally classified into four main classes, according to Table 4-1 and rated from 2.5 to 10 to generate Figure 6-13 (on the right).

This Figure 6-13 (on the right) shows that the low groundwater levels over the whole study area act as significant contributors to SWI by creating a landward hydraulic gradient that dramatically emphasizes the phenomenon of SWI. Those results are in line with the general topography of the area depicted earlier in Figure 5-7 and that shows that a large part of the coastal areas in the provinces of Ferrara and Ravenna are located b.m.s.l. or only a few meters a.m.s.l., due to former anthropic subsidence. By contrast in the south of the study area this general trend tends to reverse due to the presence of the topographical relief of the Apennines foothills.

- *D*istance from the shore

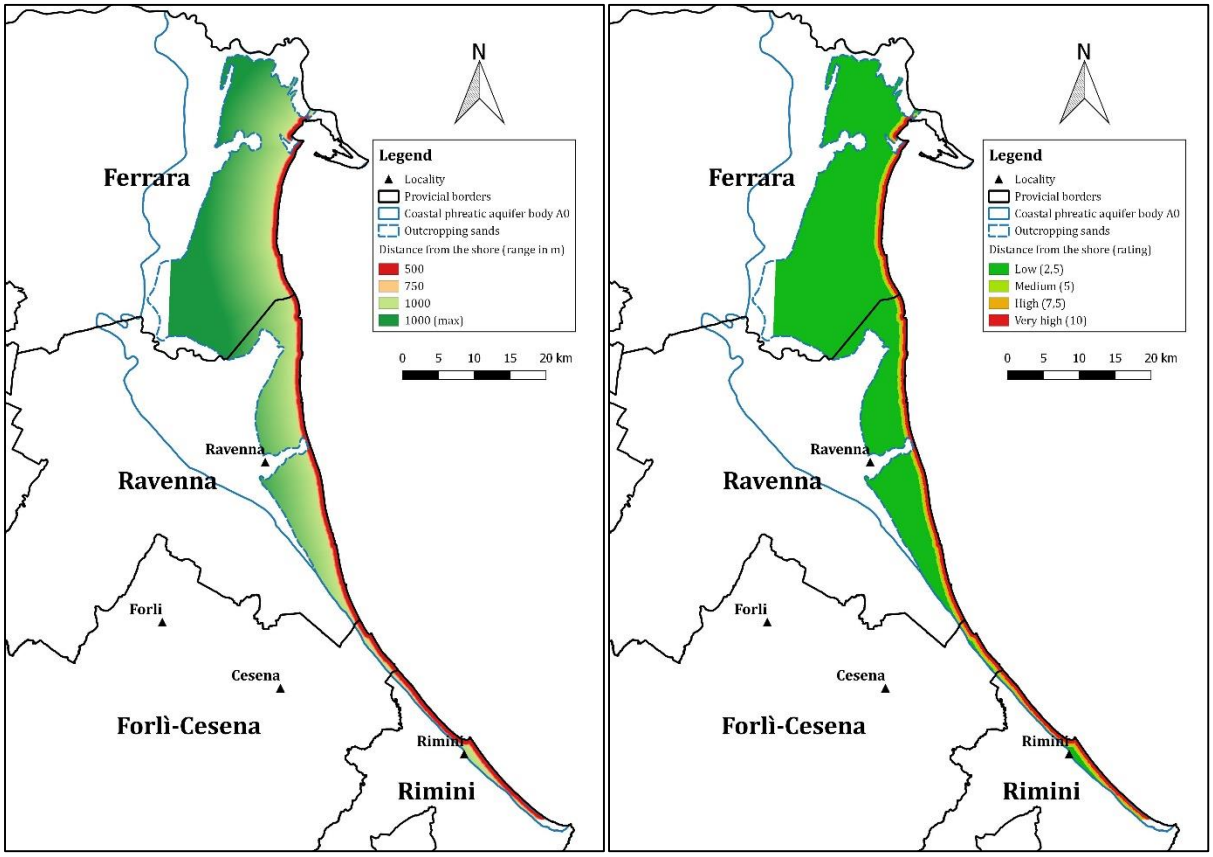

Figure 6-14: Distance from the shore (D) for the phreatic aquifer A0 - range (on the left) and rating (on the right)

The distance from the shore (D) was estimated for every point of the study area by using the "Distance Matrix" tool of the software QGIS© (see the table in Appendix B (B.3)). The Figure 6-14 (on the left) was secondly obtained by plotting the results while considering three different reference distances perpendicular to the coastline (i.e. 500, 750 and 1000m).

All the values were finally classified into four main classes, according to Table 4-1 and rated from 2.5 for a distance higher than 1000m to 10 for a distance lower than 500m (see Figure 6-14, on the right). Indeed the impact of SWI decreases when moving perpendicularly from the shore towards the land. The further away the groundwater is from the shore, the lesser the pressure from seawater to infiltrate. [46]

At this point an important remark concerns the presence of brackish surface water bodies (such as the Pialasse basin or the Comacchio Lake that are shown in Figure 5-8) in the study area. In theory those water bodies have the same effect in terms of SWI in the area as those of the coastal zone and should therefore be treated as such. In this study, it has however been decided to only consider the SWI coming from the sea.

➢ *I*mpact of existing status of SWI in the area

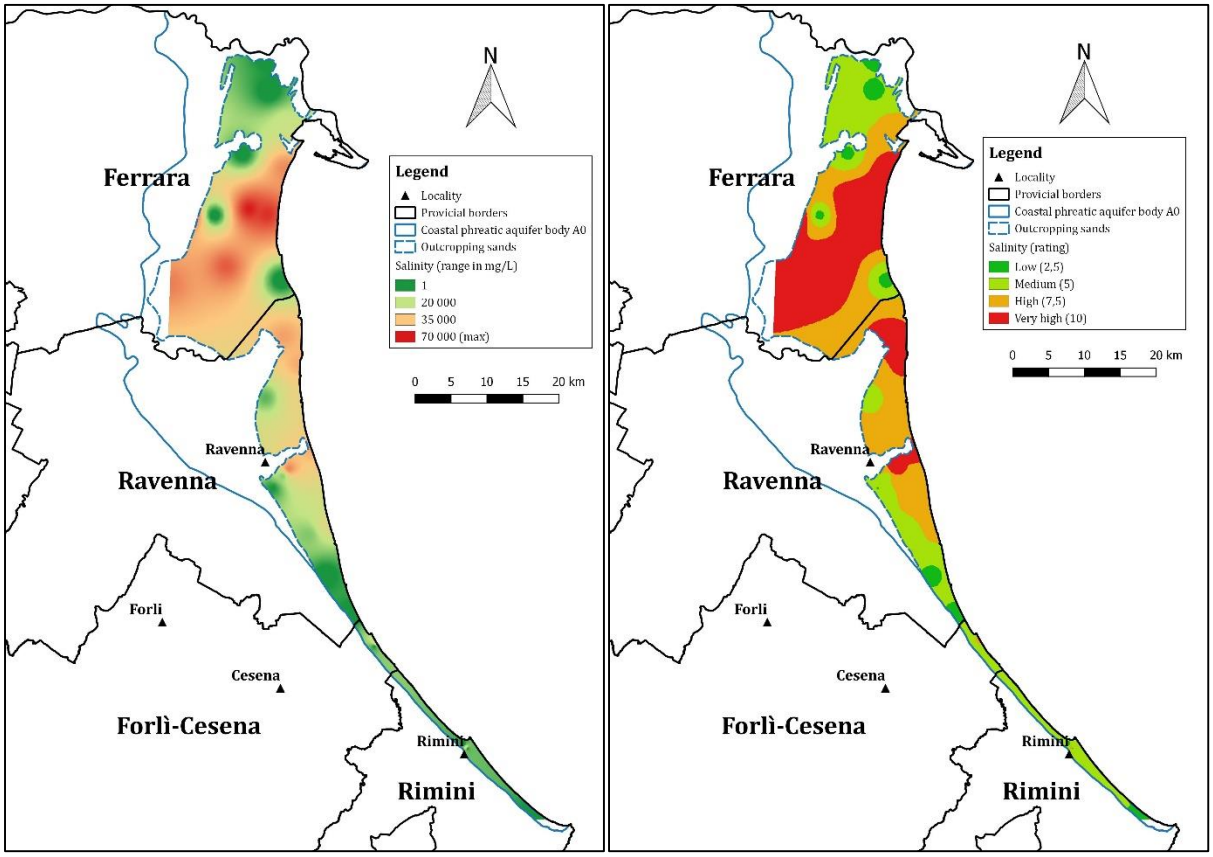

Figure 6-15: Impact of existing status of SWI in the phreatic aquifer A0 (I) - range (on the left) and rating (on the right)

To evaluate the impact of existing status of SWI in the study area (I), the classical approach consists in evaluating the ratio $\frac{Cl^-}{HCO_3^-+CO_3^{2-}}$. Since the data about the chemical composition of groundwater were not available, an alternative approach had to be considered which relies on the computation of the salinity[16] based on the measurements of the groundwater temperature T (in °C) and of the electrical conductivity EC (in mS/cm).

Those two parameters were extracted from the measurements that have been conducted since 2009 over the whole network of 32 piezometers that covers the study area. It has been decided to consider the maximum electrical conductivity and the average temperature at a depth of 6m b.m.s.l. among the different sequences of measurements that were available for each well (see the example in Appendix B (B.1)). This choice is obviously arbitrary but was motivated by the desire to use values that are representative of the general behaviour of the aquifer and that are therefore recorded more or less in the middle of the aquifer thickness. Those values were finally converted into salinity values (expressed in mg of TDS per litre) by using an online salinity calculator (such as http://www.mt-oceanography.info/Utilities/salcon.html) and interpolated over the whole study area by using the IDW method to produce the map depicted in Figure 6-15 (on the left).

[16] The concept of salinity was introduced in the section 3.2.1 and may be expressed through the use of 3 proxies. Here this is the approach based on the content of Total Dissolved Solids (TDS) that has been selected.

Since this approach presents a different range of values with respect to what was presented in Table 4-1 for the classical approach, it is required to re-derive the numeric rating that has to be assigned to this factor. A first attempt for the re-classification of this factor, based on the water salinity classification that was presented in Table 3-3, is proposed in Table 6-1 herebelow and is the one that has been used in this thesis to generate the Figure 6-15 (on the right).

Table 6-1: New ratings adopted for the GALDIT parameter (I)

Factor	Weight	Rating			
		Very low 2.5	Low 5	Medium 7.5	High 10
I (salinity in mg/L)	1	<1,000	1,000-20,000	20,000-35,000	>35,000

- ***T***hickness of the aquifer

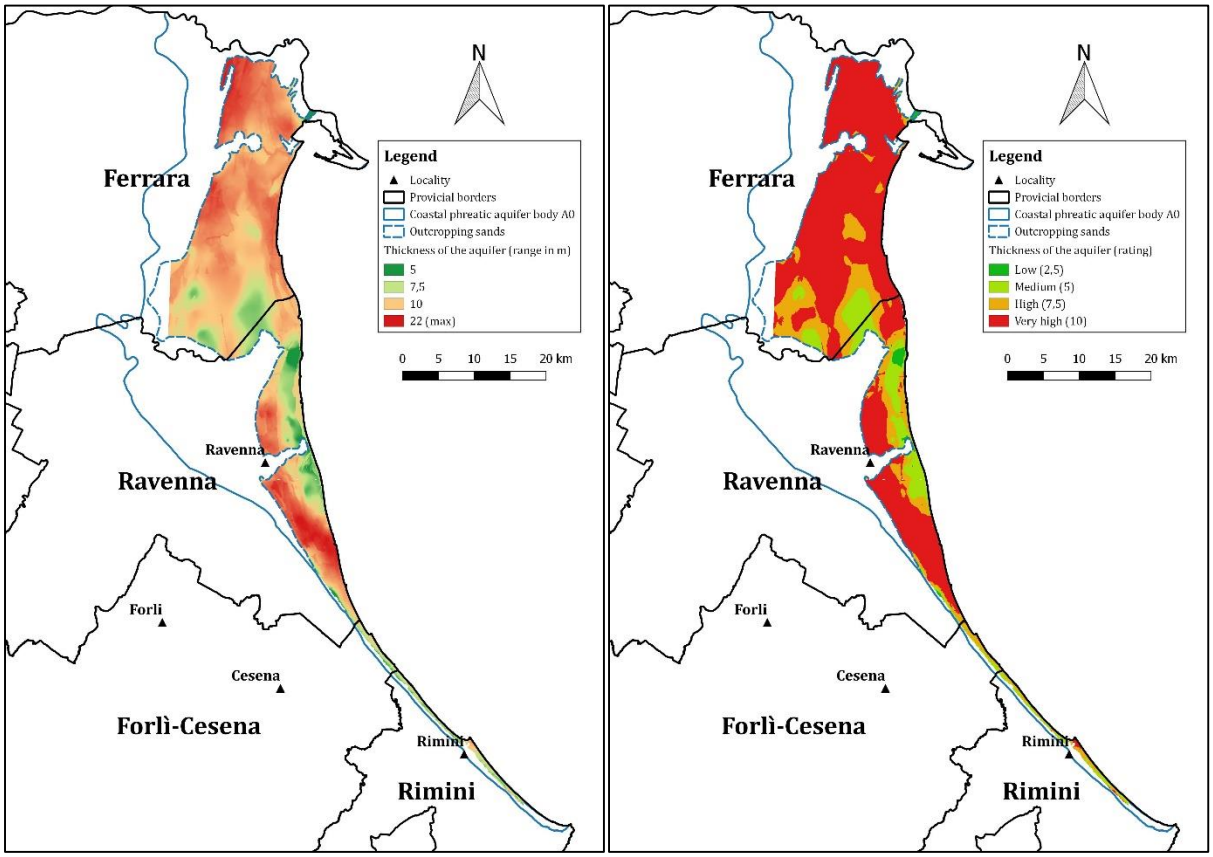

Figure 6-16: Thickness of the phreatic aquifer A0 (T) - range (on the left) and rating (on the right)

The thickness of the aquifer (T) was extracted from the two maps depicting the bottom and the top of the phreatic aquifer (see Appendix B (B.2)). The former map was subtracted from the latter one by using the "Raster Calculator" tool of the software QGIS© in order to produce the Figure 6-16 (on the left). These newly-computed values were then classified into four main classes, according to Table 4-1, and rated from 2.5 to 10 to generate Figure 6-16 (on the right).

The results depicted in Figure 6-16 are in line with the ones that were presented earlier in Figure 6-8 for the area of Ravenna alone and show that the thickness of the aquifer is larger than 7.5m over most of the study area, indicating that the thickness is a rather high contributor to SWI.

6.3.3. GALDIT vulnerability assessment

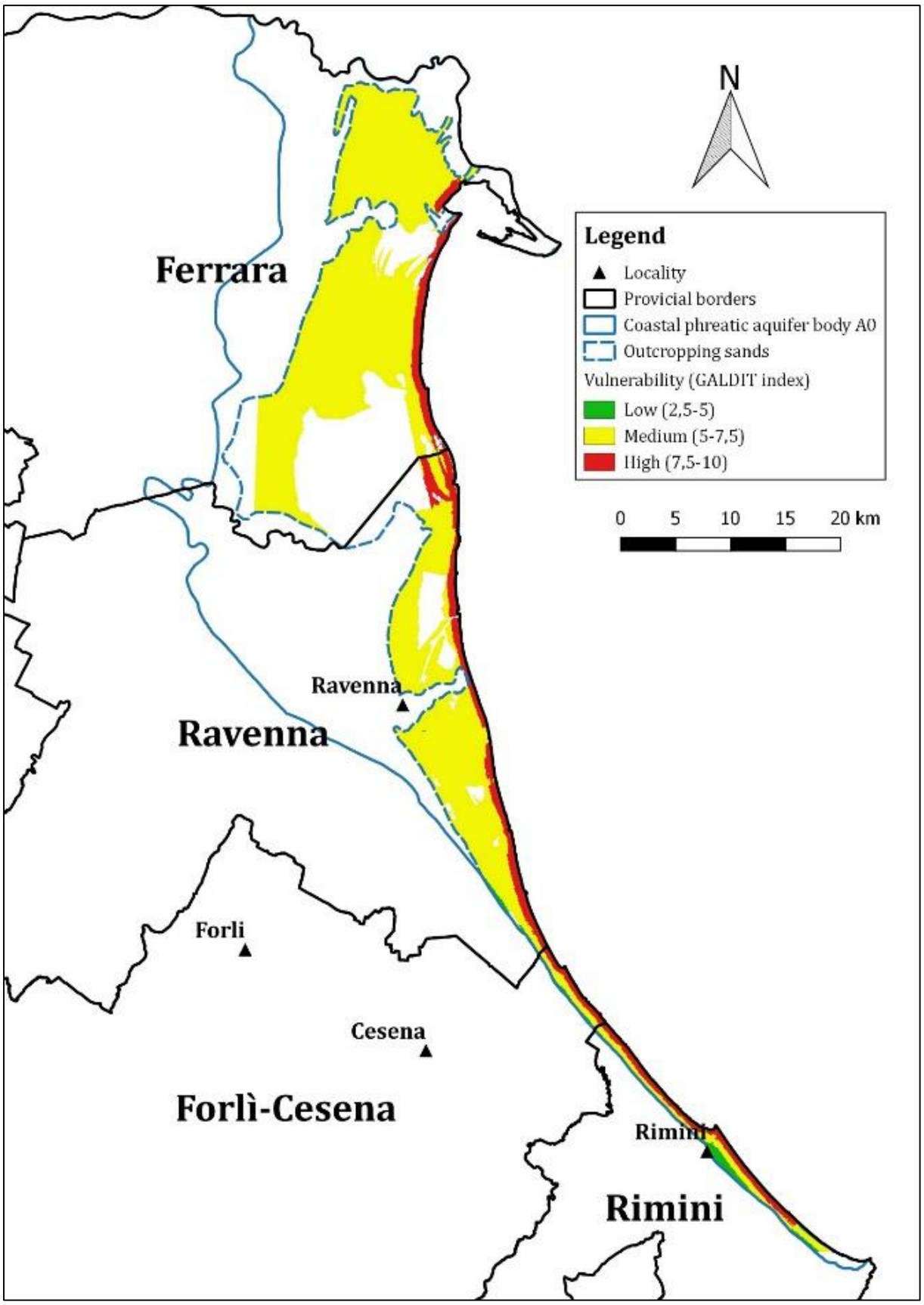

Figure 6-17: GALDIT vulnerability assessment for the phreatic aquifer A0

Figure 6-17 gives an overview of the spatial distribution of the GALDIT-Index in the study area. It has been prepared by applying equation (23) to the 6 parameter layers that were presented in the previous section 6.3.2.

The range of the GALDIT-Index scores (i.e. 2.5 to 10) is divided into three classes: 2.5–5, 5–7.5 and 7.5–10 denoted, respectively, as low, moderate and high vulnerability. Generally speaking, the higher the index, the greater the vulnerability to SWI. The use of this index therefore enables to highlight the areas that are likely to be more susceptible to SWI.

From Figure 6-17, it can be seen that the study area presents the following general trend: the most vulnerable area consists of a narrow buffer zone along the coast on the eastern side of the study area and then the vulnerability tends to decrease while moving landwards. This can be explained by the fact that those highly vulnerable zones are characterized by a high proximity to the sea and by a low elevation (i.e. a low height of the groundwater table) and those two factors (i.e. L and D) turn out to be the most significant ones when deriving the GALDIT-Index (see the weights in Table 4-1).

Generally speaking the low topographic level of the Emilia-Romagna coastal plain has a dramatic impact on the phenomenon of SWI by creating a negative landward hydraulic gradient. Close to the sea this general trend is even more emphasized due to the direct proximity of the sea. By contrast, the southern part of the study area is characterized by a lower vulnerability to SWI due to the rapid increase of the topography towards the Apennines foothills, which tends to restore a positive hydraulic gradient towards the sea.

Finally from a statistical point of view, it is interesting to note that 24% of the study area is covered by surface water bodies (that were not included in the study itself due to the lack of data). Among the remaining 76% the percentage distribution between low, moderate and high vulnerability zones is 1.5%, 86.5% and 12% respectively.

6.4 Emilia-Romagna confined aquifer A

6.4.1. Monitoring network

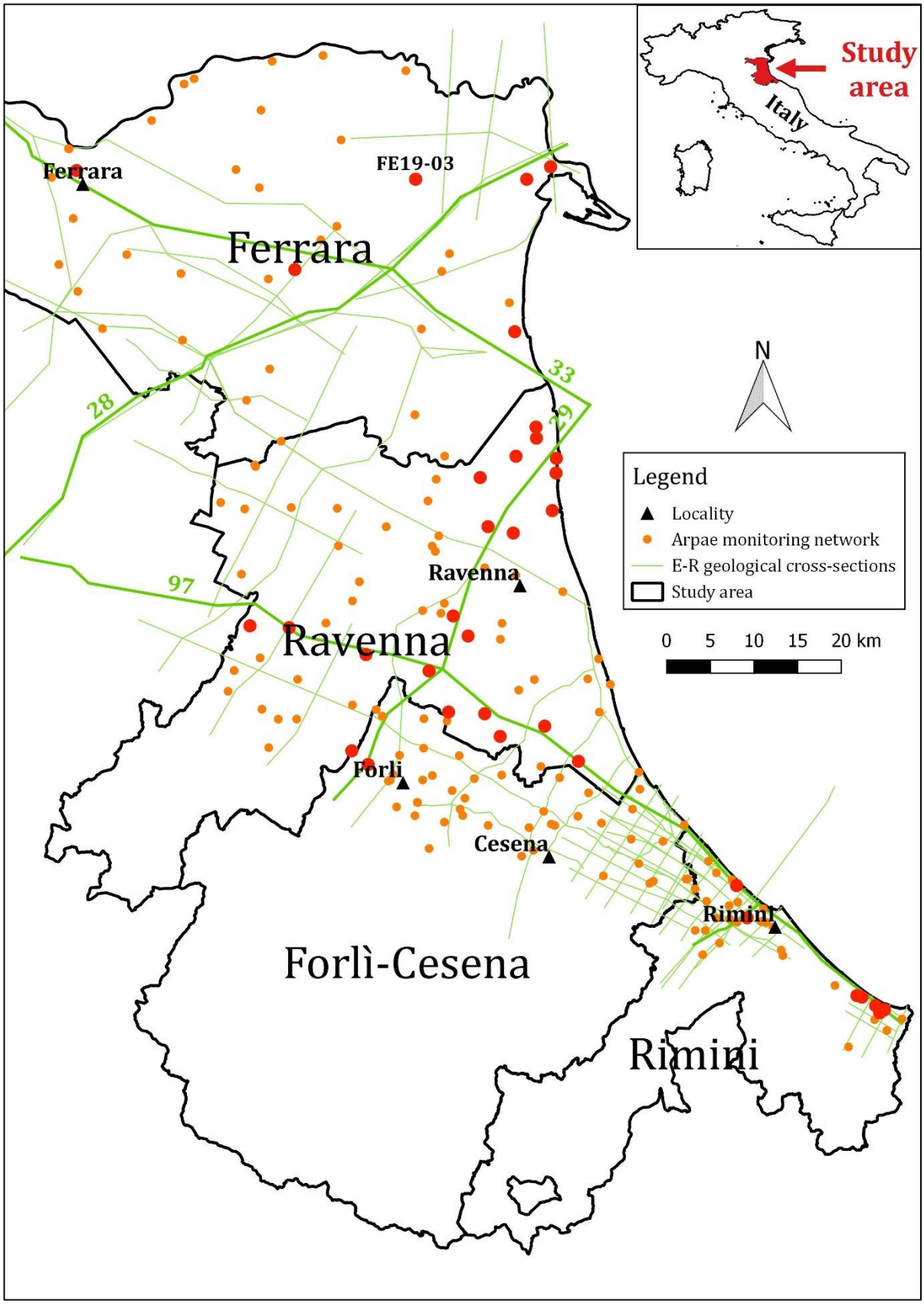

Figure 6-18: ARPAE monitoring network and geological cross-sections

As described in section 5.3, the subsurface of the Emilia-Romagna flood plain is characterized by the alternation of high-permeable and low-permeable layers coming respectively from marine and continental sedimentations that have been affecting the region over the past million years according to the climatic fluctuations. Some of those permeable layers are interconnected and can therefore be grouped into larger hydrostratigraphic units called respectively "A, B, C…" (when moving downwards) and that consist of huge regional confined aquifers.

The scope of this thesis has been limited to the study of the shallowest hydrostratigraphic unit "A" because it is the most likely one to be exploited for the extraction of fresh groundwater, the others being buried too deeply. This unit is composed of 4 permeable layers called respectively A1 to A4 (from the surface to the bottom) and that are grouped into the upper confined aquifer (A1+A2) and the lower confined aquifer (A3+A4). However in this work no distinction is made between those two sub-groups and the confined aquifer body "A" is considered as a single body. Furthermore only the coastal provinces of the Emilia-Romagna Region, i.e. the provinces of Ferrara, Ravenna, Forli-Cesena and Rimini are part of the scope of this study, as described in Figure 6-18.

The agency that is in charge of the surveillance of the groundwater for the Emilia-Romagna Region is called ARPAE, this acronym standing for the Regional Agency for Prevention, Environment and Energy of Emilia-Romagna, i.e. Agenzia regionale per la prevenzione, l´ambiente e l´energia dell´Emilia-Romagna. The key goal of this agency is the protection of human health and territorial competitiveness through the control of the state of the environment and through the support of the sustainability of human activities.

Two types of monitoring networks are used by this agency for the control of the sub-surface groundwater bodies: (1) a quantitative monitoring network that mainly measures the level of the groundwater table (in m); (2) a qualitative monitoring network that provides the detailed chemical composition of the groundwater. In total 195 piezometers cover the whole study area and are distributed as follows: 51 in the province of Ferrara, 65 in Ravenna, 47 in Forli-Cesena and 32 in Rimini, as depicted in Figure 6-18. It is important to note that some of those wells combine both the qualitative and quantitative monitoring, while some others only have the qualitative or quantitative feature. Excel spreadsheets summarizing all the data for the period 2010-2015 are freely available on the ARPAE website: https://www.arpae.it/elenchi_dinamici.asp?tipo=dati_acqua&idlivello=2020.

In order to overcome the lack of information required for the derivation of the GALDIT-Index, secondary data were collected from the literature in addition to the direct field data. Those secondary data consist of 70 geological cross-sections that are depicted in green in Figure 6-18 (an example of one of these 70 cross-sections is provided in Appendix C (C.1)). A table summarizing all the relevant information for this particular case study is provided in Appendix C (C.2).

6.4.2. Mapping of the parameters

- Groundwater occurrence

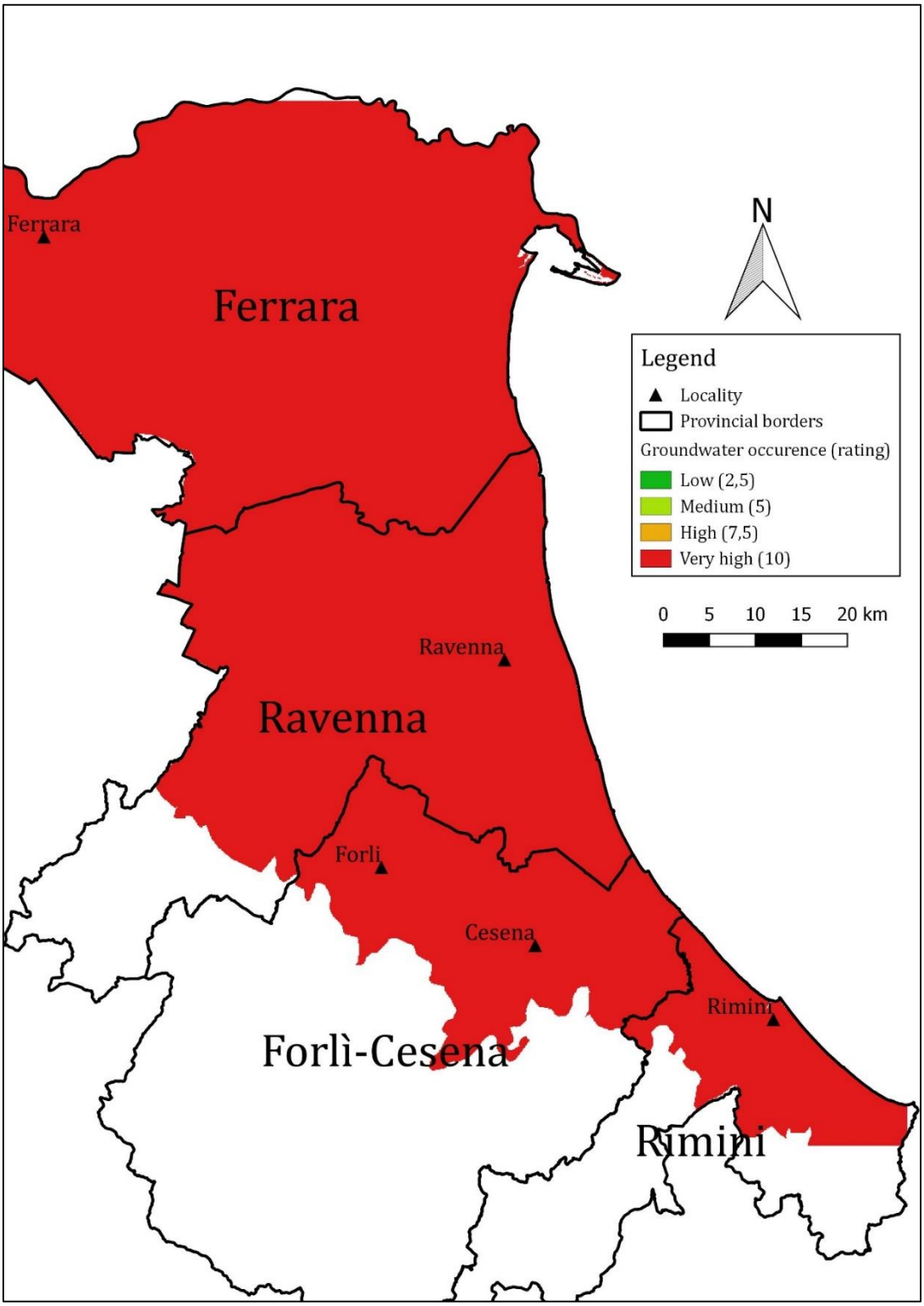

Figure 6-19: Groundwater occurrence (G) for the confined aquifer A - rating

As mentioned hereabove, the analysis focuses only on the shallowest confined aquifer body "A" and is limited to the coastal provinces of the Emilia-Romagna Region. Therefore the rating for the groundwater occurrence corresponds to 7.5 (see Figure 6-19).

➢ Aquifer hydraulic conductivity

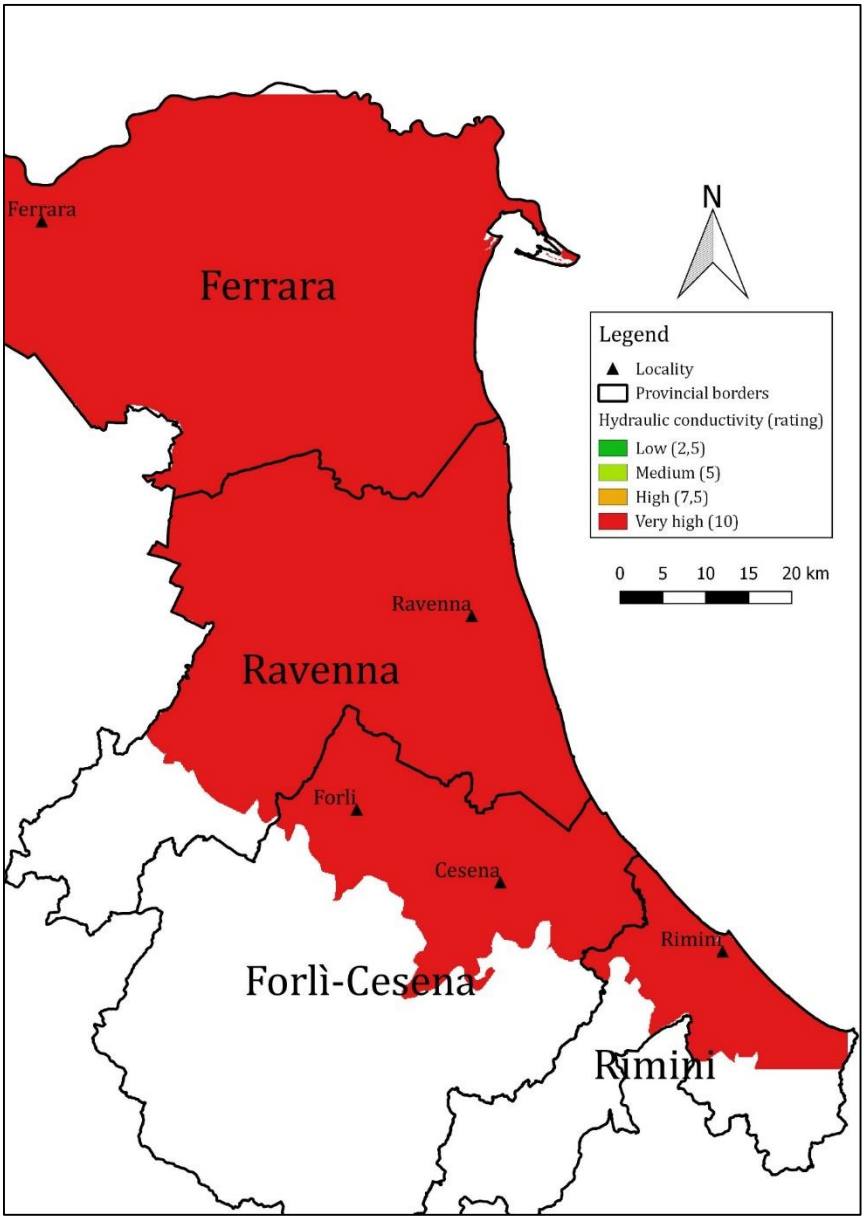

Figure 6-20: Aquifer hydraulic conductivity (A) for the confined aquifer A - rating

The data for the hydraulic conductivity (A) were extracted from a limited number of geological cross-sections that cross the 4 coastal provinces and that are assumed to be representative of the whole study area. Those cross-sections (5 in total) are highlighted in green in Figure 6-18. The hydraulic conductivity was then computed for all the wells located in the vicinity of those representative cross-sections. In total, 41 wells were selected and are highlighted in red in Figure 6-18.

The approach behind the derivation of the hydraulic conductivity relies on the concept of equivalent hydraulic conductivity and is described in details in Appendix C (C.1) by means of an example (the well FE 19-03 located in the geological section n°28). The results for the 41 selected wells are summarized in the table given in Appendix C (C.2). By proceeding in this manner it was quickly established that the equivalent hydraulic conductivity was higher than 40m/day over the whole study area and this area was therefore assigned a rating of 10, as depicted in Figure 6-20. This means that the hydraulic conductivity acts as a major contributor to SWI.

➢ Height of groundwater ***L***evel a.m.s.l.

The height of groundwater level a.m.s.l. (L) was computed from the measurements that were conducted over the whole network of piezometers that covers the study area during the period 2010-2015. Unlike the two previous case studies it has been decided to take the dynamic aspect of this parameter into account. To do so, the yearly lowest value of the groundwater level was selected among the sequence of measurements that was available at each well. This approach aims at giving an insight into the effect of the annual variability of this parameter on the vulnerability assessment. The extreme values are summarized in the table given in Appendix C (C.1) and those values were interpolated over the whole study area by using the IDW method in order to produce the series of maps depicted in Figure 6-21 to Figure 6-24 (on the left).

It can be seen from these 4 figures that the central and the western parts of the study area are characterized by a very low groundwater level. The explication is relatively straightforward by taking into consideration the very low topography of this area as well as the fact that the confined aquifer is not outcropping in this area but rather deeply buried under the coastal phreatic aquifer. Then the height of groundwater level a.m.s.l. tends to increase towards the south and towards the west where the confined aquifer becomes outcropping and the relief more pronounced.

The groundwater levels were finally classified into four main classes, according to Table 4-1 and rated from 2.5 to 10 to generate Figure 6-21 to Figure 6-24(on the right). By having a closer look at those pictures, it turns out that the interface between the red and green parts slowly tends to be pushed back towards the sea. This observation may be explained either by an increase of the freshwater recharge, or by a decrease of the extractions or by a combination of these two factors.

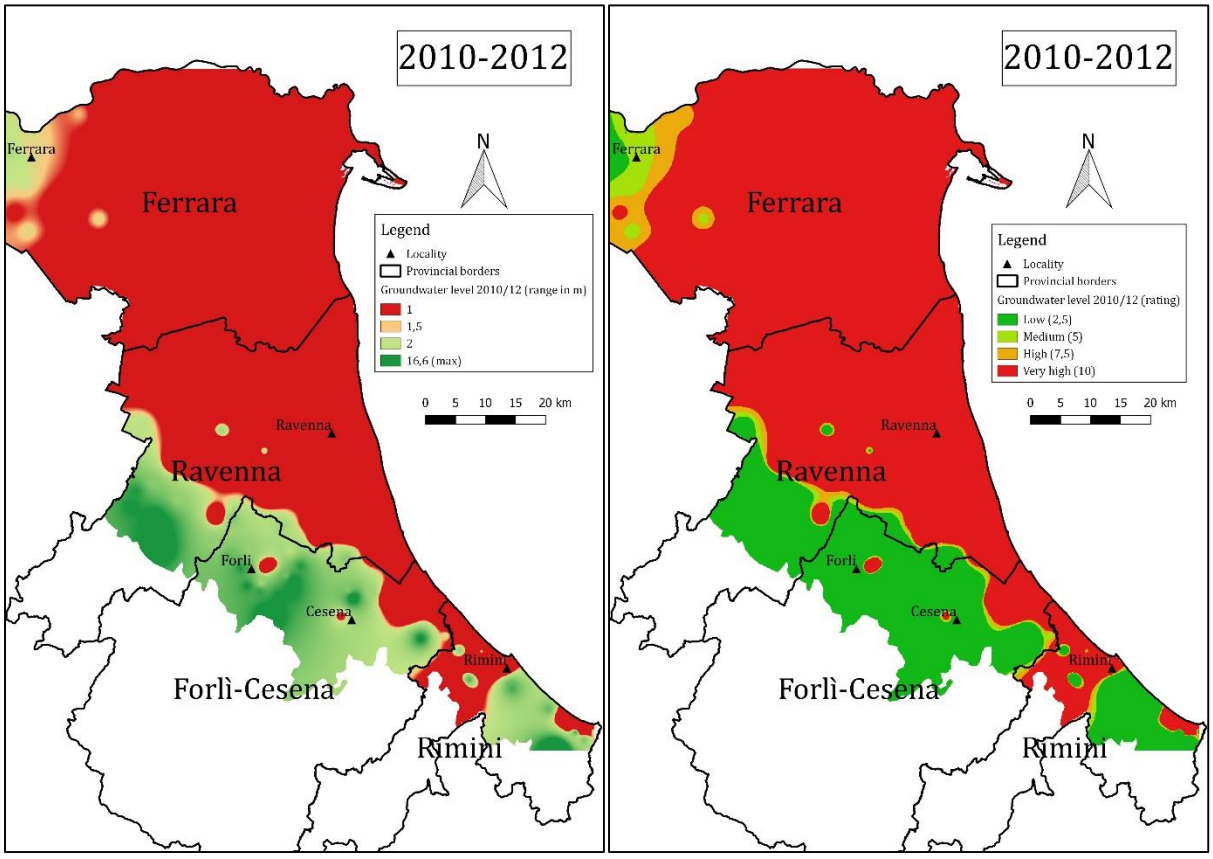

Figure 6-21: Height of groundwater level a.m.s.l. (L) in 2010/12 - range (on the left) and rating (on the right)

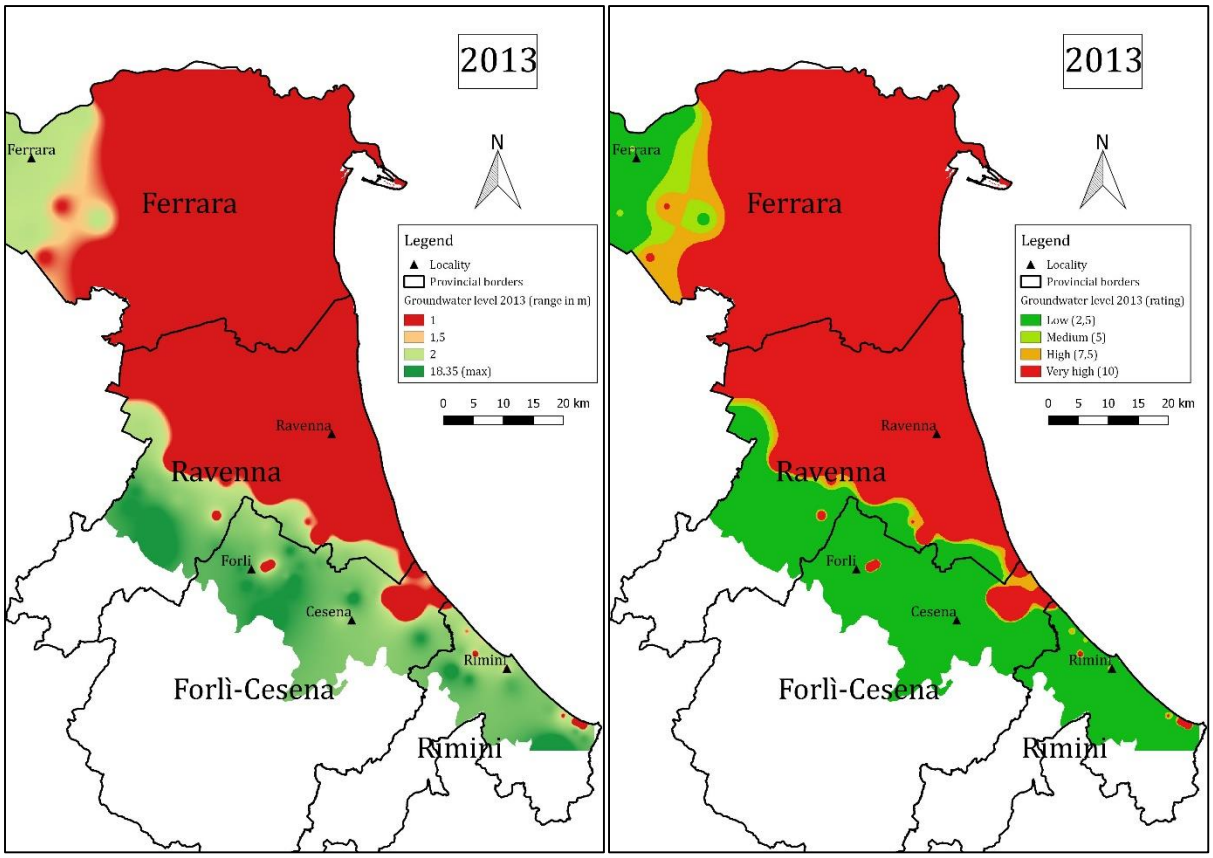

Figure 6-22: Height of groundwater level a.m.s.l. (L) in 2013 - range (on the left) and rating (on the right)

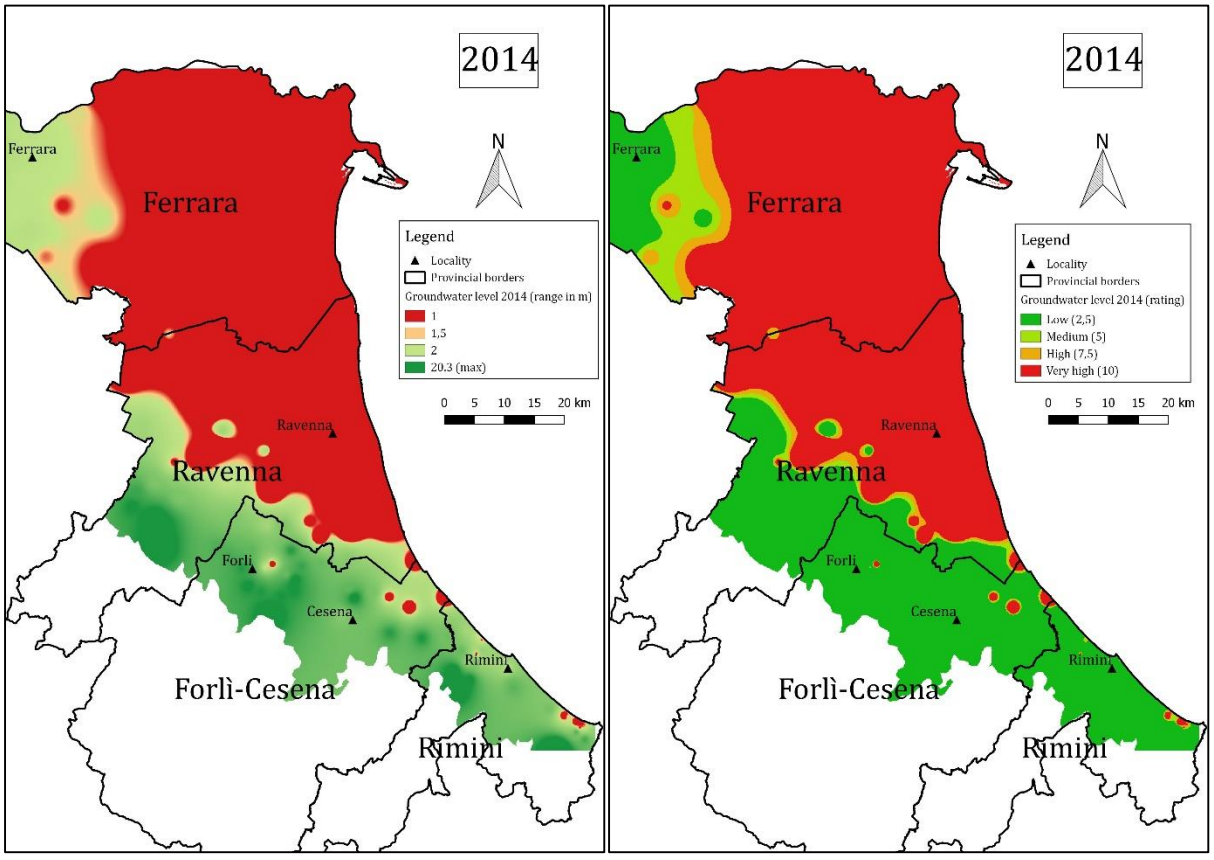

Figure 6-23: Height of groundwater level a.m.s.l. (L) in 2014 - range (on the left) and rating (on the right)

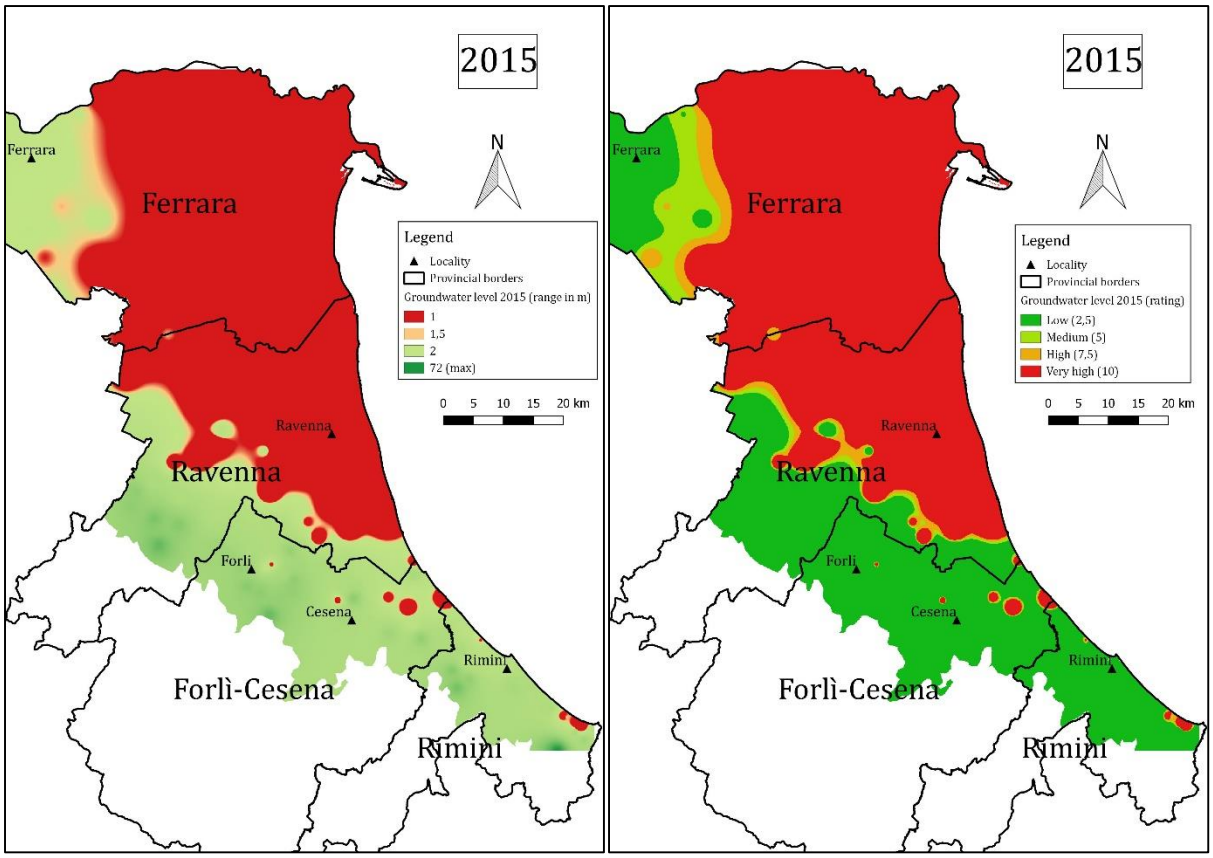

Figure 6-24: Height of groundwater level a.m.s.l. (L) in 2015 - range (on the left) and rating (on the right)

➢ *D*istance from the shore

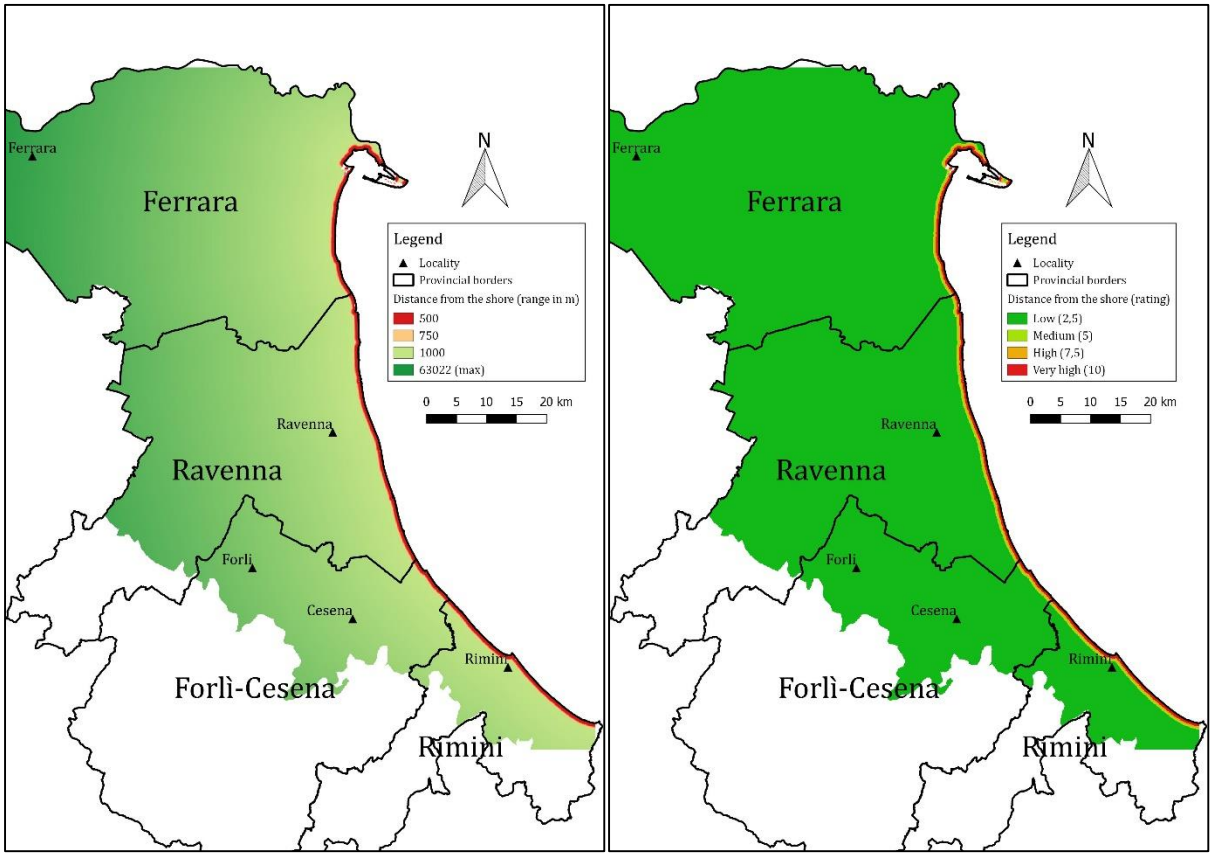

Figure 6-25: Distance from the shore (D) for the confined aquifer A - range (on the left) and rating (on the right)

The distance from the shore (D) was estimated for every point of the study area by using the "Distance Matrix" tool of the software QGIS© (see the table in Appendix C (C.2)). The Figure 6-25 (on the left) was secondly obtained by plotting the results while considering three different reference distances perpendicular to the coastline (i.e. 500, 750 and 1000m).

All the values were then classified into four main classes, according to Table 4-1 and rated from 2.5 for a distance higher than 1000m to 10 for a distance lower than 500m (see the Figure 6-25, on the right). Indeed the impact of SWI decreases when moving perpendicularly from the shore towards the land. The further away the groundwater is from the shore, the lesser the pressure from seawater to infiltrate. [46]

➢ *I*mpact of existing status of SWI in the area

To evaluate the impact of existing status of SWI in the study area (I), it is recommended to consider the ratio $\frac{Cl^-}{HCO_3^- + CO_3^{2-}}$. The chemical parameters used in this ratio were collected from the measurements that were conducted over the whole network of monitoring wells that covers the study area during the period 2010-2015. Unlike the two previous case studies it has been decided to take the dynamic aspect of this parameter into account. To do so, the yearly highest ratio was selected among the sequence of ratios that was available at each well. This approach aims at giving an insight into the effect of the annual variability of this parameter on the vulnerability assessment in the area. The extreme values of the ratios are summarized in the table given in Appendix C (C.2) and were interpolated over the whole study area by using the IDW method in order to produce the series of maps depicted in Figure 6-26 to Figure 6-29 (on the left).

It can be seen from these 4 figures that the impact of existing status of SWI is really low over the study area and this area was therefore mostly assigned a rating of 2.5, as depicted in Figure 6-26 to Figure 6-29 (on the right). This means that this confined aquifer has so far been relatively well preserved from any pollution caused by SWI.

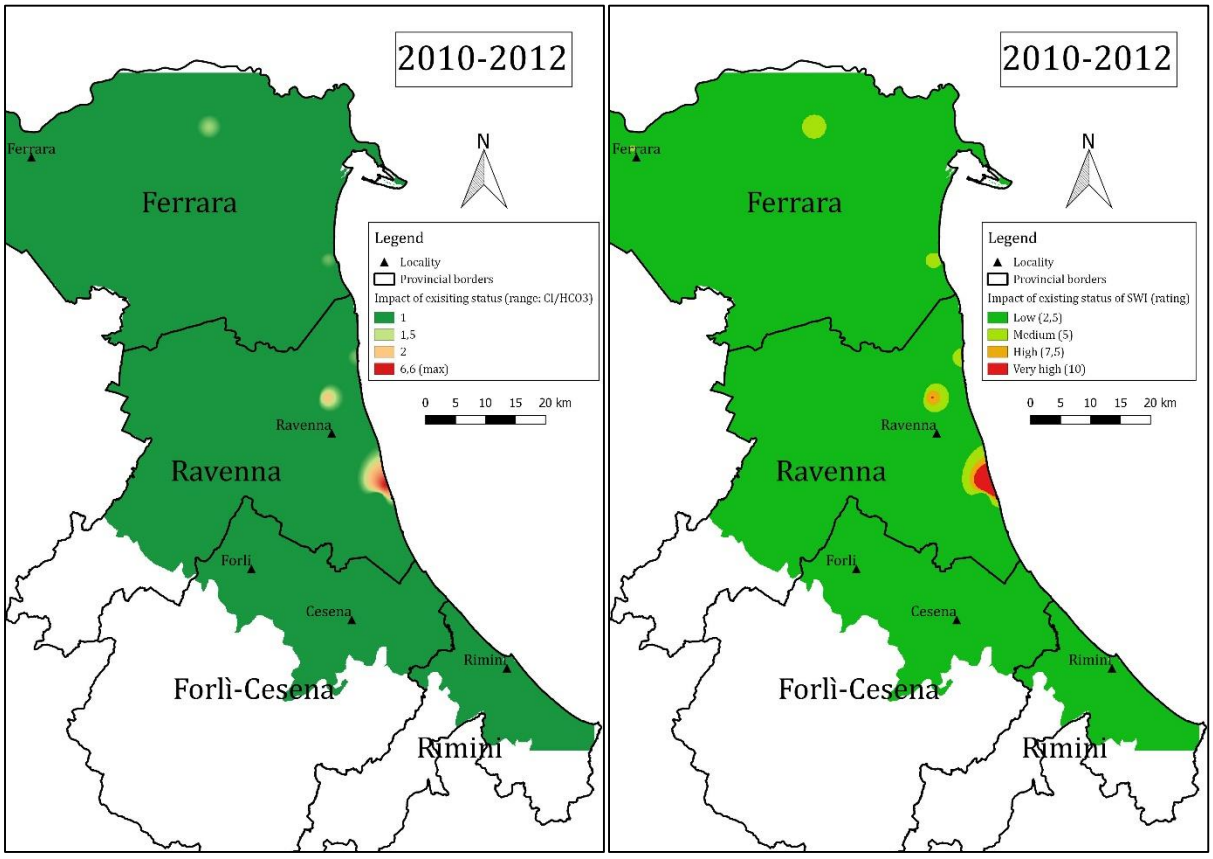

Figure 6-26: Impact of existing status of SWI in 2010/12 (I) - range (on the left) and rating (on the right)

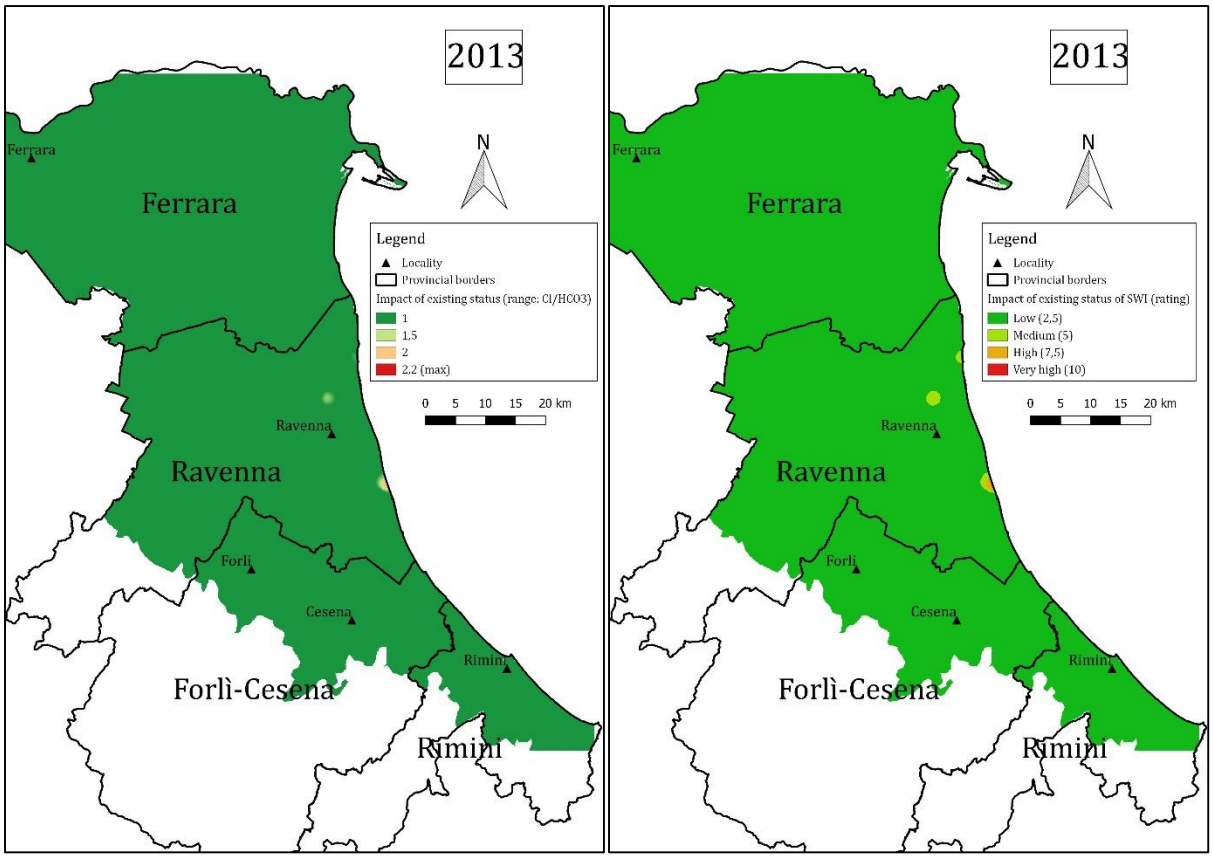

Figure 6-27: Impact of existing status of SWI in 2013 (I) - range (on the left) and rating (on the right)

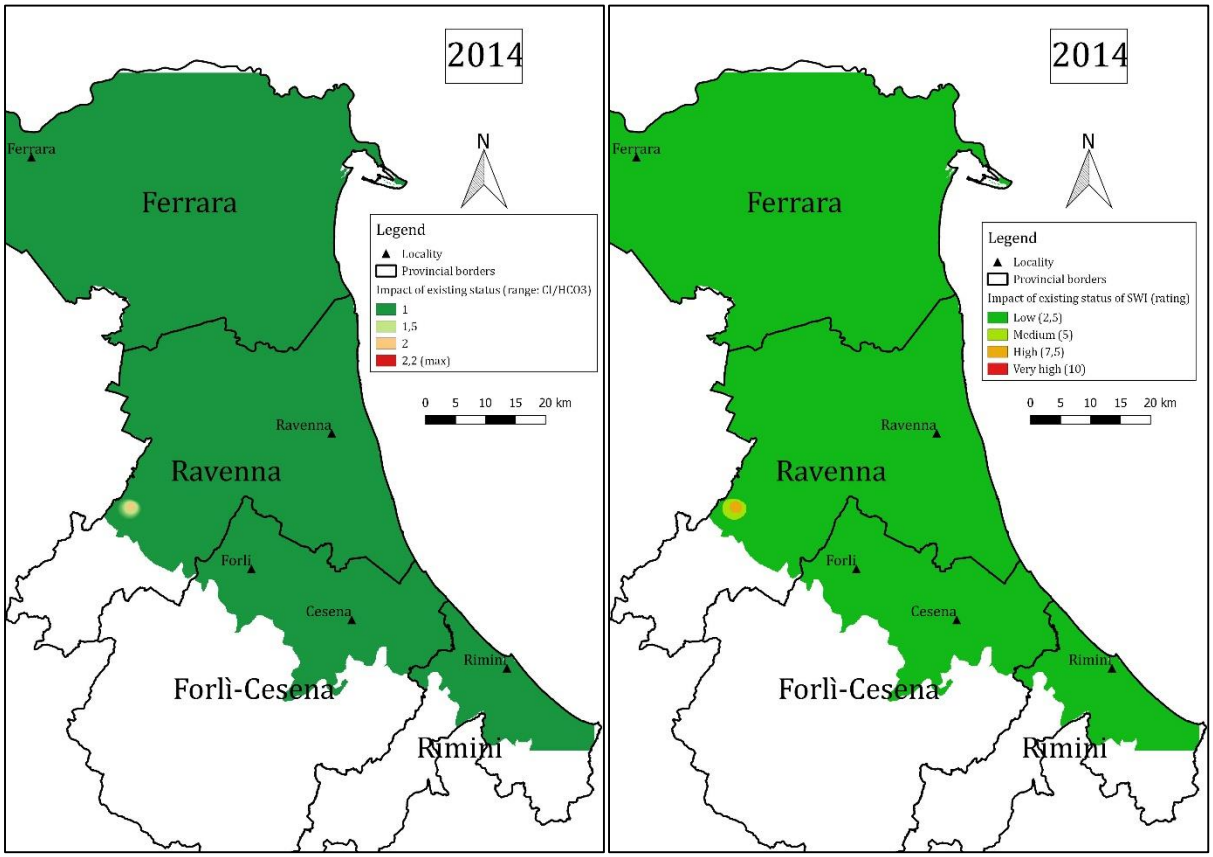

Figure 6-28: Impact of existing status of SWI in 2014 (I) - range (on the left) and rating (on the right)

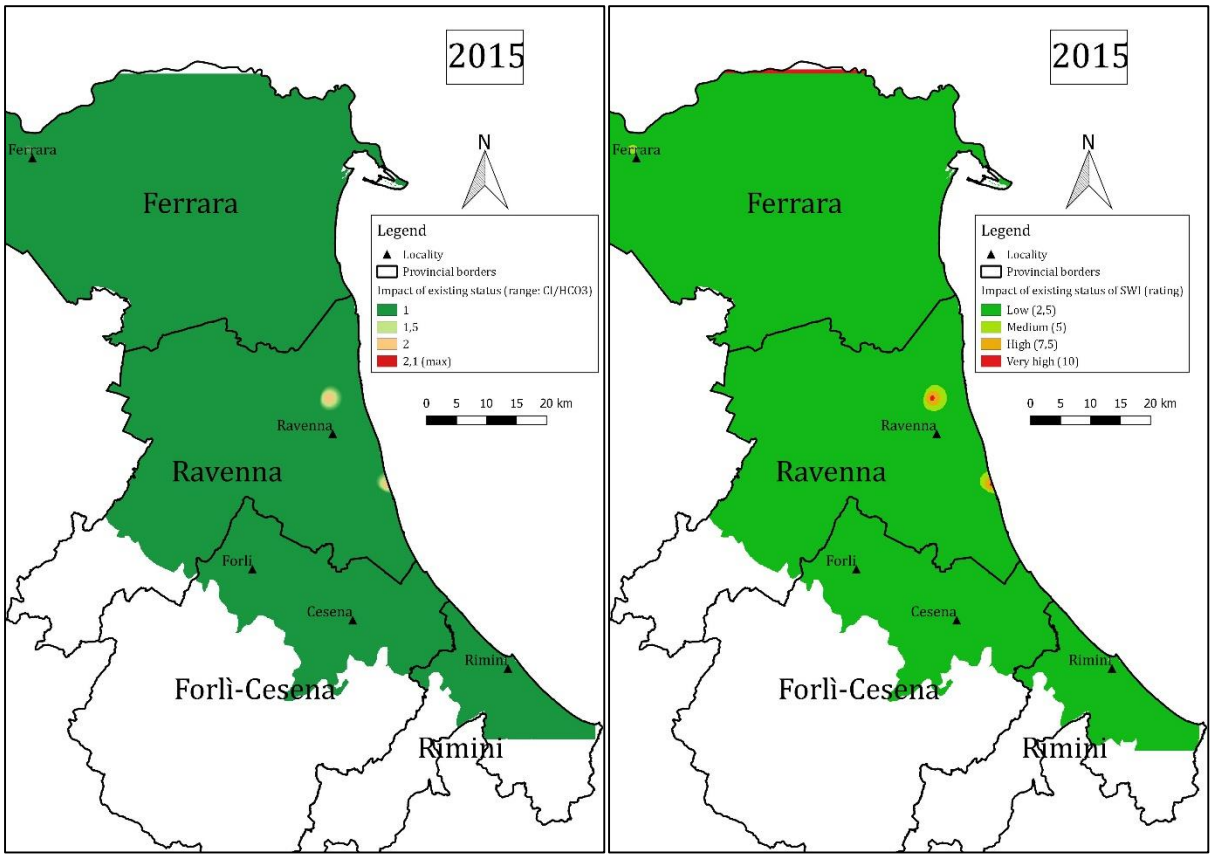

Figure 6-29: Impact of existing status of SWI in 2015 (I) - range (on the left) and rating (on the right)

➢ Thickness of the aquifer

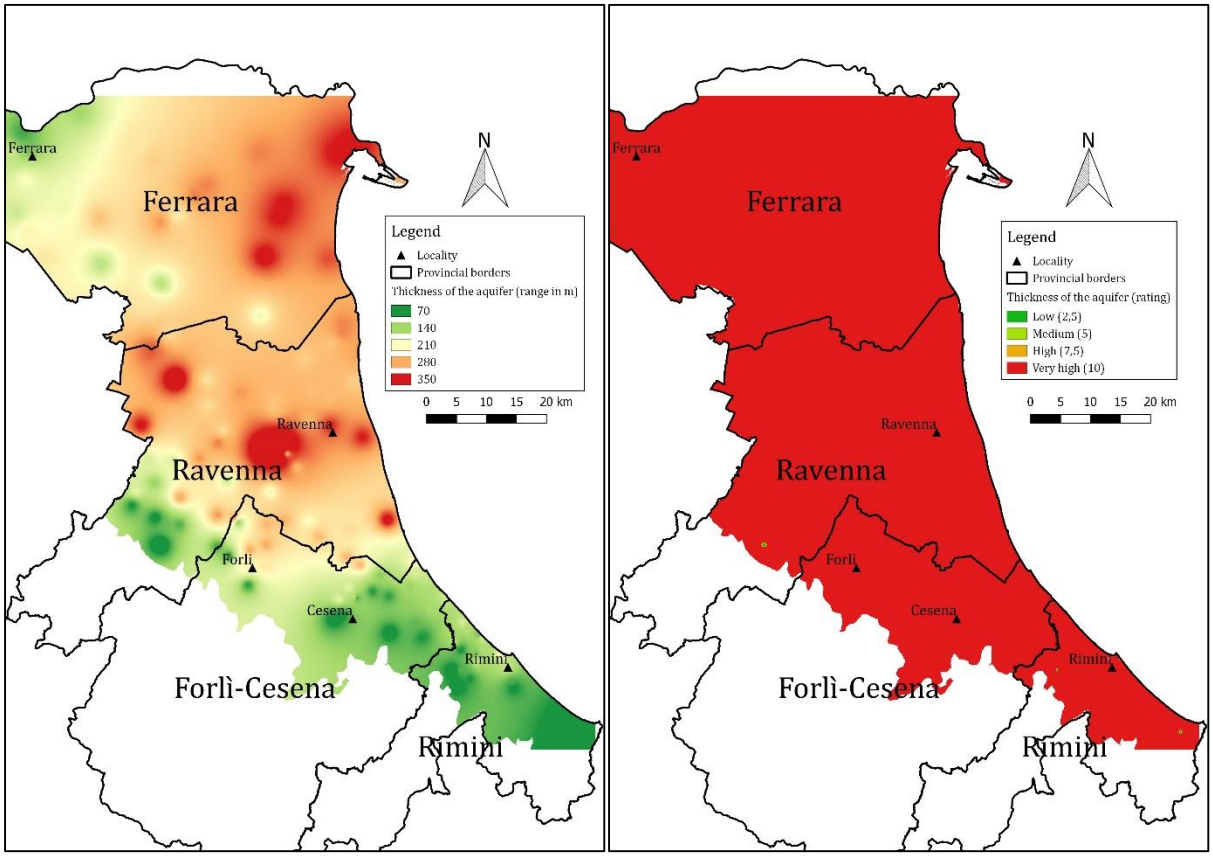

Figure 6-30: Thickness of the confined aquifer A (T) - range (on the left) and rating (on the right)

The data for the thickness of the aquifer (T) were extracted by hand for each well based on the 70 available cross-sections. An example of the manual procedure is presented in Appendix C (C.1) (for the well FE 19-03 in the cross-section n°28) and the approximate results are summarized in the table in Appendix C (C.2). No value has been assigned to the wells that were not located in the direct vicinity of a cross-section. The IDW method was secondly used to produce the map depicted in Figure 6-30 (on the left) by interpolating those known values over the whole study area.

It can be seen from Figure 6-30 (on the left) that the confined aquifer body A is characterized by very large thicknesses in the central part of the study area and tends to shrink when proceeding southwards in the direction of the Apennines. The range of thicknesses varies from a minimum value of 70m to a maximum value of more than 350m. Since those values are much higher than 10m, the whole study area was assigned a rating of 10, as depicted in Figure 6-30. This means that the aquifer thickness has a rather important contribution to SWI.

6.4.3. GALDIT vulnerability assessment

Figure 6-31 to Figure 6-34 give an overview of the spatial distribution of the GALDIT-Index in the study area. They have been prepared by applying equation (23) to the 6 parameter layers that were presented in the previous section 6.4.2 and considering two different colour scales.

The range of the GALDIT-Index scores (i.e. 2.5 to 10) is traditionally divided into three classes: 2.5–5, 5–7.5 and 7.5–10 denoted, respectively, as low, moderate and high vulnerability. Generally speaking, the higher the index, the greater the vulnerability to SWI. The use of this index therefore enables to highlight the areas that are likely to be more susceptible to SWI.

Considering Figure 6-31 to Figure 6-34 (on the left), the conclusions are basically the same as the ones that were drawn for the phreatic aquifer, namely: the most vulnerable area consists of a narrow buffer zone along the coast on the eastern side of the study area and then the vulnerability tends to decrease while moving landwards. This may be explained by the fact that those highly vulnerable zones are characterized by a high proximity to the sea and by a low elevation (i.e. a low height of the groundwater table) and those two factors (i.e. L and D) turn out to be the most significant ones when deriving the GALDIT-Index (see the weights in Table 4-1).

The same pictures were then plotted with a more refined colour scale (see Figure 6-31 to Figure 6-34, on the right) and present a general trend that is relatively similar to the one that was obtained for the parameter "L" in the section 6.4.2. Indeed it can be seen that the interface between the areas respectively characterized by a high and a low level of vulnerability slowly moves backwards towards the sea over time which is a positive feature. It shows that the groundwater level becomes the most significant parameter for the areas located further from the coast because, as it was pointed out a number of times before in this work, this parameter reflects the potential (i.e. the hydraulic pressure) that the aquifer can oppose to the inland motion of the seawater front.

From a statistical point of view, the percentage distribution between low, moderate and high vulnerable zones is summarized in Table 6-2 for the 4 time periods that were considered. These statistics translate into figures the same general trend as the one that was described hereabove, namely a very slow decrease in the vulnerability of the study area over time.

Table 6-2: Percentage distribution of the vulnerability for the confined aquifer A

Percentage [%]		Vulnerability		
		Low	Moderate	High
Time period	2010/12	0	96.6	3.4
	2013	0.01	97.97	2.02
	2014	0.01	98.2	1.79
	2015	0.02	97.91	2.07

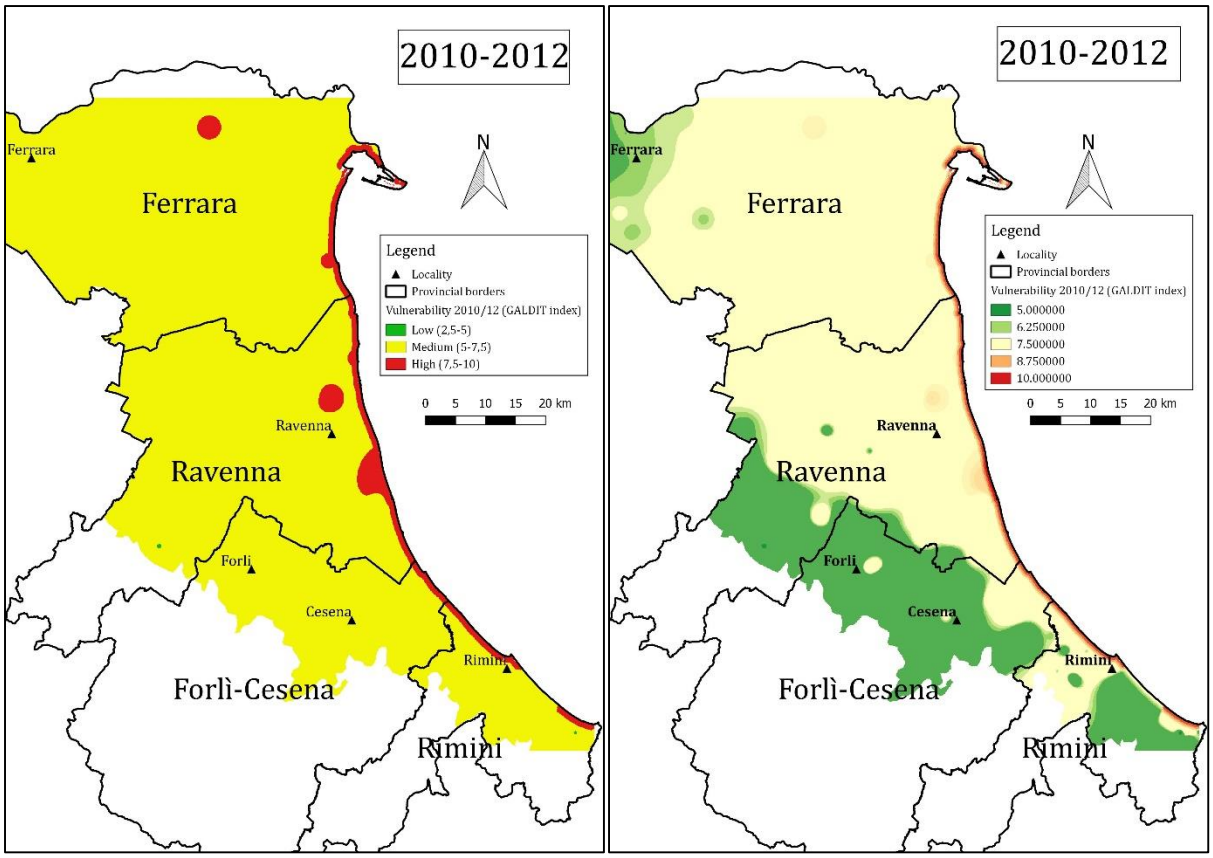

Figure 6-31: GALDIT vulnerability assessment for the confined aquifer A in 2010/12

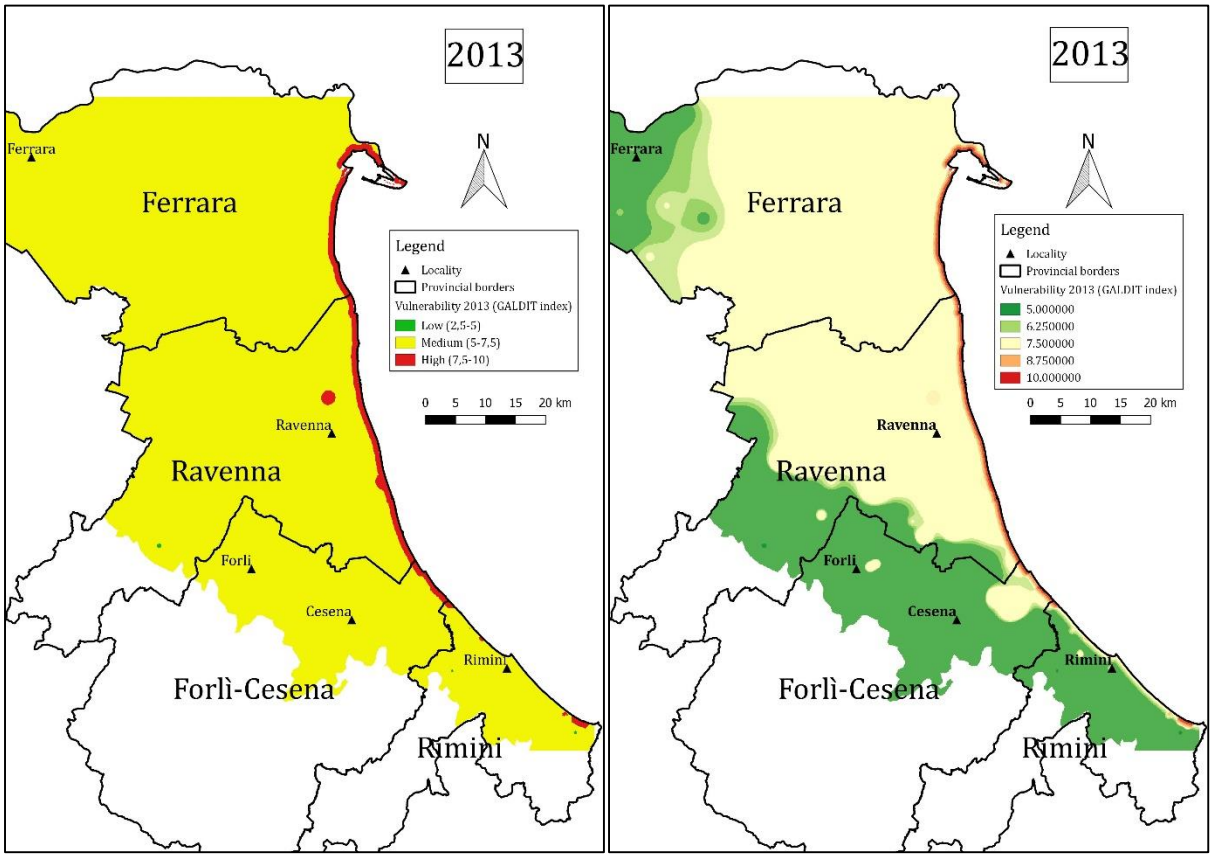

Figure 6-32: GALDIT vulnerability assessment for the confined aquifer A in 2013

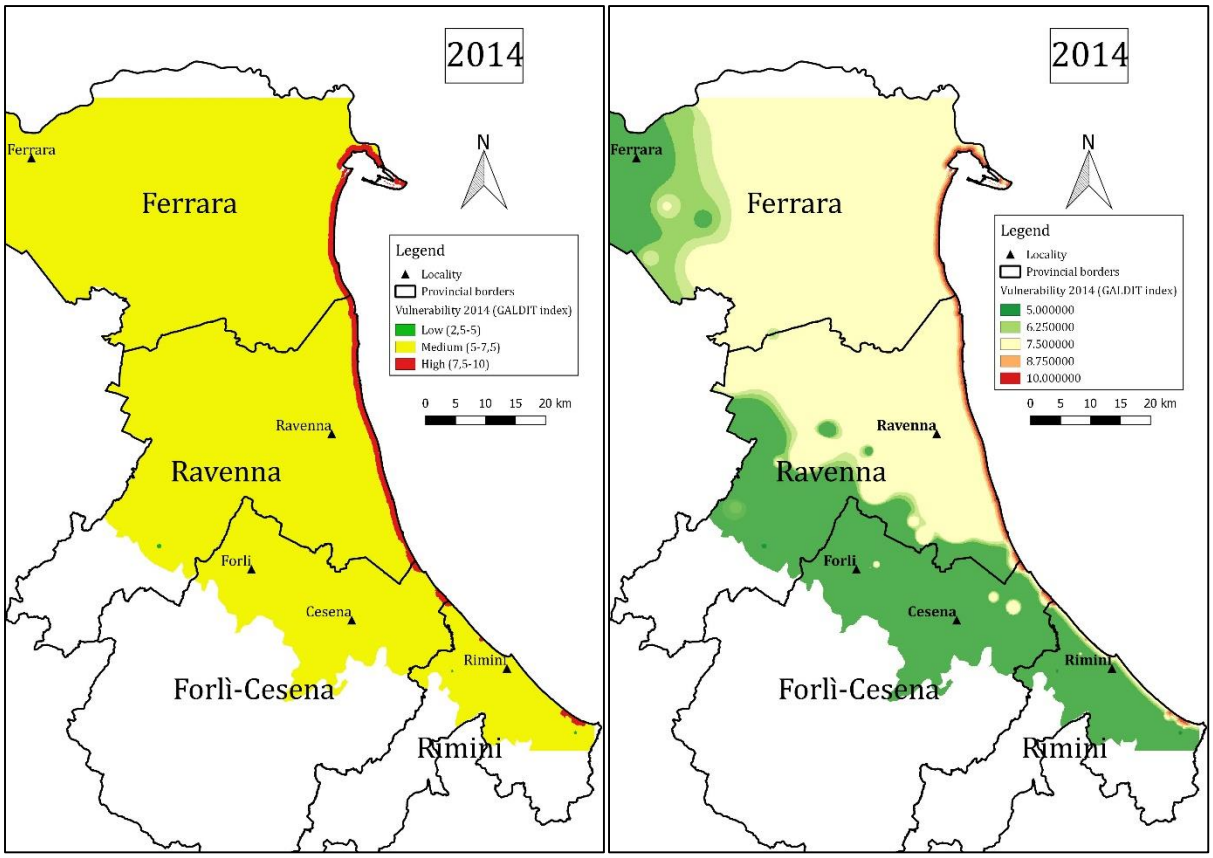

Figure 6-33: GALDIT vulnerability assessment for the confined aquifer A in 2014

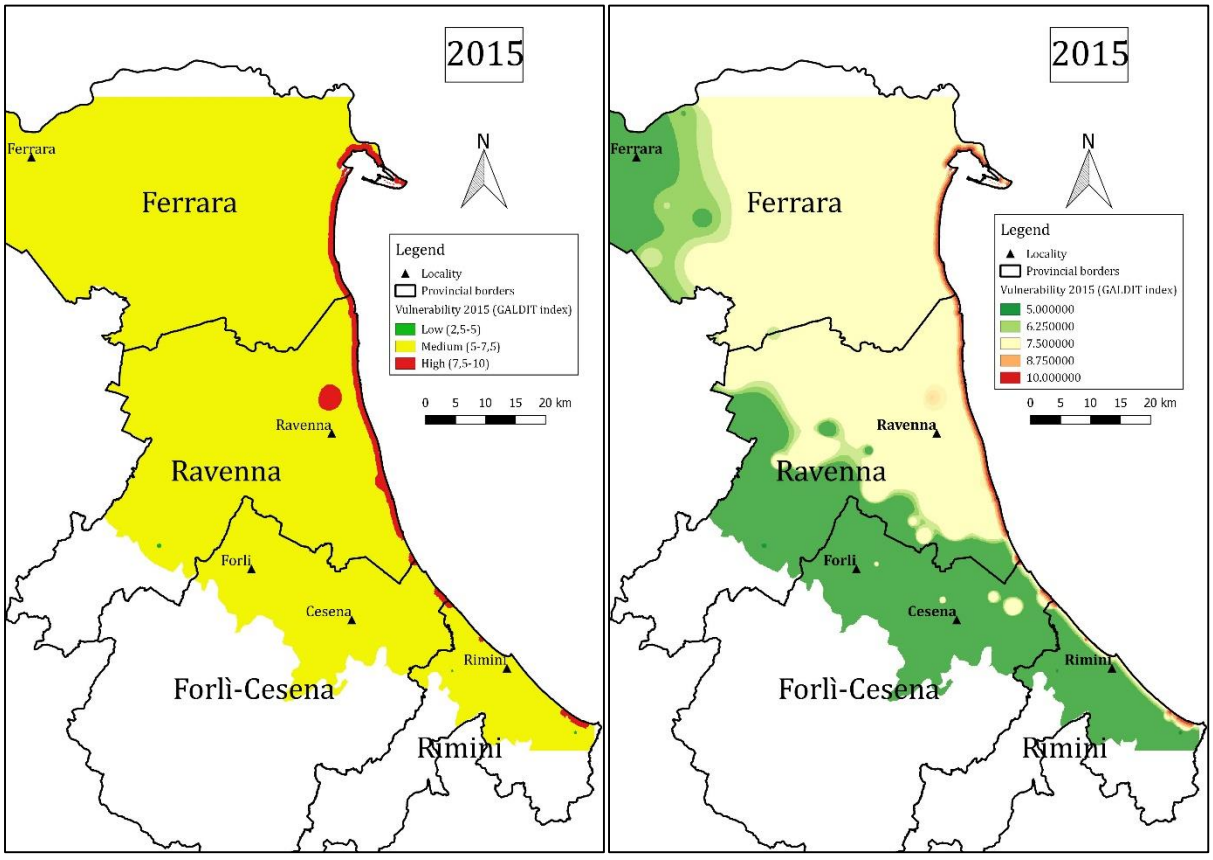

Figure 6-34: GALDIT vulnerability assessment for the confined aquifer A in 2015

Chapter 7
Conclusion

In conclusion, this master thesis consisted of a case study and aimed at assessing the vulnerability of the Emilia-Romagna coastline (Italy) to SWI. This assessment process was carried out by applying the GALDIT-Index to the study area, which basically considers 6 parameters that are presumed to control the phenomenon of SWI:

- The ***G***roundwater occurrence;
- The ***A***quifer hydraulic conductivity;
- The ***L***evel of groundwater above the mean sea-level;
- The ***D***istance from the shore;
- The ***I***mpact of existing status of SWI;
- The ***T***hickness of the aquifer;

The scope of the work was limited to the surface phreatic aquifer and the underlying shallowest confined unit "A" that stretch across the coastal provinces of Ferrara, Ravenna, Forli-Cesena and Rimini. These two bodies were of particular interest since they are the ones that can be exploited for the extraction of freshwater from a technical and economical point of view.

In practice, the contamination of these two bodies by saltwater occurs through two preferential pathways, namely: (1) by lateral intrusion from the sea due to SLR or water over-abstractions; (2) by upward intrusion of relic hypersaline groundwater due to upward hydraulic gradients imposed by anthropic activities (i.e. drainage systems, pumping wells). However, the general structure of the GALDIT-Index doesn't allow to take into account the SWI due to upwelling of relic saline groundwater. The possible future lateral SWI due to SLR was not either part of the scope of this work.

The maps of the 6 parameters were prepared in a GIS environment where they were rated, weighted and overlaid in order to produce the two GALDIT vulnerability maps. The 6 following conclusions were drawn from these two maps:

- Both aquifers present more or less the same general vulnerability pattern, namely a few kilometre wide buffer of very high vulnerability located directly along the coastline and the coastal plain characterized by a moderate vulnerability;
- The high vulnerability of the coastline is due to its direct proximity to the sea and to its low topographic level (i.e. low groundwater level) and these two parameters turn out to be the most significant ones when deriving the GALDIT-index;
- In particular the very low topography, that is emphasized in the study area by natural and anthropogenic subsidence rates, can have a dramatic impact on SWI by lowering the

level of the groundwater table, therefore creating a negative hydraulic gradient towards the land and causing the saltwater to be actively drawn into the aquifer;
- When moving landwards, the vulnerability level naturally tends to be reduced due to the increasing distance from the saltwater source and due to the higher topography and subsequently the higher level of the groundwater table. This is particularly true in the south of the study area with the presence of the Apennines foothills;
- Under the current circumstances the confined aquifer seems to be relatively preserved from SWI even though it is characterized by a high vulnerability. The study of the time evolution of the vulnerability pattern over the period 2010-2015 reveals that the vulnerability doesn't increase and even tends to be slightly reduced over time indicating a generally good balance between abstraction and recharge;
- By contrast the phreatic part seems to be more affected by the problematic of SWI especially in those zones characterized by a very low topography.

The practical goal of those vulnerability maps is to provide a qualitative overview of the problematic of SWI in the study area. They turn out to be a useful tool for the people involved with coastal zone management (i.e. policy makers, local governments, environmental managers…) because they offer them a quick and cost-effective means to prioritize the areas requiring more detailed investigations, to decide where corrective measures have to be taken or where money has to be invested.

<u>Perspectives:</u>

The steps that were necessary to bring this work to an end could be roughly summarized as follows: setting of the initial objectives, deepening of knowledge of the topic through the review of the scientific literature, collection and analysis of the data, computation of the results, analysis of the results and drawing of the conclusions.

However writing a master thesis is a long-run process which implies that some of the initial objectives have inevitably been redefined, refined or prioritized at the expense of some others throughout the life of the project to finally come up with the present work. These changes were set based on the new ideas that came out of the discussions I had with my supervisors and in order to stay in line with the time and data availability constraints.

This being said, a non-exhaustive list of 5 paths that would have been interesting to explore is provided herebelow. These latters can be seen as possible future contributions to enlarge the scope of the present study:

- Studying the effect of SLR in the study area through the use of projections of future potential climatic scenarios;
- Performing a refined analysis of the confined body by considering separately the upper (A1+A2) and lower (A3+A4) parts;
- Applying the second method for the assessment of SWI that was introduced in this work, namely the GQI_{SWI}, and comparing the results with those obtained in the present work;

- Integrating the results of this study into a broader analysis of the risk of the region to SWI by considering the hazards due to human activities in addition to the natural vulnerability of the aquifer. This assessment could be conducted by applying one of the approaches that were briefly reviewed in the bibliographic part of this thesis;
- Discussing the possible remediation techniques that could be applied to the Emilia-Romagna coastline;

Appendix A
UniBo monitoring network

Monitoring Well	Geographical coordinates EPSG12832 - ETRS89 32N		Groundwater occurrence	Hydraulic conductivity (m/day)	Groundwater level (m)	Distance from the shore (m)	Impact of existing status of SWI (-)	Thickness of the aquifer (m)
	X - UTM	Y - UTM						
PZMR4B	760175,44	4935278,1	phreatic	80	2,5	514,328735	4,6952807	6,4
PZMR3B	760476,75	4935288,8	phreatic	80	1,45	214,4729	4,6952807	6,4
PZBEV2G	765486,79	4915293,5	phreatic	80	1,3	89,5285492	4,6952807	6,6
PZMR3A	760458,76	4935397,9	phreatic	80	1,67	218,293564	4,6952807	6,4
PZMRPC	760471,76	4935325,9	phreatic	80	1,54	218,293564	4,6952807	6,4
PZBEV2A	764950,75	4917209,2	phreatic	80	2,21	112,047455	4,6952807	6,6
PZBEV2F	754701,5	4928590,8	phreatic	80	0,77	Out of the study area	4,6952807	6,6
PZBEV3F	765287,39	4916007,1	phreatic	80	1,24	48,0917969	4,6952807	6,6
PZMAR3	765119,96	4915946,7	phreatic	45	2,24	237,148849	5,1085736	16,5
PZBEV3G	754703,48	4928509,7	phreatic	80	1,5	Out of the study area	4,6952807	6,6
PZLD3	765365,46	4915249,3	phreatic	52	1,35	272,441528	4,6952807	8
PZLD1	764456,34	4918600,5	phreatic	48	1,6	288,28006	4,6952807	8
PZMAR2	764467,41	4919407,6	phreatic	45	2,41	169,065292	5,1085736	16,5
PZBEV1G	765514,02	4915303,1	phreatic	80	1,3	89,5285492	4,6952807	6,6
PZMAR4	754806,05	4928401,2	phreatic	45	1,72	Out of the study area	5,1085736	16,5
PZBEV2B	765024,8	4916964,2	phreatic	80	3,75	43,1557693	4,6952807	6,6
PZBEV1F	765314,34	4916013,7	phreatic	80	1,73	21,0803108	4,6952807	6,6
PZLD2	764508,46	4917707	phreatic	62	1,4	354,513428	4,6952807	8

Monitoring Well	Geographical coordinates EPSG12832 - ETRS89 32N		Groundwater occurrence	Hydraulic conductivity (m/day)	Groundwater level (m)	Distance from the shore (m)	Impact of existing status of SWI (-)	Thickness of the aquifer (m)
	X - UTM	Y - UTM						
PZMAR5	754793,03	4928564,8	phreatic	45	2,43	Out of the study area	5,1085736	16,5
PZMAR6	754796,87	4928509,4	phreatic	45	2,17	Out of the study area	5,1085736	16,5
PZSV3	757252,87	4929080	phreatic	36,4	1,472	4221,99316	25,569775	11
PZSV12	757392,89	4932740,9	phreatic	30,6	1,008	3448,64038	1,0725823	11,4
PZSV14	757154,86	4933940,9	phreatic	66,8	1,502	3575,39087	5,1085736	11,4
PZMAR7	754797,93	4928455,7	phreatic	45	2,19	Out of the study area	5,1085736	16,5
PZSV16	757413,83	4935268,9	phreatic	36,4	1,334	3214,10962	7,6806492	9,5
PZSV9	757091,83	4931827,9	phreatic	36,4	1,827	3786,42529	6,9085606	11,4
PZSV2	756629,84	4928956	phreatic	30,6	1,91	4829,31055	1,0725823	11,4
PZSV17	756000,84	4934228,8	phreatic	36,4	1,878	4636,29785	0,2944785	9,5
PZSV18	755688,87	4934319,9	phreatic	36,4	1,199	Out of the study area	0,2944785	8
PZSV19	757578,81	4936058,8	phreatic	2,9	1,83	3082,95728	5,6049344	11,4
PZSV8	756641,86	4930710,9	phreatic	36,4	1,322	4510,52441	0,4977401	11,4
PZSV15	756889,88	4935214,9	phreatic	48,1	2,275	3714,10327	7,6806492	10
PZSV10	756571,83	4931844	phreatic	36,4	1,623	4384,93994	0,4977401	11,4
PZSV22	758490,76	4938825,8	phreatic	36,4	1,876	2227,96826	0,2944785	11,4
PZSV20	757767,84	4936802,9	phreatic	30,6	1,646	2863,21533	1,0725823	11,4
PZSV11	756627,82	4932687,9	phreatic	48,1	1,783	4251,08301	0,124898	10,5
PZSV13	756718,82	4933917,9	phreatic	33,8	1,889	3973,61035	5,1085736	11,4
PZSV21	758035,83	4937692,8	phreatic	36,4	1,535	2567,50879	0,683025	11,4
PZCL2	760844,86	4917976,7	phreatic	17	3,4	3839,00171	5,4428839	18,5
PZSV32	755655,04	4929340,7	phreatic	2,9	0,463	5762,58691	5,1085736	10,7
PZSV26	755736,31	4930196,4	phreatic	36,4	0,066	5520,98535	0,7486889	10,7
P9S	754284,14	4916458,1	phreatic	30	2,889	Out of the study area	0,1507584	2

Monitoring Well	Geographical coordinates EPSG12832 - ETRS89 32N		Groundwater occurrence	Hydraulic conductivity (m/day)	Groundwater level (m)	Distance from the shore (m)	Impact of existing status of SWI (-)	Thickness of the aquifer (m)
	X - UTM	Y - UTM						
PZSV36	757417,14	4929452,3	phreatic	2,9	0,815	3971,34912	19,82957	11,4
PZSV37	755690,84	4928742,7	phreatic	2,9	0,471	5746,61377	2,2467172	9,9
PZSV23	756212,95	4930458,8	phreatic	36,4	0,652	4953,13916	1,7195864	11,4
PZSV35	757389,27	4929675	phreatic	30,6	0,51	3937,83325	5,9474249	10,4
PZSV24	756574,65	4931065,3	phreatic	36,4	0,647	4501,2583	7,3060034	11,4
PZSV33	756325,1	4929303,7	phreatic	2,9	0,793	5089,0127	5,9474249	10,4
PZCL1	760463,2	4918594,6	phreatic	17	3,18	4135,48633	5,4428839	20
PZSV28	756686,66	4929927,6	phreatic	36,4	0,691	4681,13672	4,4369622	11,4
PZSV34	756730,97	4929360,6	phreatic	2,9	1,401	4678,43262	5,9474249	11,4
PMSV7	756796,84	4930440,9	phreatic	48,1	0,442	4387,36133	1,087258	11,4
PZSV31	757365,91	4929979,4	phreatic	2,9	0,723	3995,77783	24,390657	11,4
PMSV6	756504,91	4928478	phreatic	33,6	0,622	5005,32031	10,726563	11,4
PZSV30	757343,66	4930285,4	phreatic	2,9	0,848	3931,06909	12,680755	11,4
PZLA2	760754,04	4924830	phreatic	46	0	2075,88696	11,259858	5,3
P11S	759073,54	4915284,1	phreatic	46	-1,643	Out of the study area	0,2931034	10
PZSV27	756239,43	4929880,3	phreatic	36,4	0,563	5093,44727	24,390657	11,4
PZLA1	760683,25	4923844,4	phreatic	46	0	2448,42529	1,9205064	5,3
PMSV8	757398,87	4928954	phreatic	36,4	1,004	4034,99902	1,7903561	11,4
P8S	757378,16	4916481,6	phreatic	120	0,531	Out of the study area	0,2931034	1,9
P1N	756722,34	4934168,9	phreatic	48,1	1,938	3950,42993	1,0725823	11,4
P19S	764708,58	4910313,2	phreatic	52	1,174	2316,1936	0,9513816	10,5
P2N	760583,15	4933035,8	phreatic	60	1,641	253,284851	4,3519599	9,3
P17S	764206,8	4912593	phreatic	52	1,169	2131,74634	0,9513816	9,4
P13S	761377,49	4914441,7	phreatic	10	1,166	4216,3833	1,3151032	18,7
P6S	758344,29	4916292,8	phreatic	60	-0,118	Out of the study area	0,2931034	13,5

Monitoring Well	Geographical coordinates EPSG12832 - ETRS89 32N		Groundwater occurrence	Hydraulic conductivity (m/day)	Groundwater level (m)	Distance from the shore (m)	Impact of existing status of SWI (-)	Thickness of the aquifer (m)
	X - UTM	Y - UTM						
P10S	759124,1	4915321,7	phreatic	60	-1,695	Out of the study area	5,5056922	10,3
P18S	766400,14	4910768,2	phreatic	46	2,067	685,333191	1,2634178	8,3
P12S	762482,57	4915106,7	phreatic	8	1	3083,17798	2,1874501	14,8
P4S	761630,13	4917299,4	phreatic	40	0,292	3249,57813	1,7776926	14,2
P16S	766014,3	4912695	phreatic	60	1,111	336,641846	5,1172027	7,2
P3S	762656,17	4917539,3	phreatic	60	0,513	2229,80933	9,3144012	7,3
P1S	764266,17	4918978,4	phreatic	58	0,363	417,015564	23,960694	8
P2S	764643,44	4917685,1	phreatic	58	1,029	254,522156	14,032583	8,2
P15S	765571,46	4914727,5	phreatic	58	1,544	240,8806	21,602219	9,7
P5S	760297,44	4916941,4	phreatic	12	1,195	4603,79932	5,4428839	3,5
P14S	762392,22	4913645,4	phreatic	80	1,604	3524,30493	0,4327076	22,3

Appendix B
Collection of the data for the phreatic aquifer A0

B.1 Monitoring network from the Emilia-Romagna Region (Monography for the piezometer P1)

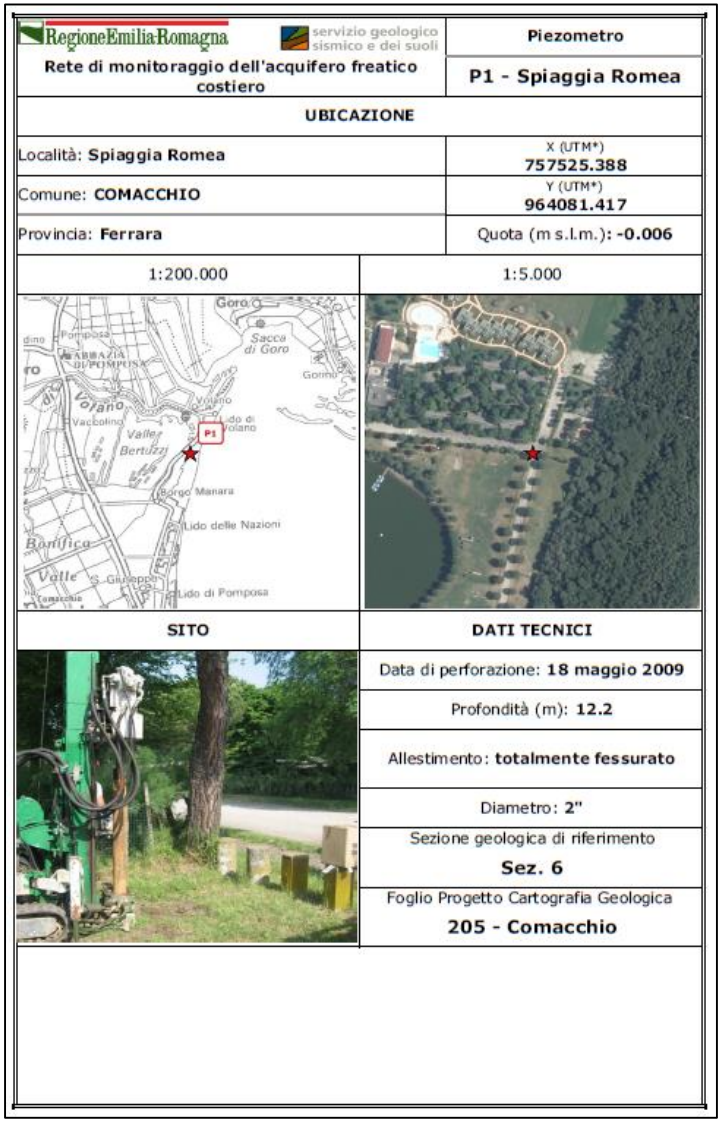

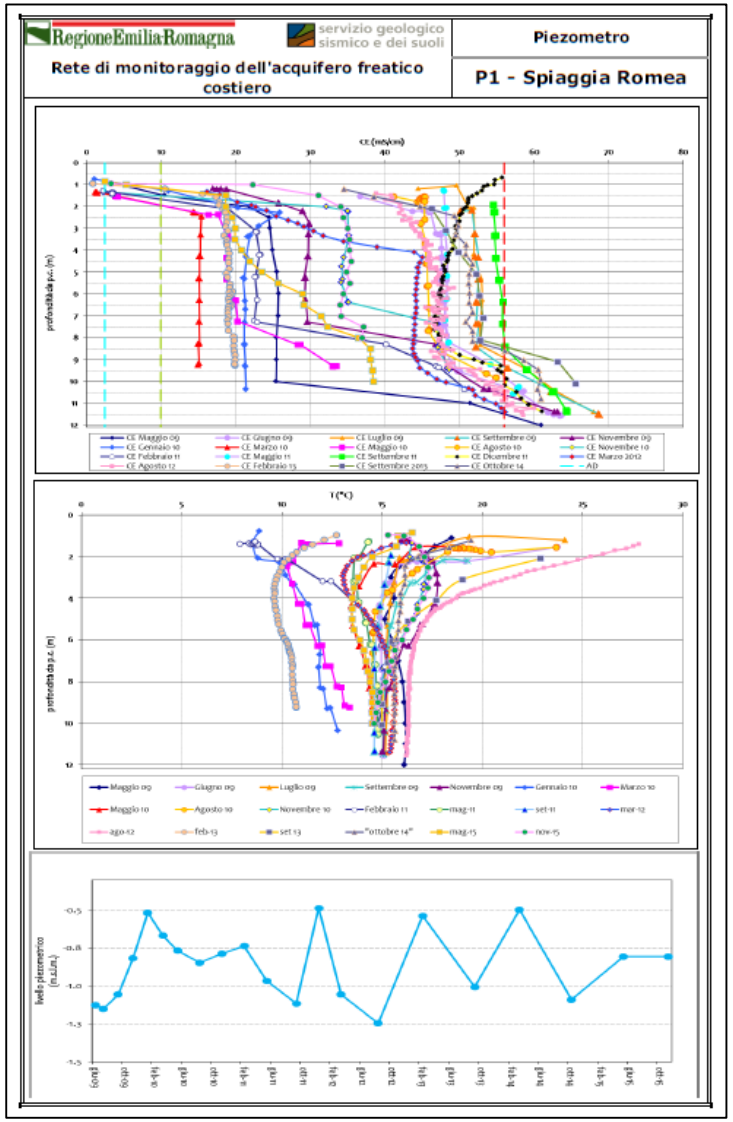

B.2 Maps coming from the literature

➢ Aquifer hydraulic conductivity

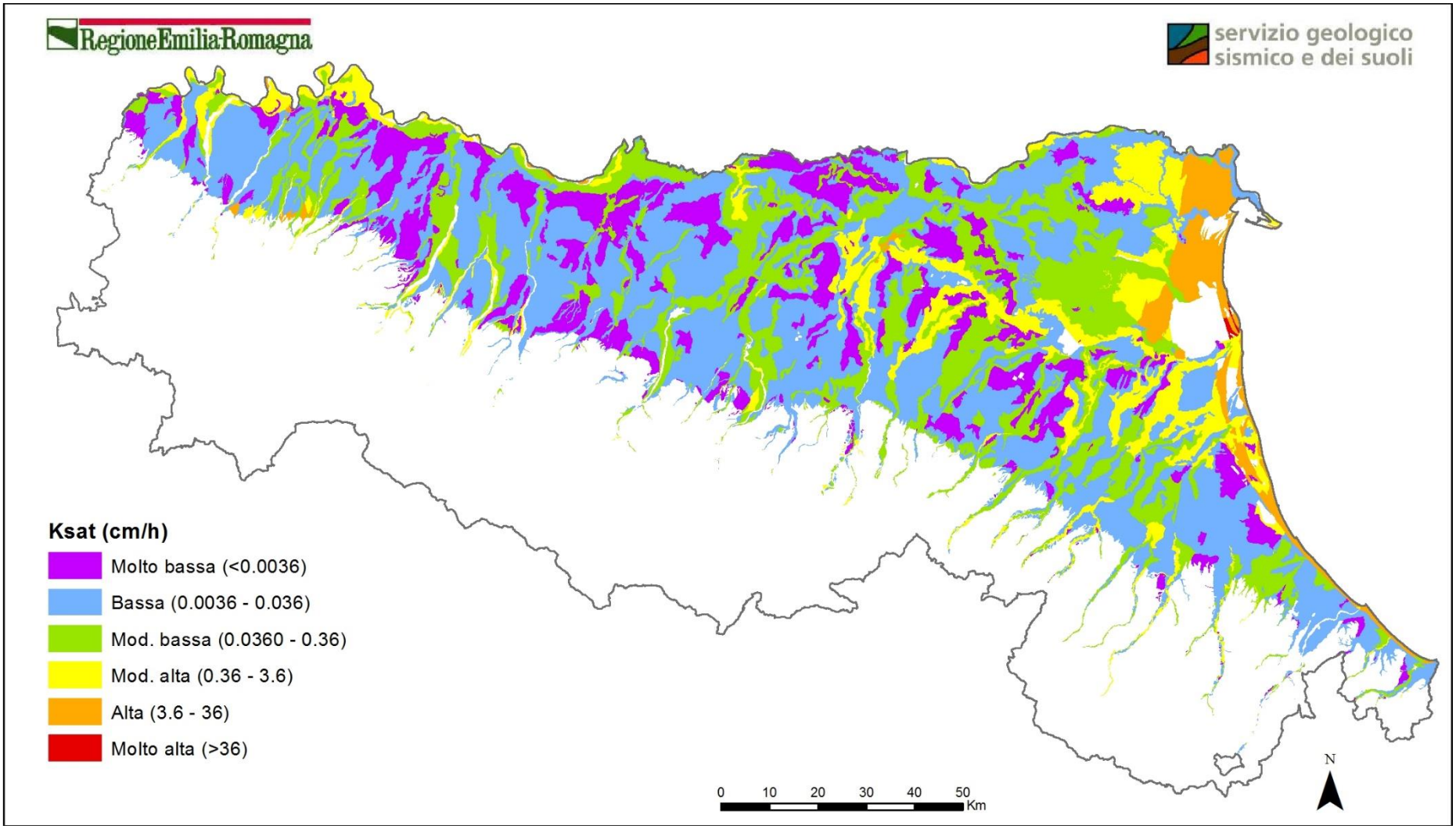

➢ Top and bottom of the phreatic aquifer A0

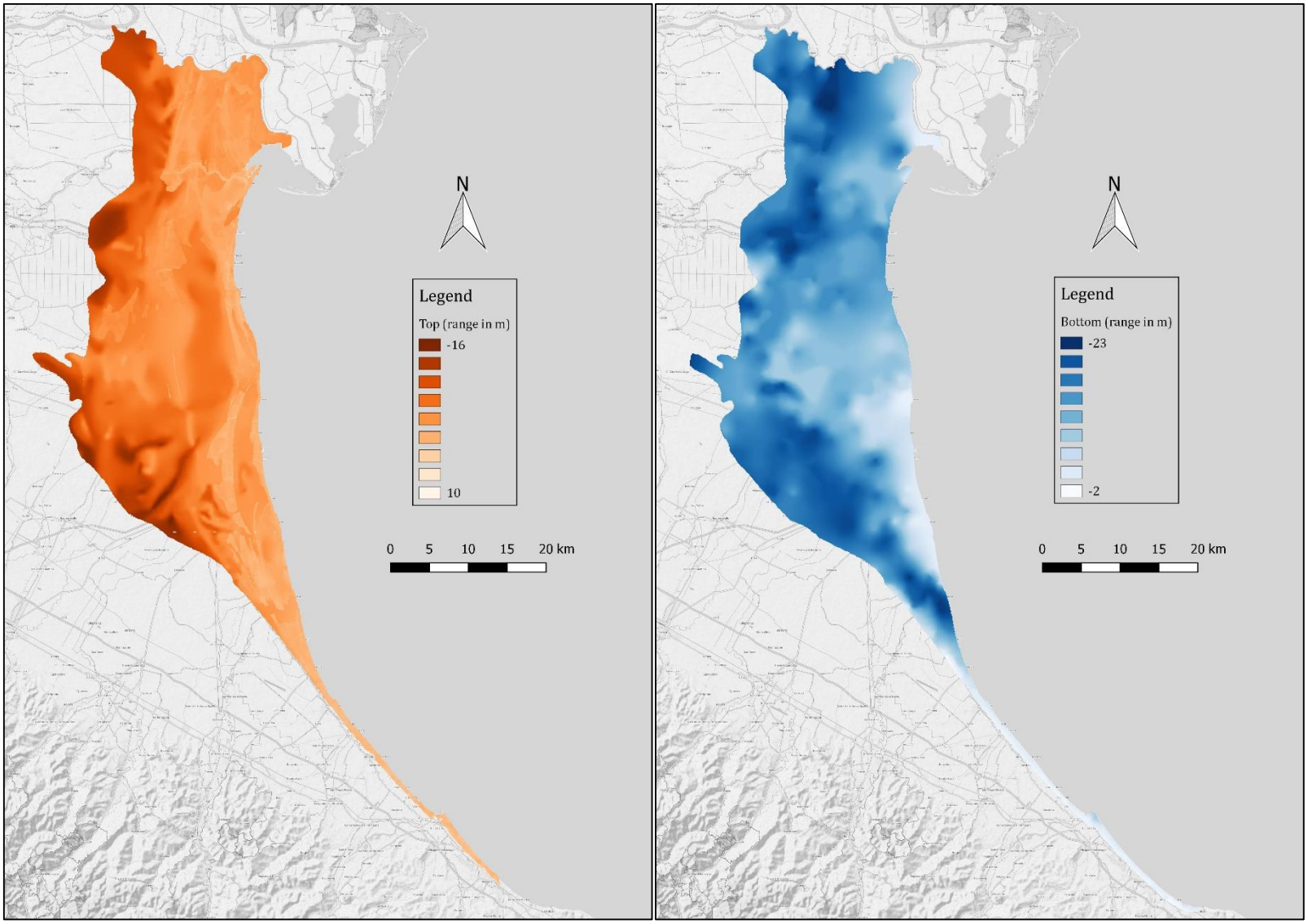

B.3 Summary of the relevant information

Monitoring Well	Geographical coordinates EPSG12832 - ETRS89 32N		Groundwater occurrence	Hydraulic conductivity (m/day)	Groundwater level (m)	Distance from the shore (m)	Salinity (g/L)	Thickness of the aquifer (m)
	X - UTM	Y - UTM						
P1 - Spiaggia Romea	757439,71	4963883,32	phreatic	8,64	-1,3	351,72	47,25	13,27
P2 - Elciola	757072,7	4970270,19	phreatic	8,64	-2,41	1980,72	21,418	17,114
P3 - Volania	748043,92	4957254,4	phreatic	8,64	-3,26	8696,99	0,948	16,55
P4 - Mesola	755221,69	4979547,01	phreatic	0,00864	-3,25	Out of the study area	0,474	13,59
P5 - Bosco Mesola	754911,72	4974386,11	phreatic	8,64	-2,47	6046,89	1,622	15,75
P7 - Vaccolino	751608,82	4965795,26	phreatic	8,64	-3	6448,05	1,622	12,82
P8 - San Giuseppe	755249,78	4957681,42	phreatic	8,64	-2,1	1510,87	65,293	14,9
P9 - Lido di Spina	757562,77	4948709,6	phreatic	24	-0,3	663,52	0,808	13,13
P10 - Collettore Pega	749934,02	4950308,19	phreatic	8,64	-4,085	7447,33	56,792	14
P11 - Collettore Fosse	742300,07	4947683,56	phreatic	8,64	-5,26	15470,00	49,823	13,07
P12 - Reno	758264,79	4941064,75	phreatic	0,864	-1,53	2405,58	42,776	10,35
P13 - Casal Borsetti	760533,76	4937343,83	phreatic	8,64	0,24	46,91	40,616	6,45
P14 - Porto Corsini	760723,78	4932539,92	phreatic	8,64	-0,47	263,03	30,281	9,11
P15 - San Romualdo	751927,95	4931914,9	confined	0,00864	-1,2	Out of the study area	28,561	7,25
P16 - Mezzano	746589,06	4928572,94	confined	0,864	-1,83	Out of the study area	14,523	14,5
P17 - Porto Fuori	758805,86	4921795,12	phreatic	0,864	-1,4625	4952,60	15,51	14,66
P18 - Classe	757546,89	4920065,15	phreatic	0,864	-1,9	6756,71	4,85	20,56
P19 - Punta Marina	762542,77	4925535,06	phreatic	0,00864	0,4	122,67	39,684	7,26
P20 - Lido di Classe	765347,76	4915212,27	phreatic	0,864	-0,1	286,49	27,522	9,88
P21 - Savio	762651,82	4913771,29	phreatic	8,64	-0,35	3282,50	14,345	20,65
P22 - Rimini Chiesa	785847,49	4885407,92	phreatic	8,64	0,175	1029,53	31,148	7
P24 - Pinarella	769142,74	4903206,51	phreatic	8,64	-0,14	640,92	1,602	9,33
P25 - Cesenatico	772460,69	4898843,61	phreatic	8,64	0,11	495,39	4,165	7,37

Monitoring Well	Geographical coordinates EPSG12832 - ETRS89 32N		Groundwater occurrence	Hydraulic conductivity (m/day)	Groundwater level (m)	Distance from the shore (m)	Salinity (g/L)	Thickness of the aquifer (m
	X - UTM	Y - UTM						
P26 - Misano	797110,32	4875834,14	phreatic	8,64	1,39	Out of the study area	1,622	7,25
P27 - Rimini Stazione	785980,49	4885294,92	phreatic	8,64	1,14	1137,94	1,525	5,25
P28 - Rimini Scuola	785408,5	4885902,9	phreatic	8,64	0,6	580,03	1,282	7,15
P29 - San Vitale	756054,87	4932484,9	phreatic	8,64	-0,61	4859,72	11,029	10,48
P31 - Ravenna Est	759666,84	4922871,1	phreatic	0,864	-1,13	3810,39	47,867	8,65
P33 - Corte Ancona	745107,98	4956866,4	phreatic	0,0864	-6,56	Out of the study area	51,12	15,95
P34 - Taglio Nuovo	752822,82	4958263,4	phreatic	8,64	0,86	3929,91	69,3	12,15
P35 - Milano Maritima	765362,79	4908417,4	phreatic	8,64	-0,67	2195,93	1,643	13,71
P37 - Cesenatico nuit	772605,69	4899297,6	phreatic	8,64	-0,3	106,62	30,763	9,7

Appendix C
Collection of the data for the confined aquifer A

C.1 Computation of the thickness and the equivalent hydraulic conductivity

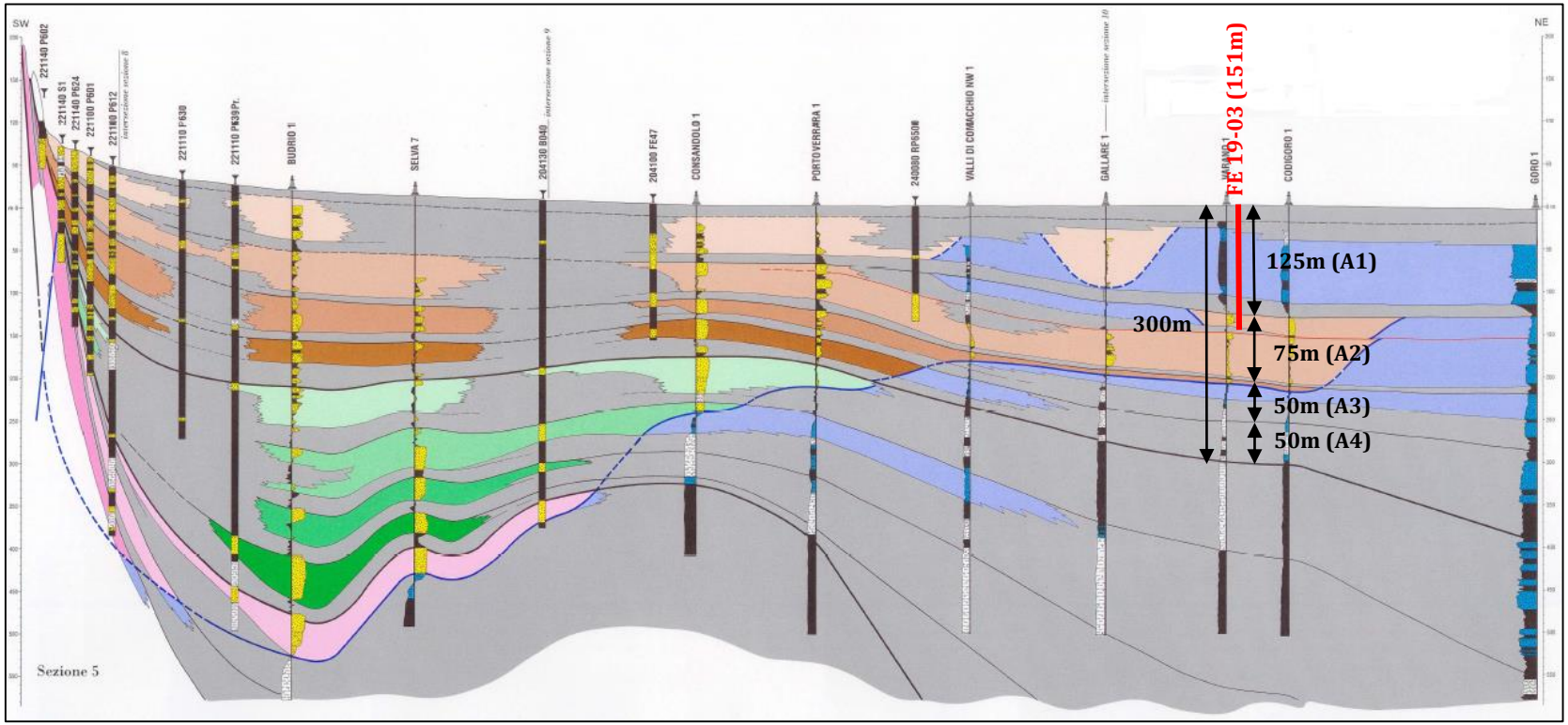

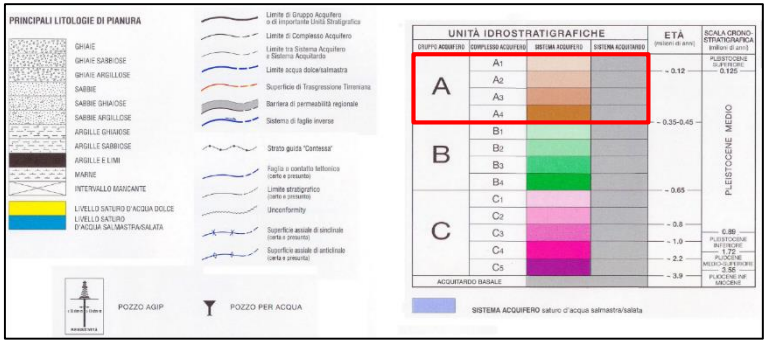

Procedure:

1. Localization of the interface between the interface between the hydrostratigraphic units A & B in the geological section;
2. Localization of the well in the geological section;
3. Measurement of the thickness of the hydrostratigraphic unit A in the geological section;
4. Measurement of the different thicknesses of each layer separately in the geological section;
5. Application of the formula: $\boxed{K_x = \frac{\sum_{i=1}^{n} K_{ix} d_i}{\sum_{i=1}^{n} d_i}}$

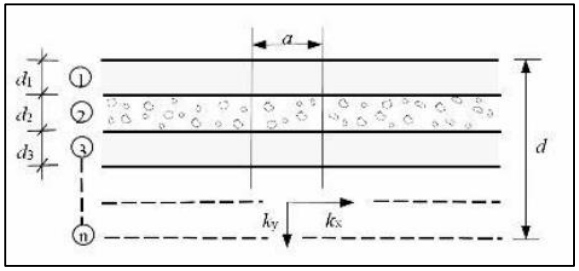

Numerical example:

- Thicknesses

Layer	A1	A2	A3	A4	A
Thickness (m)	125	75	50	50	300

- Hydraulic conductivities (adapted from [67])

Layer		Hydraulic conductivity (m/s)		
		Max	Min	Mean
A1	A1.1	2×10^{-3}	2×10^{-5}	5.85×10^{-4}
	A1.2	3×10^{-4}	2×10^{-5}	
A2	A2.1	2×10^{-3}	2×10^{-6}	7.515×10^{-4}
	A2.2	1×10^{-3}	4×10^{-6}	
A3		2×10^{-3}	1×10^{-5}	10^{-3}
A4		7×10^{-4}	2×10^{-5}	3.6×10^{-4}

- Equivalent hydraulic conductivity

$$K_x(A) = \frac{\sum_{i=1}^{n} K_{ix} d_i}{\sum_{i=1}^{n} d_i} = \frac{5.85 \times 10^{-4} \times 125 + 7.515 \times 10^{-4} \times 75 + 10^{-3} \times 50 + 3.6 \times 10^{-4} \times 50}{300} = 0.0006583 m/s = \boxed{56.88 m/day}$$

C.2 Summary of the relevant information

Monitoring well	Geographical coordinates EPSG12832 - ETRS89 32N		Groundwater occurrence	Hydraulic conductivity (m/day)	Groundwater level (m)				Distance from the shore (m)	Ratio: $\frac{Cl^-}{HCO_3^- + CO_3^{2-}}$				Aquifer thickness (m)
	X - UTM	Y - UTM			2010/12	2013	2014	2015		2010/12	2013	2014	2015	
FE01-01	690795	4978495	Confined	61	2,6	3,1	6,1	5,2	53896	0,04	0,03	0,02	0,04	90
FE05-02	704595	4973733	Confined		2,5	3,8	2,8	2,9	53787	0,12	0,07			90
FE05-03	704670	4973700	Confined		1,2	3,3			41416	0,11	0,13	0,03	0,19	
FE07-01	718990	4981747	Confined		-2,3	-0,6	-1,6	-0,5	31621	0,06	0,04	0,03	0,05	250
FE12-00	726466	4969250	Confined		-2,6	-2	-1,5	-1,4	29126	0,13	0,09	0,09	0,09	
FE13-01	733775	4984419	Confined		-1,5	-1,1	-0,8	-1,5	20365					
FE15-00	743260	4982671	Confined		-2	-1,6	-1,8	-1,7	12880	0,35	0,31	0,2	0,33	
FE16-00	747705	4938463	Confined		-6,6	-7,7	-5	-4,6	13950	0,05	0,05	0,12	0,08	300
FE19-03	744381	4970223	Confined	56,88					824	0,22	0,21	0,04	0,22	380
FE21-00	759844	4971650	Confined	20,97	-2,1	-1,7	-1,8	-1,7	71651					180
FE22-00	685137	4960021	Confined		3,6	5,1	5,6	4,9	66468	0,22	0,21			260
FE23-00	690581	4964056	Confined		3	3,8	4,5	4	75735	0,01	0,01	0,14	0,02	140
FE24-02	680922	4954694	Confined						53377	0,01	0,01		0,01	170
FE30-00	703494	4960438	Confined		0,8	2	2,5	2,1	45648	0,03	0,02	0,06	0,02	200
FE33-00	711280	4961583	Confined		-0,4	1	0,9	1,5	48254	0,03	0,02	0,07	0,03	230
FE35-00	708486	4953080	Confined		0,4	0,9	1,2	1	26279			0,03	0,02	225
FE38-00	730536	4959854	Confined	44,93	-1,5	-1,3	-1,7	-1,3	29331	0,08	0,07	0,04	0,08	290
FE39-01	727496	4958786	Confined		-2,4	-0,9	-0,6	-1,2	23620	0,06	0,05	0,06	0,08	300
FE41-01	733513	4963263	Confined		-0,7			0,2	39107					160
FE47-01	717666	4951764	Confined		-1,4	-0,6	-0,6	-1,1	29530					160
FE48-00	727660	4948452	Confined		-1,5	-0,7	-0,8	-0,4	32827	0,24	0,18	0,08	0,19	230
FE49-00	725007	4944875	Confined		-3,2	-2,9	-2,7	-2,7	78450	0,19	0,35	0,25	0,21	250
FE52-00	680585	4979784	Confined	58,9	5,2		5,5		72251	1,26	1,07	0,11	1,27	

Monitoring well	Geographical coordinates EPSG12832 - ETRS89 32N		Groundwater occurrence	Hydraulic conductivity (m/day)	Groundwater level (m)				Distance from the shore (m)	Ratio: $\frac{Cl^-}{HCO_3^-+CO_3^{2-}}$				Aquifer thickness (m)
	X - UTM	Y - UTM			2010/12	2013	2014	2015		2010/12	2013	2014	2015	
FE53-00	685655	4972210	Confined		6,9	6,1	6,9	5,3	8849	0,36	0,28	0,07	0,31	360
FE54-02	748261	4961674	Confined				-1,5	-1,4	55192			0,17	0,25	170
FE56-00	702655	4970438	Confined		3,3	3,8	3,7	3,8	52474	0,05	0,04	0,18	0,06	110
FE58-02	705536	4971213	Confined	60	1,6	1,9	2,5	2,6	52111	1,13	1,03	0,16	1,19	210
FE60-00	705138	4965716	Confined		2	2,8	2,3	2,4	44843	0,03	0,02	0,03	0,03	140
FE61-01	714115	4976957	Confined		1,4	2,6	1,8	2	77938	0,07	0,03	0,05	0,03	140
FE63-00	678700	4954402	Confined		4,3	6,5	7,1	7	33866	0,01	0,01	1,3	0,01	
FE64-00	727936	4983760	Confined		-0,5		1	-0,1	23196	0,04	0,02	0,09	0,04	
FE65-00	735836	4974726	Confined		-4,2	-3,3	-3,2	-3,2	11677	1,41	0,86	0,13	0,93	375
FE69-00	745041	4953044	Confined		-2,1	-1,5	-1,6	-1,6	74390	0,33	0,28	0,12	0,34	170
FE72-00	682383	4958363	Confined		9,1	10,8	11,2	10,9	51069	0,01	0,05	0,09	0,01	220
FE73-00	705664	4957355	Confined		1,8	3	3,5	3	15024	0,12		0,06	0,05	200
FE74-00	744292	4943212	Confined		-2,7	-2,6	-2,6	-2,6	34557	0,35	0,29	0,05	0,3	230
FE75-00	723796	4971332	Confined		-0,4	-0,2	0,2	-0,2	1139	0,52	0,42	0,01	0,43	325
FE76-00	755741	4952731	Confined	56,3					60422	1,26	0,88	0,01	0,73	175
FE77-00	697179	4968963	Confined		3,9	5,1	5	4,7	68130	0,05	0,04	0,02	0,05	70
FE78-01	689953	4972978	Confined	55,94			8,2	7,8	79016			0,02	0,5	255
FE80-00	679931	4979526	Confined	58,6	5,7	4,7		5,6	76034					210
FE81-00	682819	4978747	Confined	60,06	6	6,2		5,9	71623					150
FE-F01-00	686604	4974399	Confined		4,8	5,3		5,3	70387	0,15	0,02	0,02	0,07	200
FE-F04-01	686434	4961020	Confined				12,2	12,3	39345			0,02	0,03	260
FE-F09-00	717485	4959398	Confined		1,7	2,2	2,3	2,3	32982	0,06	0,08	0,02	0,07	
FE-F13-00	726662	4978146	Confined		-1,7	-1,2	-0,6	-1	42276	0,15	0,13	0,02	0,1	
FE-F15-00	717844	4981138	Confined				0,2	-0,4	1570			0,02	0,05	
FE-F21-00	755130	4956058	Confined		-0,8	-0,7	-0,2	-0,4	9498	0,16	0,06	0,04	0,03	360

Monitoring well	Geographical coordinates EPSG12832 - ETRS89 32N		Groundwater occurrence	Hydraulic conductivity (m/day)	Groundwater level (m)				Distance from the shore (m)	Ratio: $\frac{Cl^-}{HCO_3^- + CO_3^{2-}}$				Aquifer thickness (m)
	X - UTM	Y - UTM			2010/12	2013	2014	2015		2010/12	2013	2014	2015	
FE-F22-00	747369	4959658	Confined		-4,3	-4,5	-4,7	-3,7	1898	0,12	0,13	0,05	0,1	360
FE-F24-00	757112	4970216	Confined	42	-2,2	-1,9	-2,1	-1,8	22018	0,15	0,05	0,02	0,04	300
FE-F26-00	735355	4964826	Confined		0,3	0,4	0,4	0,3	53896	0,15	0,11	0,03	0,1	90
RA02-02	730127	4932569	Confined						30575	0,03	0,03		0,03	440
RA03-00	724418	4924919	Confined		2,5	3,9	5,7	6,3	37158					360
RA05-00	741015	4930369	Confined		-4,2	-3,7	-2,8	-3	19939					290
RA08-00	738690	4915703	Confined	58	-0,2	0,7	2,2	2,1	26000					175
RA09-00	758180	4941791	Confined	56	0,9	0,9	0,9	0,9	2480					300
RA09-01	758227	4940523	Confined	56	-1,8	-1,9	-1,8	-1,5	2420	0,07	0,07	0,05	0,07	300
RA12-01	755883	4938447	Confined	57,32	-0,5	-0,2	-0,2	-0,1	4818					260
RA13-02	756201	4911624	Confined		-7,3	-6,8	-6,8	-6,7	10023	0,46	0,49	0,05	0,46	
RA14-01	745922	4913833	Confined	59,892	-7,6	-6,7	-7,6	-7	19312	0,04	0,04	0,04	0,04	200
RA15-00	723585	4913863	Confined		16,2	18,2	16,8	22,8	40760	0,06	0,04	0,06	0,04	190
RA17-01	730858	4912855	Confined		5,8	6,5	8,9	9,4	34279	0,04	0,04	0,12	0,04	280
RA18-00	726769	4909433	Confined		26,2	27,9	31,5	31	39004					50
RA20-02	748148	4909107	Confined	57,5					18528	0,04	0,04		0,04	275
RA21-01	766702	4912271	Confined		-3,5	-3,1	-2,1	-2,8	55					
RA23-01	745794	4933322	Confined						14959	0,04	0,07		0,05	270
RA24-00	760513	4938208	Confined	55,92	-1,6	-1,5	-1,2	-1,2	204					285
RA24-01	760474	4936523	Confined	55,92	-0,7	-1,3	-0,5	-0,6	157	1,29	1,15	0,13	0,74	285
RA29-00	760044	4932212	Confined	56,7	-2,4	-2,2	-1,7	-1,7	862					250
RA30-00	752680	4930373	Confined	55,42	-6,2	-5,2	-5,1	-5,2	8445	0,04	0,05	0,12	0,06	265
RA33-01	761243	4922912	Confined					-3	2284		0,29	0,12	0,26	350
RA34-02	754282	4919291	Confined		-6,7	-5,8	-5,1	-5,2	10141	0,18	0,21	0,19	0,1	
RA35-00	750390	4917832	Confined	56,25	-7,7	-7,1	-4,8	-6,4	14238					270

Monitoring well	Geographical coordinates EPSG12832 - ETRS89 32N		Groundwater occurrence	Hydraulic conductivity (m/day)	Groundwater level (m)				Distance from the shore (m)	Ratio: $\frac{Cl^-}{HCO_3^- + CO_3^{2-}}$				Aquifer thickness (m)
	X - UTM	Y - UTM			2010/12	2013	2014	2015		2010/12	2013	2014	2015	
RA38-00	759174	4907496	Confined	57,53	-5,9	-5,8	-9,6	-5,6	8420					240
RA39-00	754064	4906316	Confined	57,53	-5,2	-5,3	-4,9	-4,6	13632					265
RA41-02	764107	4912914	Confined		-5,8	-4,8	-4,8	-4,8	2145	0,13	0,12	0,18	0,13	
RA42-01	755862	4924811	Confined		-0,5	0,4	0,3	0,4	6642					350
RA44-00	722038	4933143	Confined		-2,1	-1,7	-1,6	-1,3	38632	0,04	0,05	0,02	0,03	
RA45-01	751774	4936004	Confined	56,7	-2,6	-2,5	-2,6	-2,3	8867					250
RA47-00	746633	4927545	Confined		-5,8	-4,9	-4,3	-4,3	14909					260
RA47-01	746274	4928145	Confined						15181	0,16	0,16		0,17	260
RA48-01	737141	4909916	Confined		-6	-1,1		8,5	28771					290
RA49-00	752304	4925658	Confined		-7,9	-8,6	-7,9	-0,4	9716					270
RA53-04	765442	4909103	Confined		-13,9	-9,3	-11,6	-11,3	1920	0,48	0,65	0,04	0,48	370
RA55-02	729890	4918790	Confined	57	-3	-3,2	0,6	-1,8	33250	0,08	0,07	0,05	0,11	180
RA58-00	735531	4928175	Confined		-6,5	-5,9	-5,3	-5,1	25671					240
RA59-01	737143	4921852	Confined		-7	-6,3	-5,7	-5,5	25375	0,15	0,12	0,09	0,12	300
RA60-01	735399	4932471	Confined		-9,1	-8,4	-7,3	-7,5	25398	0,04	0,04	0,06	0,04	235
RA65-01	754103	4917457	Confined						10609	0,09	0,08	0,03	0,16	
RA66-01	757991	4912838	Confined		-6,1	-5	-4,4	-4,3	8029					
RA67-00	747675	4921574	Confined		-7,4	-7	-6,2	-6,6	15474					600
RA67-01	747277	4920444	Confined		-8,9	-8,1	-6,8	-7,4	16236	0,04	0,04	0,03	0,04	600
RA70-01	763042	4903465	Confined		-2,5				5993	0,05	0,05	0,01	0,05	200
RA71-00	726046	4937271	Confined		-6,7	-6,2	-7,5	-4,4	34152					320
RA71-01	725959	4937443	Confined						34175	0,05	0,08		0,07	320
RA73-00	769981	4902222	Confined		-3,1	-2,1	-2	-1,5	360					225
RA74-00	725394	4918993	Confined	56,7					37524	0,05	0,03		0,03	180
RA75-00	724792	4932409	Confined						35977	0,09	0,06		0,04	

Monitoring well	Geographical coordinates EPSG12832 - ETRS89 32N		Groundwater occurrence	Hydraulic conductivity (m/day)	Groundwater level (m)				Distance from the shore (m)	Ratio: $\frac{Cl^-}{HCO_3^- + CO_3^{2-}}$				Aquifer thickness (m)
	X - UTM	Y - UTM			2010/12	2013	2014	2015		2010/12	2013	2014	2015	
RA76-03	734106	4919319	Confined		-13,2	-9,7	-5,7	-6,9	28959	0,06	0,06	0,04	0,06	290
RA77-00	722887	4911491	Confined		18,2	20,7	21,6	22,7	42242	0,05	0,05	1,98	0,05	70
RA78-00	730747	4908299	Confined					26,3	35393	0,05	0,06		0,06	100
RA79-00	726558	4915324	Confined		6,9	8,9	9,2	11,2	37432	0,23	0,24	0,07	0,23	135
RA80-02	748688	4920131	Confined	56,25		-4	-3,4	-3,8	15041		0,09	0,01	0,08	275
RA81-01	746740	4935810	Confined						13870	0,05	0,04	0,02	0,05	
RA82-00	747033	4929315	Confined		-8,8	-7,8	-6,9	-7,1	14133					260
RA84-01	752295	4908913	Confined	56,6	-0,4	0,9	-0,3	0,1	14608	0,55	0,64	0,03	0,55	210
RA85-00	737064	4904662	Confined	58,7	5,6	14,2	14,5	16,9	30404	0,11	0,08	0,04	0,07	90
RA89-00	728640	4908289	Confined		18,4	19,4	21,6	22,1	37426	0,04	0,05	0,07	0,04	110
RA90-00	727550	4905022	Confined		39,2	39,9	40,3	39,9	39360	0,1	0,11	0,06	0,07	
RA-F01-00	728959	4940178	Confined		0,7	-0,6	1,6	1,4	30452	0,12	0,09	0,05	0,06	240
RA-F06-00	755574	4929643	Confined	55,42	-0,8		-0,8	0,1	5802	2,02	1,37	0,07	2,1	265
RA-F13-01	737935	4924053	Confined		4,4		5,5	5,1	24098	0,08	0,04	0,06	0,05	240
RA-F14-00	745191	4920756	Confined		2,4		3,7	3,5	18097	0,81	0,21	0,04	0,24	600
RA-F16-00	765347	4915210	Confined		-0,1	0,2	-0,1	-0,1	290	6,56	1,92	0,06	2,03	
RA-F22-00	747972	4908087	Confined		4,8	8,6	9,5	9,6	18996	0,1	0,09	0,11	0,07	
RA-F23-01	758727	4902869	Confined		6,8	7,1	8,2	8,3	10210	0,1	0,09	0,11	0,16	270
FC03-02	742205	4898227	Confined		17	20,5	22,5	25,2	27267					80
FC04-00	749779	4897241	Confined		19,3	20	21,2	21,7	20659					
FC07-01	769967	4891732	Confined					4,7	7051	0,14	0,15	0,17	0,15	105
FC12-00	745330	4908338	Confined		3,1	4	5,1	9,2	21406					270
FC13-00	742537	4904150	Confined		5,6	10,5	12,7	10,2	25309					280
FC14-02	748563	4900097	Confined		8,8	10,3	11,5	12,3	20734	0,08	0,09	0,19	0,09	
FC16-01	775163	4896146	Confined		-9,9	-3,9	-4,3	-7,9	262	0,13	0,14		0,18	175

Monitoring well	Geographical coordinates EPSG12832 - ETRS89 32N		Groundwater occurrence	Hydraulic conductivity (m/day)	Groundwater level (m)				Distance from the shore (m)	Ratio: $\frac{Cl^-}{HCO_3^- + CO_3^{2-}}$				Aquifer thickness (m)
	X - UTM	Y - UTM			2010/12	2013	2014	2015		2010/12	2013	2014	2015	
FC17-01	769237	4897971	Confined						3465	0,09	0,09	0,1	0,08	135
FC18-00	769089	4894534	Confined		-9,5	-11	-2,5	-6	5749					130
FC19-00	739849	4909389	Confined		7,2	8,1	9,2	10	26345					290
FC19-01	740540	4908651	Confined						25974	0,1	0,11	0,1	0,08	130
FC20-00	741466	4901290	Confined		12,5	15,3	17,3	16,6	27129					210
FC20-01	741781	4901960	Confined						26652	0,06	0,07		0,07	230
FC22-00	749384	4904116	Confined		2,6	18,7	19	19,3	18742					
FC25-00	765677	4896373	Confined		-5,5	-4	-0,9	-1,2	7201	0,08	0,09	0,04	0,08	80
FC27-00	759064	4897716	Confined		6,9	9,4	12,2	10,8	12103					190
FC28-02	756529	4892579	Confined						16864	0,07	0,07	0,05	0,07	30
FC41-00	762976	4897161	Confined		5,2	7,2	10	6,5	9008					75
FC43-00	772727	4894282	Confined						3306	0,79	0,9		0,82	145
FC50-02	745193	4901314	Confined		-7,9	-4,7	1,9	2,8	23559	0,06	0,07			230
FC51-01	745296	4904972	Confined						22498	0,07	0,07		0,07	280
FC52-00	754245	4901885	Confined			12,2	11,9	11,8	14.771	0,32	0,5		0,46	
FC53-00	749482	4897978	Confined		19	21,6	21	21,3	20663					
FC56-00	760890	4901578	Confined						8773	0,06	0,06	0,17	0,05	270
FC57-03	765900	4890320	Confined				18,4	15,5	10917			0,16	0,05	30
FC58-01	776391	4888819	Confined						4187	0,05	0,05	0,15	0,05	155
FC70-00	775377	4889943	Confined		2	8,1	11	10,5	4285					135
FC70-01	775555	4889980	Confined						4038	0,07	0,07	0,06	0,07	150
FC71-00	741252	4901195	Confined		17,2	17,9	20,1	20,8	27349					210
FC73-00	744301	4897221	Confined		15	17,8	19,6	23,5	25659					
FC77-00	751113	4901473	Confined		15,8	16,2	17	14,4	17809					
FC78-01	771623	4889715	Confined						71730	0,1	0,15	0,1	0,14	75

Monitoring well	Geographical coordinates EPSG12832 - ETRS89 32N		Groundwater occurrence	Hydraulic conductivity (m/day)	Groundwater level (m)				Distance from the shore (m)	Ratio: $\frac{Cl^-}{HCO_3^- + CO_3^{2-}}$				Aquifer thickness (m)
	X - UTM	Y - UTM			2010/12	2013	2014	2015		2010/12	2013	2014	2015	
FC79-01	752692	4896108	Confined						18550	0,59	0,59	0,05	0,65	
FC80-01	757380	4895857	Confined					-1,5	14492			0,06	0,66	190
FC81-03	770077	4900261	Confined					12,4	1346	0,08	0,06	0,02	0,06	180
FC83-00	744569	4898758	Confined		4,4				24935	0,06	0,05	0,08	0,06	
FC83-01	744603	4898725	Confined						28842					
FC85-00	747675	4896484	Confined		19,3	19,7	20,4	20,6	22904					
FC86-00	738934	4903088	Confined	58,835	10,7	14	15,7	17,9	29069	0,1	0,1	0,07	0,12	75
FC89-00	745925	4893453	Confined		38,5	38,8	38,8	39	25709	0,12	0,11	0,02	0,1	
FC90-00	757882	4893250	Confined		-0,3	3,4	7,7	13,5	15389	0,11	0,06	0,02	0,03	50
FC91-00	764203	4899837	Confined						6529	0,05	0,04	0,13	0,04	130
FC92-00	760325	4896103	Confined						11787	0,05	0,05	0,05	0,05	95
FC93-00	746304	4901831	Confined		-4	-3,4	-2	-0,2	22268	0,08	0,08	0,16	0,08	
FC-F04-00	750030	4899225	Confined		22,2	22,8	23,9	23,3	19620	0,08	0,08	0,04	0,06	
FC-F06-00	759933	4896258	Confined		22,8	23,4	24,1	23,3	12021	0,1	0,12	0,05	0,09	170
FC-F07-00	771211	4889465	Confined		18	18,5	19,9	20	7626	0,07	0,07	0,07	0,04	65
RN02-00	797566	4874609	Confined	50,5	-15,6		0,7	-7,2	1226					50
RN03-00	777283	4881282	Confined		-17,1		42,5	33,4	8883					30
RN04-00	784553	4884990	Confined		-3,9		6,5	6,4	1668					165
RN05-00	780345	4885373	Confined		-14,3		10,6	7,2	3771					175
RN06-00	798105	4874950	Confined	50,5	-10,3		2,4	-4,4	636					50
RN08-01	777954	4892011	Confined		-14,4				950	0,04	0,04	0,04	0,04	180
RN21-02	779194	4882616	Confined		10,9	18,8	22,9	20,9	6586	0,16	0,12	0,07	0,08	65
RN29-00	777722	4887408	Confined		5,1	9,5	11,6	11,5	4188	0,04	0,04	0,04	0,04	55
RN30-00	781291	4887309	Confined		1,7	4,5	6,6	6,2	1783	0,05	0,06	0,05	0,06	155
RN31-01	783994	4885076	Confined		-0,8	4,3	4,7	5,2	1816	0,11	0,08	0,07	0,06	140

Monitoring well	Geographical coordinates EPSG12832 - ETRS89 32N		Groundwater occurrence	Hydraulic conductivity (m/day)	Groundwater level (m)				Distance from the shore (m)	Ratio: $\frac{Cl^-}{HCO_3^- + CO_3^{2-}}$				Aquifer thickness (m)
	X - UTM	Y - UTM			2010/12	2013	2014	2015		2010/12	2013	2014	2015	
RN33-00	777584	4884052	Confined						6631	0,03	0,03	0,03	0,03	100
RN33-01	776419	4884064	Confined			26,6	28,8	26,2	7396	0,13	0,05	0,04	0,03	
RN34-00	785354	4884462	Confined		-2	0,8	1,8	2,4	1979	0,12	0,07	0,08	0,06	170
RN36-00	794961	4876586	Confined	50,5	-4,1	0,6	-1,4	-1,3	925	0,15	0,13	0,11	0,12	40
RN38-01	798396	4872593	Confined		7,6	14	15,4	15,4	2851	0,15	0,12	0,12	0,11	25
RN59-00	778854	4890670	Confined		-1,2	1,2	5,1	5,2	1130	0,05	0,05	0,05	0,05	150
RN60-01	778815	4885449	Confined		-1,4	4	6,5	5,3	4722	0,04	0,04	0,03	0,04	110
RN61-00	784243	4886555	Confined						415	0,06	0,05	0,05	0,05	220
RN62-00	800113	4873916	Confined		2,7	5,8	7	6,9	1154	0,15	0,15	0,14	0,14	45
RN63-01	786274	4881805	Confined		10,5	12,6	12	12	3118					95
RN66-00	792434	4877742	Confined		9,6	10,3	10,4	10,6	1599					
RN67-00	798091	4874982	Confined	50,5	-11,6	-5,3	-0,7	2,5	659	0,59	0,68	0,63	0,64	50
RN68-00	797093	4875432	Confined	50,5	-13,6	-2	-3,2	-2,7	668	0,24	0,16	0,1	0,09	40
RN70-00	796986	4873830	Confined		12	12,6	13,5	12,5	2103					
RN71-00	780313	4886907	Confined		-4,2	-1,1	0,7		2684	0,05	0,04	0,04	0,04	115
RN72-00	781199	4884985	Confined		-3,2	3,6	5,7	6	3542	0,09	0,1	0,1	0,1	140
RN73-00	782375	4885516	Confined	52,31	-0,5	2,3	4,2	4,3	2321	0,06	0,04	0,03	0,03	145
RN74-00	780624	4889890	Confined		-0,3	2	2	2	366	0,06	0,05	0,05	0,05	120
RN76-00	793995	4870706	Confined		70,3	71,2	69,7	71,2	6287	0,16	0,18	0,15		10
RN-F01-00	781166	4889206	Confined	56,5	0,3	1,5	1	0,6	491	0,07	0,05	0,06	0,05	175
RN-F02-00	786461	4881183	Confined		12,9	13,3	13,3	13,2	3365	0,11	0,06	0,09	0,08	45
RN-F03-00	795537	4876404	Confined	50,5	-0,4	2	1,7	1,6	730	0,12	0,12	0,11	0,14	40

Bibliography

[1] K. Ivkovic, P. Dixon-Jain, S. Marshall, B. Sundaram, J. Clarke, L. Wallace and A. Werner, "A national-scale vulnerability assessment of seawater intrusion: Literature review, data review, and method development.," *Geoscience Australia,* p. 172, 2013.

[2] G. Wriedt and B. Fayçal, "Large scale screening of seawater intrusion risk in Europe: Methodological development and pilot application along the Spanish Mediterranean coast," Office for Official Publications of the European Communities, Luxembourg, 2009.

[3] M. Dentoni, "Risk Analysis and Mitigation of Seawater Intrusion," Cagliari, Esame finale anno accademico 2011 – 2012.

[4] D. Dunn, "SALTWATER INTRUSION, NON-TECHNICAL," [Online]. Available: http://www.dunnhydrogeo.com/home/saltwater-intrusion-pompano-t/saltwater-intrusion-nt. [Accessed March 2017].

[5] P. M. Barlow, "Ground Water in Freshwater-Saltwater Environments of the Atlantic Coast," *U.S. Geological Survey,* no. circular 1262, p. 113, 2003.

[6] J. P. LOBO FERREIRA and A. G. CHACHADI, "Assessing aquifer vulnerability to sea-water intrusion using GALDIT method: Part 2 – GALDIT Indicators Description," in *The Fourth Inter-Celtic Colloquium on Hydrology and Management of Water Resources*, Guimarães, Portugal, 2005.

[7] J. Bear, A. Cheng, S. Sorek, D. Ouazar and I. Herrera, Seawater Intrusion in Coastal Aquifers Concepts, Methods and Practices (Theory and Applications of Transport in Porous Media), Berlin, 1999, p. 640.

[8] V. Post, H. Kooi and C. Simmons, "Using Hydraulic Head Measurements in Variable-Density Ground Water Flow Analyses," *GROUND WATER,* vol. 45, no. 6, pp. 664-671, November-December 2007.

[9] Solinst Canada Ltd - High Quality Groundwater & Surface Water Monitoring Instrumentation, "Pump/Recharge Rate Affects Saltwater Intrusion," [Online]. Available: https://www.solinst.com/resources/papers/101c4salt.php. [Accessed 14 mars 2017].

[10] F. Van Weert, J. Van Der Gun and J. Reckman, "Global Overview of Saline Groundwater Occurrence and Genesis," International Goundwater Resources Assessment Centre, Utrecht, July 2009.

[11] Y. Y. Y. Agarwadkar, "Thesis: Salinity Mapping In Coastal Area Using GIS and Remote," International Institute for Geo-information Science and Earth Observation, Enschede, The Nederlands, 2005 (February).

[12] I. Shiklomanov, "World fresh water resources," in *Water in Crisis: A Guide to the World's Fresh Water Resources*, New York, Oxford University Press, 1993, p. 346.

[13] I. S. Zektser and L. G. Everett, Groundwater Resources of the World and their Use, Vols. IHP-VI, SERIES ON GROUNDWATER NO. 6, I. S. Zektser, Ed., Paris: United Nations Educational Scientific and Cultural Organization (UNESCO), 2004.

[14] T. N. G. W. A. (NGWA), "Facts About Global Groundwater Usage," Westerville, Ohio, U.S.A., 2016.

[15] A. Franek, E. Koncagul, R. Connor and D. Hunziker, "WATER FOR A SUSTAINABLE WORLD : FACTS AND FIGURES," Division of Water Sciences, UNESCO, Perugia, Italy, 2015.

[16] D. Hinrichsen, "Ocean planet in decline," May 2010. [Online]. Available: http://www.peopleandtheplanet.com/index.html@lid=26188&section=35&topic=44.html. [Accessed 15 March 2017].

[17] P. M. Barlow and E. G. Reichard, "Saltwater intrusion in coastal regions of North America," *Hydrogeology Journal,* no. 18, pp. 247-260, February 2010.

[18] E. Bocanegra, G. J. Cardoso Da Silva, E. Custodio, M. Manzano and S. Montenegro, "State of knowledge of coastal aquifer management in South America," *Hydrogeology Journal,* no. 18, pp. 261-267, 10 October 2009.

[19] E. Custodio, "Coastal aquifers of Europe: An overview," *Hydrogeology Journal,* no. 18, pp. 269-280, February 2009.

[20] G. Steyl and I. Dennis, "Review of coastal-area aquifers in Africa," *Hydrogeology Journal,* no. 18, pp. 217-225, February 2010.

[21] L. K. Morgan and A. D. Werner, "A national inventory of seawater intrusion vulnerability for Australia," *Journal of Hydrology: Regional Studies,* no. 4, pp. 686-698, September 2015.

[22] A. D. Werner, M. Bakker, V. E. Post, A. Vandenbohede, C. Lu, B. Ataie-Ashtiani, C. T. Simmons and D. A. Barry, "Seawater intrusion processes, investigation and management: Recent advances and future challenges," *Advances in Water Resources,* no. 51, pp. 3-26, 2013.

[23] G. A. G. Ferguson and T. Gleeson, "Vulnerability of coastal aquifers to groundwater use and climate change," *Nature Climate Change,* vol. 2, pp. 341-345, May 2012.

[24] L. K. Morgan, "Practical approaches to seawater intrusion investigation and management," 2014.

[25] J. Traverse, D. Chastanet, A. Vanden Berghe, L. Roger and J.-M. Dufond, "Nouvelles approches et capteurs innovants pour la connaissance et le suivi des aquifères côtiers. Application à la surveillance des intrusions salines dans le bassin sédimentaire du Roussillon (France) - Tâche 4: Etat de l'art concernant ...," Février 2014 [French].

[26] P. Stuyfzand, "A new hydrochemical classification of water types," *RegionalCfiaracterizaiionof WaterQua,* no. 182, pp. 89-98, May 1989.

[27] P. Mollema, M. Antonellini, E. Dinelli, G. Gabbianelli, N. Greggio and P. Stuyfzand, "Hydrochemical and physical processes influencing salinization and freshening in Mediterranean low-lying coastal environments," *Applied Geochemistry,* vol. 34, p. 207–221, July 2013.

[28] Anonymous, "Electrical resistivity and conductivity," Wikipedia - The Free Encyclopedia, 25 March 2017. [Online]. Available: https://en.wikipedia.org/wiki/Electrical_resistivity_and_conductivity#General_definition. [Accessed 14 April 2017].

[29] Anonymous, "Piper diagram," Wikipedia - The Free Encyclopedia, 2 March 2017. [Online]. Available: https://en.wikipedia.org/wiki/Piper_diagram. [Accessed 8 April 2017].

[30] Anonymous, "What is a piper plot?".

[31] Anonymous, "Stiff diagram," Wikipedia - The Free Encyclopedia, 11 September 2016. [Online]. Available: https://en.wikipedia.org/wiki/Stiff_diagram. [Accessed 19 April 2017].

[32] Anonymous, "Hydrochemical study of the Griffy Lake [Public Domain]," [Online]. Available: https://www.google.it/search?q=durov+diagram&ie=utf-8&oe=utf-8&client=firefox-b-ab&gfe_rd=cr&ei=XDH3WLP8AbHBXpmnuLAJ#. [Accessed 19 April 2017].

[33] K. Hinsby, "Environmental tracers, groundwater age and vulnerability," Burval, pp. 141-148.

[34] Schlumberger, "Oilfield Glossary - seismic velocity," Schlumberger Limited - All rights reserved ©, 2017. [Online]. Available: http://www.glossary.oilfield.slb.com/Terms/s/seismic_velocity.aspx. [Accessed 15 April 2017].

[35] Zonge International, "Geophysical Survey Methods," 2017 Zonge International - All rights reserved ©, [Online]. Available: http://zonge.com/geophysical-methods/. [Accessed 15 April 2017].

[36] T. Dahlin, "The development of electrical imaging techniques," *Computers and Geosciences,* no. 27(9), pp. 1019-1029, 01 January 2001.

[37] A. Bourhane, HAL (archives-ouvertes.fr), 2014.

[38] Anonymous, "Transient electromagnetics," Wikipedia - The Free Encyclopedia, 16 March 2017. [Online]. Available: https://en.wikipedia.org/wiki/Transient_electromagnetics. [Accessed 14 April 2017].

[39] Geophysics GPR International Inc., "Heliborne Time-Domain EM (GPRTEM)," © COPYRIGHT Geophysics GPR International Inc., [Online]. Available: http://airborne.geophysicsgpr.com/en/techniques/electromagnetic-tdem-and-vlf/heliborne-time-domain-em-gprtem/. [Accessed 16 April 2017].

[40] D. Oldenburg, F. Jones, L. Heagy, R. Cockett, T. Astic and S. Devriese, "Ground Penetrating Radar," Copyright 2014-2016, UBCGIF ©, [Online]. Available: http://gpg.geosci.xyz/content/GPR/index.html. [Accessed 15 April 2017].

[41] Enviroscan Inc., "Seismic Refraction Versus Reflection," Copyright Enviroscan, Inc. - All Rights Reserved ©, 2017. [Online]. Available: http://www.enviroscan.com/home/seismic-refraction-versus-reflection. [Accessed 16 April 2017].

[42] Southern Rural Water - Managing Water. Serving Communities, "Where does groundwater come from and where does it go?," Spatial Vision Innovations Pty Ltd ©, 27 May 2015. [Online]. Available: http://gwhub.srw.com.au/where-does-groundwater-come-and-where-does-it-go. [Accessed 22 April 2017].

[43] C. D. Langevin and M. Zygnerski, "Effect of Sea-Level Rise on Salt Water Intrusion near a Coastal Well Field in Southeastern Florida," *Groundwater,* vol. 51, no. 5, pp. 781-803, September-October 2013.

[44] Food and agriculture organization of the United Nations, "Physics and mathematics," in *Seawater Intrusion in Coastal Aquifers - Guidelines for study, monitoring and control*, vol. 11, Rome, ©FAO 1997, 1997, p. 153.

[45] G. H. Oude Essink, "Density Dependent Groundwater Flow - Salt Water Intrusion and Heat Transport," Utrecht, 2001.

[46] N. Trabelsi, I. Triki, I. Hentati and M. Zairi, "Aquifer vulnerability and seawater intrusion risk using GALDIT, GQI(SWI) and GIS: case of a coastal aquifer in Tunisia," *Environ Earth Sci,* no. 75, pp. 1-19, 2016.

[47] A. HAOUCHINE, F. Z. HAOUCHINE and A. LABADI, "ASSESSMENT OF GROUNDWATER VULNERABILITY USING INDEX BASED METHOD. CASE OF SEBAOU RIVER AQUIFER (NORTHERN ALGERIA)," *Larhyss Journal,* no. 24, pp. 337-349, December 2015.

[48] GISGeography, "What is Geographic Information Systems (GIS)?," 14 March 2017. [Online]. Available: http://gisgeography.com/what-gis-geographic-information-systems/. [Accessed 26 March 2017].

[49] K. Rutledge, M. McDaniel, D. Boudreau, T. Ramroop, S. Teng, E. Sprout, H. Costa, H. Hall and J. Hunt, "GIS (geographic information system)," National Geographic Society , 26 March 2011. [Online]. Available: http://www.nationalgeographic.org/encyclopedia/geographic-information-system-gis/. [Accessed 26 March 2017].

[50] N. Dörfliger and P.-Y. Jeannin, "Water vulnerability assessment in karst environments: a new method of defining protection areas using a multi-attribute approach and GIS tools (EPIK method)," *Environmental Geology,* no. 39, pp. 165-176, December 1999.

[51] Z. Tasnim and S. Tahsin, "Application of the Method of Galdit for Groundwater Vulnerability Assessment: A Case of South Florida," *Asian Journal of Applied Science and Engineering,* vol. V, no. 1, pp. 27-40, 2016.

[52] J. P. Lobo Ferreira, A. G. Chachadi, C. Diamantino and M. Henriques, "Assessing aquifer vulnerability to seawater intrusion using the GALDIT method: part 1 - application to the Portuguese Monte Gordo aquifer," in *The Fourth InterCeltic Colloquium on Hydrology and Management of Water Resources*, Guimarães, 2005.

[53] V. Lenin Kalyana Sundaram, G. R. G. Dinesh and D. Govindarajalu, "Vulnerability assessment of seawater intrusion and effect of artificial recharge in Pondicherry coastal region using GIS," *Indian Journal of Science and Technology,* vol. I, no. 7, pp. 1-7, Dec. 2008.

[54] E. Idowu Temitope, M. Nyadawa and M. K'orowe, "Seawater Intrusion Vulnerability Assessment of a Coastal Aquifer: North Coast of Mombasa, Kenya as a Case Study," *International Journal of Engineering Research and Application,* vol. VI, no. 8, pp. 37-45, August 2016.

[55] A. Chachadi, "Seawater Intrusion Mapping Using Modified GALDIT Indicator Model - Case Study in Goa," *Jalvigyan Sameeksha,* vol. XX, pp. 29-45, 2005.

[56] S. Kumar, D. Thirumalaivasan, N. Radhakrishnan and S. Mathew, "Groundwater vulnerability assessment using SINTACS model," *Geomatics, Natural Hazards and Risk,* vol. IV, no. 4, pp. 339-354, 2013.

[57] M. Tomaszkiewicz, M. Abou Najm and M. El-Fadel, "Development of a groundwater quality index for seawater intrusion in coastal aquifers," *Environmental Modelling & Software,* no. 57, pp. 13-26, 27 March 2014.

[58] G. R. Mutasem El-Fadel, I. Alameddine and M. AbouNajm, "Vulnerability indices for SWI assessment," in *35th Annual Conference of the International Association for Impact Assessment*, Florence, 2015.

[59] A. G. Chachadi, J. P. C. Lobo Ferreira, L. Noronha and B. S. Choudri, "Assessing the impact of sea-level rise on salt water intrusion in coastal aquifers using GALDIT model," in *Seminário Sobre Águas Subterrâneas*, Lisboa, Fev. 2003.

[60] D. F. Ball and E. Campbell, "Saline intrusion: a screening tool for the assessment of risk to coastal aquifers in Scotland," Keyworth, Nottingham, 2006.

[61] Arpae - Servizio Affari istituzionali, Pianificazione e Comunicazione, "Coastal zone characteristics," 15 June 2017. [Online]. Available: https://www.arpae.it/dettaglio_generale.asp?id=1744&idlivello=1344. [Accessed 16 June 2017].

[62] Anonymous, "Emilia-Romagna," Wikipedia - The Free Encyclopedia, 23 May 2017. [Online]. Available: https://en.wikipedia.org/wiki/Emilia-Romagna#Administrative_divisions. [Accessed 16 June 2017].

[63] N. Greggio, P. Mollema, M. Antonellini and G. Gabbianelli, "Irrigation Management in Coastal Zones to Prevent Soil and Groundwater Salinization," in *Resource Management for Sustainable Agriculture*, V. Abrol and P. Sharma, Eds., 2012.

[64] N. Colombani, "HYDROGEOCHEMICAL MONITORING AND MODELLING OF SALTWATER INTRUSION IN LOWLANDS (FERRARA, IT)," Bologna, 2014.

[65] Arpae - Servizio Affari istituzionali, Pianificazione e Comunicazione, "Analisi climatica giornaliera 1961-2015," 15 June 2017. [Online]. Available: https://www.arpae.it/dettaglio_documento.asp?id=6147&idlivello=1528. [Accessed 16 June 2017].

[66] G. Felisa, "Dynamics of coastal aquifers: data-driven forecasting and risk analysis," 2015.

[67] P. Teatini, M. Ferronato, G. Gambolati, P. Severi, W. Bertoni, M. Gonella and M. Morelli, "Land subsidence due to groundwater withdrawal in the Emilia-Romagna coastland, Italy," in *Seventh International Symposium on Land Subsidence*, Shanghai, January 2005.

[68] M. Antonellini, D. Allen, P. Mollema, D. Capo and N. Greggio, "Groundwater Freshening Following Coastal Progradation and Land Reclamation of the Po Plain, Italy," *Hydrogeology Journal,* p. 40, n/a.

[69] B. M. Giambastiani, M. Antonellini, G. H. Oude Essink and R. J. Stuurman, "Saltwater intrusion in the unconfined coastal aquifer of Ravenna (Italy): A numerical model," *Journal of Hydrology,* no. 340, pp. 91-104, June 2007.

[70] E. Ulazzi, M. Antonellini and G. Gabbianelli, "Characterization of the Coastal Phreatic Aquifer of Cervia Area (NE Italy)," *Mem. Desc. Carta Geol. d'It.,* vol. LXXVI, pp. 277-288, 2007.

[71] F. Disconzi, "IDea - Open data, Web e Dolomiti," copyright ©2015 fabiodisconzi.com, all rights reserved, 2015. [Online]. Available: http://www.fabiodisconzi.com/gislocal/informazioni/30/index.html. [Accessed 2017 July 4].

[72] L. Perini, L. Calabrese, P. Luciani and P. Severi, "Integrated geological approach to the study of coastal subsidence in Emilia-Romagna".

[73] Anonymous, "Canale Emiliano Romagnolo," Wikipedia - the Free Encyclopedia, 28 January 2017. [Online]. Available: https://it.wikipedia.org/wiki/Canale_Emiliano_Romagnolo. [Accessed 21 June 2017].

[74] Environmental Systems Research Institute, Inc., "Comparing interpolation methods," Copyright © 1995–2017 Environmental Systems Research Institute, Inc., [Online]. Available: https://pro.arcgis.com/en/pro-app/tool-reference/3d-analyst/comparing-interpolation-methods.htm. [Accessed 5 July 2017].

[75] QGIS©, "Spatial Analysis (Interpolation)," Documentation QGIS 2.2, 04 December 2014. [Online]. Available: https://docs.qgis.org/2.2/en/docs/gentle_gis_introduction/spatial_analysis_interpolation.html#overview. [Accessed 05 July 2017].

[76] P. Tschakert, K. Zimmerer, B. King, S. Baum and D. Kunches, "Scale," The Pennsylvania State University, 2014. [Online]. Available: https://www.e-education.psu.edu/geog030/node/317. [Accessed 20 March 2017].

[77] Anonymous, "Equivalent (chemistry)," Wikipedia - The Free Encyclopedia, 28 March 2017. [Online]. Available: https://en.wikipedia.org/wiki/Equivalent_(chemistry). [Accessed 10 April 2017].

[78] Anonymous, "Spatial scale," Wikipedia - The Free Encyclopedia, 3 November 2016. [Online]. Available: https://en.wikipedia.org/wiki/Spatial_scale. [Accessed 20 March 2017].

[79] Anonymous, "Geophysical imaging," Wikipedia - The Free Encyclopedia, 27 January 2017. [Online]. Available: https://en.wikipedia.org/wiki/Geophysical_imaging. [Accessed 15 April 2017].

[80] Anonymous, "Tomography," Wikipedia - The Free Encyclopedia, 13 April 2017. [Online]. Available: https://en.wikipedia.org/wiki/Tomography. [Accessed 17 April 2017].

[81] Schlumberger, “Oilfield Glossary - tomography,” Schlumberger Limited - All rights reserved ©, 2017. [Online]. Available: http://www.glossary.oilfield.slb.com/Terms/t/tomography.aspx. [Accessed 15 April 2017].

[82] Anonymous, “Glossaire des termes techniques,” IRD - Institut de recherche pour le développement ©, [Online]. Available: http://www.brest.ird.fr/actualites/EGEE-2_glossaire.htm#liste. [Accessed 20 April 2017].

[83] Anonymous, “Hydrochimie [In French],” Wikipedia - The Free Encyclopedia, 19 September 2016. [Online]. Available: https://fr.wikipedia.org/wiki/Hydrochimie#Classification_hydrochimique_des_.C3.A9l.C3.A9ments_et_param.C3.A8tres_utilis.C3.A9s. [Accessed 20 April 2017].

[84] I. Clark, “What is kriging?,” Geostokos (Ecosse) Limited, [Online]. Available: http://www.kriging.com/whatiskriging.html. [Accessed 1 May 2017].

[85] Anonymous, “Marine transgression,” Wikipedia - The Free Encyclopedia, 24 June 2017. [Online]. Available: https://en.wikipedia.org/wiki/Marine_transgression. [Accessed 30 June 2017].

[86] Anonymous, “Marine regression,” Wikipedia - The Free Encyclopedia, 3 June 2017. [Online]. Available: https://en.wikipedia.org/wiki/Marine_regression. [Accessed 30 June 2017].